THE EVALUATION OF DIFFERENT TECHNIQUES OF HEPATIC ABLATION IN AN *EX-VIVO* PERFUSED PORCINE LIVER MODEL

Thesis submitted for the degree of

Doctor of Medicine

at the University of Leicester

by

Gianpiero Gravante

Department of Cancer Studies and Molecular Medicine

University of Leicester

January 2012

Abstract

Background: Electrolytic ablation (EA) is a technique of liver ablation that produces extreme pH changes in the local microenvironment. An *ex-vivo* perfused liver model compared EA vs. radiofrequency ablation (RFA) and analysed biochemical, immunological and histologic parameters. **Methods:** Seventeen pigs were perfused extracorporeally with normothermic autologous blood, five of which underwent RFA and five EA after one hour from reperfusion. Arterial, venous blood samples and histologic specimen were collected hourly and analysed for 1) arterial blood gases content, 2) biochemical parameters, 3) cytokines, 4) and tissue modifications. **Results:** No significant differences were registered among techniques for biochemical and immunologic parameters investigated. EA created a smaller transitional zone of ablation compared to RFA and histologically a particular pattern of changes in which the coagulative necrosis and hemorrhages affected mainly the peripheral area of the lobule, while the sinusoidal dilatations the centrilobular area. No significant changes were found for the apoptosis and the regeneration activity. **Conclusions:** Although results of the histological changes are interesting, the technical complexity of the *ex-vivo* model increased the number of parameters to monitor, especially concerning the liver viability and the administration of external substances to maintain a physiologic environment. Furthermore, the high portal vein pressures used and long warm ischemia times registered could have biased results. For the purpose of this study an *in-vivo* model would have been more appropriate.

Acknowledgments

I am indebted to many people and organisations that allowed the completion of this study. I am very grateful to **Mr Ashley Dennison** for giving me the opportunity to undertake this work and for his continuing personal and scientific support. I'm also indebted to **Prof. Michael Nicholson** for the possibility to use his laboratories and facilities and to **Mrs. Seok Ling Ong** for her constant patience and friendship throughout the entire project. A special thank to **Mr Roberto Sorge**, professor of Medical Statistics at the University "Tor Vergata" in Rome, not only for his statistical support but especially for his rigorous teaching towards evidence-based research. I want also to thank **Mr Matthew Metcalfe** for his input on the thesis format and scientific background of the project and **Mr David Lloyd** for his enthusiasm and advices. I am definitely grateful to **Mrs Severine Illouz**, **Mrs Cristina Pollard**, **Mrs Balu M'Webb, Dr Wen Yung Chuan** and **Mrs Sarah Hosgood** for their invaluable scientific suggestions and personal support. My thanks are finally due to the staff of the Intensive Care Unit at the Leicester General Hospital with particular mentions to **Dr Andrew Fox** and to the Department of Histopathology at the Leicester Royal Infirmary with particular mentions to **Dr Angus McGregor** and **Dr Kevin West**.

Publications and presentations from this thesis

Publications

1. Gravante G, Ong SL, Metcalfe MS, Sorge R, Bikhchandani J, Lloyd DM, Dennison AR. Effects of hypoxia due to isovolemic hemodilution on an ex vivo normothermic perfused liver model. J Surg Res. 2010 May 1;160(1):73-80.
2. Gravante G, Ong SL, Metcalfe MS, Sorge R, Overton J, Lloyd DM, Maddern GJ, Dennison AR. Cytokine response of electrolytic ablation in an ex vivo perfused liver model. ANZ J Surg. 2010 Jul-Aug;80(7-8):537-41.
3. Gravante G, Ong SL, Metcalfe MS, Sorge R, Fox AJ, Lloyd DM, Maddern GJ, Dennison AR. Changes in acid-base balance during electrolytic ablation in an ex vivo perfused liver model. Am J Surg. 2010 May 5. (Epub ahead of print)
4. Gravante G, Ong SL, Metcalfe MS, Sorge R, Sconocchia G, Orlando G, Lloyd DM, Dennison AR. Cytokine response to ischemia/reperfusion injury in an ex vivo perfused porcine liver model. Transplant Proc. 2009 May;41(4):1107-12.
5. Gravante G, Ong SL, Metcalfe MS, Lloyd DM, Dennison AR. The porcine hepatic arterial supply, its variations and their influence on the extracorporeal perfusion of the liver. J Surg Res. 2011 Jun 1;168(1):56-61.
6. Gravante G, Sconocchia G, Ong SL, Dennison AR, Lloyd DM. Immunoregulatory effects of liver ablation therapies for the treatment of primary and metastatic liver malignancies. Liver Int. 2009 Jan;29(1):18-24.

7. Gravante G, Ong SL, Metcalfe MS, Bhardwaj N, Maddern GJ, Lloyd DM, Dennison AR. Experimental application of electrolysis in the treatment of liver and pancreatic tumours: principles, preclinical and clinical observations and future perspectives. Surg Oncol. 2011 Jun;20(2):106-20.
8. Gravante G, Ong SL, Metcalfe MS, Bhardwaj N, Lloyd DM, Dennison AR. The effects of radiofrequency ablation on the hepatic parenchyma: histological bases for tumor recurrences. Surg Oncol. 2011 Dec;20(4):237-45.
9. Gravante G, Ong SL, Metcalfe MS, Strickland A, Dennison AR, Lloyd DM. Hepatic microwave ablation: a review of the histological changes following thermal damage. Liver Int. 2008 Aug;28(7):911-21.
10. Gravante G, Knowles T, Ong SL, Al-Taan O, Metcalfe M, Dennison A, Lloyd D. Future clinical applications of bile analysis. ANZ J Surg. 2010 Oct;80(10):679-80.
11. Gravante G, Knowles T, Ong SL, Al-Taan O, Metcalfe M, Dennison AR, Lloyd DM. Bile changes after liver surgery: experimental and clinical lessons for future applications. Dig Surg. 2010;27(6):450-60.
12. Gravante G, Overton J, Sorge R, Bhardwaj N, Metcalfe MS, Lloyd DM, Dennison AR. Radiofrequency ablation versus resection for liver tumours: an evidence-based approach to retrospective comparative studies. J Gastrointest Surg. 2011 Feb;15(2):378-87.
13. Gravante G, Ong SL, Cameron IC, Richards C, Metcalfe MS, Dennison AR, Lloyd DM. Two primary tumours metastasizing to the liver in a collision phenomenon. ANZ J Surg. 2010 May;80(5):368-9. PubMed PMID: 20557514.

14. Gravante G, Ong SL, McGregor A, Sorge R, Metcalfe MS, Lloyd DM, Dennison AR. Histological changes during extracorporeal perfusions of the porcine liver: implications for temporary support during acute liver failures. J Artif Organs. 2013 Jun;16(2):218-28.

15. Gravante G, Ong Sl, Kevin W, McGregor A, Chung WY, Al-Leswas D, Maddern GJ, Metcalfe MS, Lloyd DM, Dennison AR. Patterns of histological changes following hepatic electrolytic ablation in an *ex-vivo* perfused model. Pathol Oncol Res. 2012 Oct;18(4):1085-9.

16. Ahmad F, Gravante G, Bhardwaj N, Strickland A, Basit R, West K, Sorge R, Dennison AR, Lloyd DM. Changes in interleukin-1β and 6 after hepatic microwave tissue ablation compared with radiofrequency, cryotherapy and surgical resections. Am J Surg. 2010 Oct;200(4):500-6.

17. Ahmad F, Gravante G, Bhardwaj N, Strickland A, Basit R, West K, Sorge R, Dennison AR, Lloyd DM. Renal effects of microwave ablation compared with radiofrequency, cryotherapy and surgical resection at different volumes of the liver treated. Liver Int. 2010 Oct;30(9):1305-14.

18. Ahmad F, Gravante G, Bhardwaj N, Strickland A, Basit R, West K, Sorge R, Dennison AR, Lloyd DM. Large volume hepatic microwave ablation elicits fewer pulmonary changes than radiofrequency or cryotherapy. J Gastrointest Surg. 2010 Dec;14(12):1963-8.

19. Alzaraa A, Gravante G, Chung WY, Al-Leswas D, Morgan B, Dennison AR, Lloyd DM. Targeted microbubbles in the experimental and clinical setting. Am J Surg. 2012 Sep;204(3):355-66.

20. Alzaraa A, Gravante G, Chung WY, Al-Leswas D, Morgan B, Dennison AR, Lloyd DM. Contrast-enhanced ultrasound in the preoperative, intraoperative and postoperative assessment of liver lesions. Hepatol Res. 2013 Aug;43(8):809-19.

21. Alzaraa A, Al-Leswas D, Chung WY, Gravante G, Morgan B, West K, Dennison AR, Lloyd DM. Contrast-enhanced ultrasound detects perfusion defects in an *ex-vivo* porcine liver model: a useful tool for the study of hepatic reperfusion. J Artif Organs. 2013 Jun 29. (Epub ahead of print)

22. Bhardwaj N, Dormer J, Ahmad F, Strickland AD, Gravante G, West K, Dennison AR, Lloyd DM. Microwave ablation of the liver: a description of lesion evolution over time and an investigation of the heat sink effect. Pathology. 2011 Dec;43(7):725-31.

23. Bhardwaj N, Gravante G, Strickland AD, Ahmad F, Dormer J, Dennison AR, Lloyd DM. Cryotherapy of the liver: a histological review. Cryobiology. 2010 Aug;61(1):1-9.

24. Bhardwaj N, Dormer J, Ahmad F, Strickland AD, Gravante G, Beckingham I, West K, Dennison AR, Lloyd DM. Heat Shock Protein 70 Expression Following Hepatic Radiofrequency Ablation is Affected by Adjacent Vasculature. J Surg Res. 2010 Oct (Epub ahead of print)

25. Chung WY, Gravante G, Al-Leswas D, Alzaraa A, Sorge R, Ong SL, Pollard C, Lloyd DM, Metcalfe MS, Dennison AR. The autologous normothermic *ex-vivo* perfused porcine liver-kidney model: improving the circuit's biochemical and acid-base environment. Am J Surg. 2012 Oct;204(4):518-26.

26. Chung WY, Gravante G, Al-Leswas D, Alzaraa A, Sorge R, Ong SL, Pollard C, Lloyd DM, Metcalfe MS, Dennison AR. Addition of a kidney to the normothermic ex

vivo perfused porcine liver model does not increase cytokine response. J Artif Organs. 2012 Sep;15(3):290-4.

27. Chung WY, Gravante G, Al-Leswas D, Arshad A, Sorge R, Watson CC, Pollard C, Metcalfe MS, Dennison AR. The development of a multiorgan ex vivo perfused model: results with the porcine liver-kidney circuit over 24 hours. Artif Organs. 2013 May;37(5):457-66.

28. Ong SL, Gravante G, Metcalfe MS, Strickland AD, Dennison AR, Lloyd DM. Efficacy and safety of microwave ablation for primary and secondary liver malignancies: a systematic review. Eur J Gastroenterol Hepatol. 2009 Jun;21(6):599-605.

29. Ong SL, Gravante G, Sorge R, Metcalfe MS, Dennison AR, Lloyd DM. Hepatic microwave ablation in an extracorporeally haemoperfused porcine liver model: a dose-response study. Dig Surg (in press)

30. Ong SL, Gravante G, Garcea G, Bikhchandani J, Metcalfe MS, Lloyd DM, Dennison AR. History, ethics, advantages and limitations of experimental models for hepatic ablation. World J Gastroenterol. 2013 Jan 14;19(2):147-54.

Published abstracts

1. 8th Congress of the European Hepato Pancreato Biliary Association, 18–20 June 2009, Atens Hilton Hotel, Atens – Greece: "Cytokines changes obtained during the ischaemia-reperfusion injury elicited by *ex-vivo* perfused porcine livers" and "Hepatic microwave ablation in an extracorporeally haemoperfused liver model: a dose response."

2. 13th Congress of the Association of Upper Gastrointestinal Surgeons, 3–4 September 2009, East Midlands Conference Center, Nottingham – United Kingdom: “Glyceryl trinitrate (GTN) prevents post-ERCP pancreatitis: a meta-analysis.”
3. 13th National Surgery Congress of the Bulgarian Society of Surgery, 7–10 October 2010, Kempinski hotel, Sofia – Bulgaria: “Patterns of liver damage seen after electrolytic ablation are different to following thermal techniques in an *ex-vivo* perfused model”
4. Pancreatic Society of Great Britain and Ireland Meeting 2010, 2-3 December 2010, Belfry in Wishaw, Sutton Coldfield – United Kingdom: “The evaluation of end-stage chronic pancreatitis: a comparison of butterfat and the fecal elastase tests” and “Portal and central venous oxygen concentrations are an effective method of monitoring islet cell oxygen requirements in the early phase following autotransplantation”
5. Society of Academic & Research Surgery Annual Meeting, 5-6 January 2011, Royal College of Surgeons, Dublin - Ireland: “Portal and central venous oxygen concentrations are an effective method of monitoring islet cell oxygen requirements in the early phases following autotransplantation”, “The liver-kidney *ex-vivo* autologous perfused porcine model for the study of islet autotransplantation in large animals” and “The liver-kidney *ex-vivo* autologous perfused porcine model – a novel system for studying the renin-angiotensin system”
6. 4th Central European Congress of Surgery, 28-30 April 2011, Corinthia Grand Hotel Royal, Budapest - Hungary: "Cytokine changes elicited by microwave ablation in an *ex-vivo* perfused liver model"

7. 13th World Congress of International Pancreas and Islet Transplant Association (IPITA), 1-4 June 2011, Corinthia Hotel Prague, Prague – Czech Republic: “Portal venography and portal venous pressure assessment for one week following total pancreatectomy and islet auto-transplantation using a recannulated umbilical vein catheter.” and “The cytokine response in the initial phase of islet auto- and allo-transplantation.”
8. 2011 Joint International Congress of ILTS, ELITA, & LICAGE, 22–25 June 2011, Valencia Conference Centre, Valencia - Spain: "Detection of Ischaemia Reperfusion Injury in a Perfused Porcine Liver Model by Contrast-Enhanced Ultrasound"

Oral presentations

1. “1st Egyptian Forum for Liver Diseases”, “Two primary tumours metastasizing to the liver in a collision phenomenon”. (November 2008 – INVITED SPEAKER); Triumph Hotel, Cairo, Egypt
2. “10° European Association of Clinical Anatomy Congress”, “The influence of the porcine hepatic artery on *ex-vivo* perfused liver models.” (September 2009); Harbiye Millitary Museum and Culture Site, Istanbul, Turkey
3. “2nd Egyptian Forum for Liver Diseases”, “Thermal ablation techniques for the treatment of HCC” and “PET-CT for the evaluation of Hepatocellular Carcinoma”. (November 2009 – INVITED SPEAKER); Triumph Hotel, Cairo, Egypt
4. “37° European Society for Artificial Organs (ESAO) congress”, “Necrosis and regeneration in *ex-vivo* perfused porcine livers" (September 2010); Macedonian

Academy of Sciences and Arts, Skopje, Macedonia. CHAIRMAN of the session "Liver Working Group".

5. “4th Central European Congress of Surgery”, “Radiofrequency ablation versus hepatic resection for malignant primary and secondary liver tumours: a meta-analysis of comparative studies” and "Experimental applications of bile analysis" (April 2011); Corinthia Grand Hotel Royal, Budapest, Hungary
6. “57th Annual Conference of the American Society for Artificial Internal Organs”, “The Leicester Experience with an *Ex-vivo* Autologous Perfused Porcine Liver Model: Past Achievements and Potential Future Applications”. (June 2011 – INVITED SPEAKER); Washington Hilton Hotel, Washington D.C., United States of America

Table of contents

Preface

The experimental work of this thesis was performed on livers collected from dead pigs from the abattoir and not an *in-vivo* perfusion model. The candidate has received assistance from a colleague, Mrs. Seok Ling Ong, during the conduction of his experiments and has provided assistance for her experiments. Liver tissue and data collected from the controls experiments (n=7) have been shared and used in both thesis (joint control group) while the ablation experiments (radiofrequency ablation n=5, electrolytic ablation n=5) have been specifically reported in this thesis.

Introduction

Over the last two decades improvements in the preoperative assessment (1), surgical technique, anaesthesia and postoperative intensive care have all contributed to a significant reduction of morbidity and mortality following liver surgery. These factors have helped to improve the long-term survival of patients undergoing hepatic resection which has become the gold standard treatment for resectable liver tumours. However, this is not feasible for 80% of patients due to a low predicted hepatic reserve, significant co-morbidity or technical issues related to the location, number or size of the lesions. Over the last two decades a wide range of local ablative techniques has been developed for use in these patients with the aim of improving survival. Ablative treatments, in conjunction with adjuvant chemotherapy, palliate by achieving some degree of disease control and possibly prolong survival while maintaining an adequate functional hepatic reserve (2). Furthermore, the reduced invasiveness compared to standard liver resections (by means of laparoscopic and percutaneous approaches) renders them more appropriate for high-risk patients. These *in situ* techniques for the ablation of liver tumours have steadily increased in popularity and are now generally preferred to previous modalities such as chemoembolization and alcohol injection.

Local ablative techniques aim to control both primary and metastatic hepatic tumours by destroying the cancerous mass and a safe "rim" of surrounding normal liver tissue. Thermal ablation techniques achieve tissue destruction by creating extreme modifications of the local temperature (Radiofrequency ablation - RFA, Microwave Thermal ablation - MTA, ultrasound ablation, laser ablation) (3). Numerous studies

described the technical modifications of the applicators and generators (4, 5), the generic and specific complications for each technique (6-8), the pathologic mechanisms underlying tissue destruction (9-11), and the clinical results obtained. Contrasting with thermal techniques, Electrolytic Ablation (EA) does not use the direct production of thermal energy to destroy tissues. Heating is minimal and is only a minor secondary effect of the changes in the local microenvironment present during the procedure. Rather than relying on a rapid "burn", EA causes cell-death by a more subtle chemical action.

Radiofrequency ablation

History

The first experiments about the utilization of radiofrequency currents in man were conducted between the 19th and the 20th century. Initially Arsene D'Arsonval (1851-1940) hypothesized that electric currents superior to 10 KHz were able to generate heat but wouldn't give neuromuscular contractions during surgery (12, 13), a hypothesis later confirmed by Heinrich Hertz (1857-1894) (14). In 1899 Paul Marie Oudin (1851-1923) joined two D'Arsonval solenoids creating a machine ("resonator") able to generate more powerful currents and capable to destroy tissues (Figure 1) (12, 13). In the beginning of the 20th century Riviere decreased the electrodes surface to increase the electrical densities transmitted to tissues, and began using this device on small cutaneous neoplasms (15). In 1907 De Forest (1873-1961) created the triod, an electronic tube that reached 2 MHz of frequency (16). In 1926 William Bowie built an electrosurgical device

that offered both coagulating and cutting currents (17). Dr. Harvey Cushing began using such device to stop the intraoperative bleeding and cut through tissues during surgical procedures.

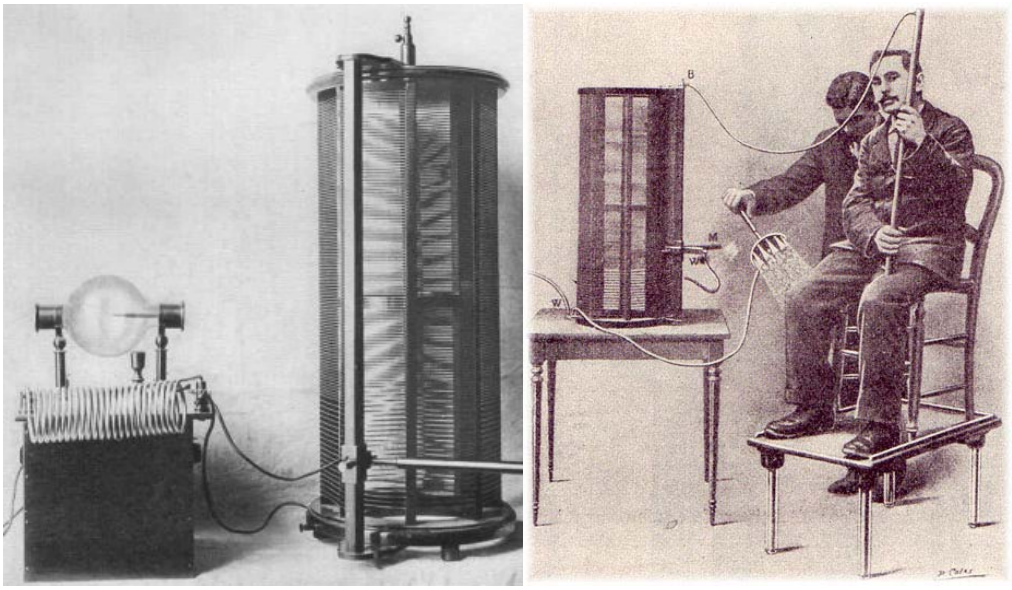

Figure 1[1]

[1] First experiments conducted with the Oudin "resonator". Left panel: resonator. Right panel: Oudin himself on the resonator.

More recently, in the 70's, the first experiments on animals began. 13.5 MHz radio waves generators were used on pigs to analyse the pattern of tissue heating on the surface and deep into tissues (18). 425 MHz to 2.45 GHz radiofrequency generators were used on rats to analyse the tissue responsiveness (19) and found that exposition to radio frequencies was compatible with life (20). Radiofrequencies were subsequently applied to various branches of medicine, mainly oncology and cardiology. Hyperthermia was used as an anticancer treatment for prostate (21), biliary tract (22), lung (23) and kidney neoplasms. During the 80's the radiofrequencies were introduced to thermally ablate stable arrhythmic foci for both supraventricular and ventricular arrhythmias (24-30).

Physics

Electromagnetic waves have a length between 3 KHz and 300 GHz and consists of the low frequencies, the intermediate frequencies and the high frequencies (31). The high frequencies include the radiofrequencies (3-300 MHz) and the microwaves (300 MHz-300 GHz) and are used for industrial and therapeutic devices (radar, MRI), domestic (cellular phones, microwaves ovens) and in every telecommunication apparatus (TV or radio station, radar, radio links**).** Most of the diathermy devices work in the range from 300 KHz to 3 MHz (intermediate frequencies) (Table 1) because values lower than 10 KHz increase the risk of neuromuscular stimulation by the patient during surgery and values higher than 3 MHz increase the risk of high frequency dispersion currents (12, 13).

Diathermy produces thermal energy by using the Joule effect developed by tissue surfaces to the passage of electric current, therefore the thermal energy is transmitted

deeply into tissues by convection lowering itself during the tract. The deeper the point to be reached, the higher the external temperatures required. Radiofrequencies work differently: they add energy to the electrons inducing a vibration of the cellular ions. This vibration, called “molecular resonance”, affects the low energy molecular bindings and generates heat. Therefore radiofrequencies develop the target temperature within the tissues producing a constant heating pattern in all the cells through the passage. Using lower external temperatures than classic diathermy (even if reaching the same target temperature inside the tissues), they have a cutting temperature of 45°C and a coagulating temperature of 65°C. Damage to tissues is still produced by protein denaturation but at lower temperatures than classic diathermy (temperatures higher than 45°C permanently damage proteins and fuse cellular membranes).

The generation of molecular resonance is strongly dependent on the frequency of the wave used (32, 33): the maximal resonance in man is approximately 35 MHz in grounded man and 70 MHz in an insulated one. For this reason radiofrequency waves are much closer to the resonant frequency of the body than 60 Hz power lines or other forms of low frequency energy and are preferred among the others. Additionally, radiofrequencies belong to the non ionizing radiations because do not alter cellular macromolecules (DNA) and therefore they are neither carcinogenic nor teratogenic (34-36).

Range	Frequency field	
3-30 KHz	VLF	Naval transmissions Video terminals (VDT) Domestic electric heat generators
30-300 KHz	LF	Naval transmissions (Loran)
300 KHz – 3 MHz	MF	AM Radio transmissions Radio amateur transmissions Industrial electric ovens Electro surgical units
3-30 MHz	HF	International transmissions Radio amateur transmissions City radio station Industrial welder Short waves diathermy **Radiofrequency ablation**
30-300 MHz	VHF	FM Radio transmissions VHF Televisions Mobile and portable transmitters Cordless phones
300-3000 MHz	UHF	UHF televisions – Cellular phones Microwaves owens and **microwaves ablation** Airports control towers
3-30 GHz	SHF	Microwave radio links Satellites Police communications
30-300 GHz	EHF	

Table 1[2]

[2] Main utilizations of radio waves (frequency range between 3 KHz and 300 GHz). Highlited are the frequencies used for clinical purposes including diathermy, radiofrequency and microwaves ablation. VLF: Very Low Frequency. MF: Medium Frequency. HF: High Frequency. VHF: Very High Frequency. UHF: Ultra High Frequency. SHF: Super High Frequency. EHF: Extra High Frequency.

Pathophysiology

During the application of radiofrequency energy a high-frequency alternating current is conducted from the electrode and is conducted through the local tissue surrounding the electrode. The rapid change in the direction of the current causes ions in the tissue to oscillate back and forth. As the ions within the tissue attempt to follow the change in direction of the alternating current, frictional heating occurs within the tissue and is transmitted by conduction (37). Ablation zones are created as the vessels with diameter inferior to 3 mm in the tissue closest to the electrodes are heated to the point of thrombosis forming a nucleus of nonperfused tissue. This nucleus will grow along the lines of RF energy until the power falls off to levels which can no longer cause thrombosis (38).

Heat distribution using a single electrode for energy delivery shows a sharp rise to 1-2 cm from the electrode (75°C) with a progressive decrease afterwards. Beyond 2-cm from the electrode the temperature is less than 60°C (39, 40). When the temperature within the tissue rises beyond 60°C, or above 45°C for more than 3 minutes, a region of coagulative necrosis surrounding the electrode develops (41, 42). This zone is surrounded by a further region or shell of ischemia in which hyperthermic but sublethal conditions are present (43). Exceptions to this pattern manifest when the ablation zone is in close proximity to a vessel larger than 3 mm in diameter. In these cases vessels remain patent and act as “heat-shields”, removing the frictional and conducted heat and protecting the tissue behind them (“heat-sink” effect) (38). Furthermore, the increase in tissue charring at the metal electrode–tissue interface results in elevated circuit impedance and markedly

reduced RF output because of tissue dryness, limiting the heat diffusion (44). Although it is technically possible to produce tissue temperatures that exceed 90°C around the electrodes by increasing the wattage and current amplitude, this actually decreases the efficiency of RFA because of rapid tissue dryness near the needles and a resultant decrease in current flow (45).

The "two-hit" hypothesis of tissue damage applies to RFA as well as to other types of thermal injuries (46). The main mechanism of destruction produced by high temperatures (first hit) derives from the direct and immediate denaturation of cellular proteins, the dissolution of the membrane phospholipid bilayer and localized dryness as extracellular and intracellular water is driven out of the tissue (46, 47) These changes lead to the classic appearance of cells with shrunken cytoplasm (48). With time the damaged area is further enlarged by microvessel spasm, thrombosis and immune activation (second hit). This in turn produces tissue ischemia and consequently apoptosis (38, 46, 49).

Liver ablation

Developments in RFA progressed rapidly over the years and allowed for the production of generators and probes that achieved reliable and safe tissue destructions. To date RFA remains the most widely used ablative technique worldwide and numerous RFA devices have been developed (50) each producing different shapes (4) and volumes of the ablated lesion. Initially the wide range of generators and probes used (and the even wider range of combinations) produced results and data that were very difficult to compare and in an attempt to overcome these difficulties researchers adopted a common

terminology (51) which has subsequently allowed results to be pooled (and resulted in a number of reviews and meta-analyses). These pooled results have demonstrated a mortality of 0.5% following RFA ablation (20/3670 patients), a complication rate of 8.9% (327/3670) and a local recurrence rate of 2-60% (2, 8, 52, 53). There is an overall survival (OS) at 5 years of 14-55% which is very encouraging especially when the initial poor prognosis of many of the patients is considered (54). Evidence from the literature also shows that local recurrences are highly dependent on the diameter of the initial lesion (53), a characteristic shared by all *in situ* ablative techniques (55-58). One centimetre is usually considered the minimum safe macroscopic margin for tumour ablation and a 5cm ablation is required for the safe destruction of a tumour (including the transitional zone) with a diameter of approximately 3cm (53, 59).

Electrolytic ablation

History

In the 1550s William Gilbert discovered the electricity (also called "amber effect"). In 1663 Otto von Guericke created the first electrostatic generator that produced static electricity by applying friction. By the mid-18th century Charles François de Cisternay Du Fay discovered two forms of static electricity called “fluids” ("two-fluid theory"), and that like fluids (charges) repel each other while unlike charges attract. He called “vitreous” the positive electricity and “resinous” the negative electricity. By the 1750s electricity produced by new generators was used to treat paralysis, muscle spasms, and to control heart rates.

In 1800, English chemists William Nicholson and Johann Wilhelm Ritter succeeded in separating water into hydrogen and oxygen by electrolysis through an electrolytic cell. Later on, iridium, osmium, palladium, rhodium, sodium and potassium were discovered with the same method as well as the alkaline earth metals.

Physics

Direct current (DC) is the passage of electrons between the anode (positive electrode) and the cathode (negative electrode) through a conductive medium. The current elicits different tissue responses depending on the voltage used. High-voltage DC heats tissues through the resistance offered to the passage of electrons (Joule effect). This

process, called electrocoagulation, burns tissues. Low-voltage DC produces new electrical and chemical compounds that create a toxic local microenvironment and electrolysis is the term used for the process.

Electrolysis is a method of using a direct electric current through an ionic substance resulting in chemical reactions at the electrodes. The main components are: an electrolyte (substance containing free ions which are the carriers of electric current), a direct current supply (to provide the necessary energy) and two electrodes (electrical conductor which provides the physical interface between the electrical circuit and the electrolyte). The key process of electrolysis is the interchange of atoms and ions by the removal or addition of electrons from the external circuit. An electrical potential is applied across a pair of electrodes immersed in the electrolyte. Each electrode attracts ions that are of the opposite charge. Positively charged ions (cations) move towards the electron-providing (negative) cathode, whereas negatively charged ions (anions) move towards the positive anode. At the electrodes, electrons are absorbed or released by the atoms and ions. Those atoms that gain or lose electrons to become charged ions pass into the electrolyte. Those ions that gain or lose electrons to become uncharged atoms separate from the electrolyte. Although the first report of DC current being employed in the liver described the use of gold electrodes, almost all the other studies have used platinum which does not corrode during the electrolytic process (producing insulation of the electrode) and is thus preferred to gold, steel, copper and silver (60-62). A few studies have also used aluminium electrodes (63-66).

Pathophysiology

The small DC current activates the electron transfer, polarizing the electrodes (67, 68), and resulting in the formation of hydrogen ions according to the following equations: Anode: $2H_2O \leftrightarrow O_2 + 4H^+ + 4e^-$, Cathode: $2H_2O + 2e^- \leftrightarrow H_2 + 2OH-$ (68, 69). In order to complete the circuit, negatively charged ions become attracted to the anode and positively charged ions to the cathode (70). A significant pH gradient forms and the anode is relatively acidic compared to the basic cathode (60, 71-75). This produces a change of the intracellular pH in surrounding tissues (70), which extend also to the healthy liver tissue up to a distance of 5 mm from the border of the electrodes (69, 76). During EA blood flow produces a homoeostatic buffering effect at the periphery of the lesion prior to definitive necrosis ("electric-sink" effect) as evidenced by the pH fluctuations present at the edge of the lesion before cell death (68).

A second consequence of the DC application is that in solution sodium chloride is ionized into Na^+ and Cl^- ions, which move toward the cathode and the anode, respectively (75). The concentrations of Na^+ and K^+ ions are higher around the cathode, where the alkalinity is also greater, while the concentration of Cl^- ions is higher around the anode (75). These ions react with the tissue water producing new chemical substances: sodium hydroxide and hydrogen at the cathode, hydrochloric acid, oxygen and chlorine at the anode according to the following reactions $2Cl^- \leftrightarrow Cl_2 + 2e^-$ and $Cl_2 + H_2O \leftrightarrow HClO + H^+ + Cl^-$ (61, 62, 69, 73-75, 77-80). Chlorine gas is a powerful oxidant that immediately attacks the surrounding tissues, while sodium hydroxide is also cytotoxic but to a less extent (62). Water is electrolysed releasing both ionic and molecular oxygen (73). Finally, haemoglobin accumulates at the anode and is transformed into hemin when the

pH value is below 2 and albumin and globulin also precipitate significantly at both electrodes (75).

Cell necrosis is probably produced by both these electric and chemical changes (70, 71) and is complete (no viable cells present) when a pH of less than 6 or greater than 9 is reached (68, 69). The acidic environment around the anode (pH 2) is known to be more toxic than the alkalinity (pH 12) at the cathode (67, 81). Compared to the cathode, different substances are responsible for the ablated zone around the anode. Chlorine acts in the inner area, hydrogen ions in the intermediate and protons in the peripheral area due to their ability to diffuse for a greater distance than the other chemical products (67, 80). However, the complexity of changes occurring in the microenvironment suggests that other factors may well be involved. Apoptosis, modifications of ion channels (67) and changes in tumor perfusion and oxygenation (82, 83) have all been suggested. Immune system modifications involve the activation of macrophages and the accumulation of leukocytes in the cathodic field by extravasation (67). Additionally, the increase in tissue turgor around the cathode also produces an impedance of the blood flow that is further enhanced by the segmental contraction of arteriolar podocytes. Finally, oxyreductases in capillary endothelial cells are activated by the superimposed electrical field and the free radicals produced in the lumen cause lysis of red blood cells producing multiple microthromboses. Since the severity of tissue destruction is in proportion to the electric charge delivered to the tissue, lowering the resistance of the target region maximizes the charge delivered under limited electric pressure and treatment time. Saturated interstitial saline injection (26% concentration) lowers tissue resistance by increasing the local concentration of sodium and chloride, and its presence creates larger ablation zones

compared to controls ("liquid electrode") (84). This effect was not found with acetic acid or normal saline (0.9% concentration) (85).

Although increases of the local tissue temperature have been reported during EA, all authors report that the thermal effect is negligible (69, 73, 79, 86, 87). In fact DC current generators are generally designed to deliver a preset current to avoid heating by making automatic voltage adjustments in response to alterations in hepatic parenchymal resistance during EA (88).

Liver ablation

Low-level direct EA has proved to be an effective, though presently little used method in the local therapy of liver tumours. It is a technique that destroys tissues by the use of electrolysis and therefore generates lower temperatures compared to RFA. Due to these characteristics it has potential advantages over more frequently used ablative procedures that employ extremes of temperatures to cause tumor necrosis. Consequently EA is not limited by the "heat-sink" effect of nearby major vascular structures (73) which reduces the effectiveness of thermal ablative techniques owing to the effect of heat dissipation secondary to local blood flow. As a result, if a tumor is adjacent to a major vessel, a cuff of viable malignant cells may be left untreated around it following RFA (70). EA is also safe in respect of thrombosis or breach of large blood vessels in close proximity to the site of electrolysis (89). This has been confirmed experimentally (70, 89) and clinically even for lesions close to the inferior vena cava or the portal vein (for pancreatic ablation) (90). With thermal ablation techniques a direct "burn" to the vessel

may result, leading to a significant rate of hemorrhages following treatment (70). This contrasts with EA that develops only minor changes in the local temperature and therefore could be used for the treatment of tumors located close to major vessels.

Currently the clinical use of EA is limited by its protracted delivery at safe current levels, that preclude the treatment of large or multiple tumors as they would necessitate long treatment times (typical treatment tymes are between 3 and 4 hours). Shortening treatment times could have been reached through the use of higher voltages but this could increase the tissue temperatures negating one of the typical characteristics of EA. Treatment times could be decreased also through the use of larger electrodes but this would preclude the percutaneous use of the technique. The combination of EA with RFA (combination called BETA modality – "Bimodal Electric Tissue Ablation") recently attempted to overcome this issue combining characteristics of both techniques (63). The BETA modality consisted in an initial application of EA to hydrate the tissue (using the electrode as a cathode and inserting the other – anode – subcutaneously) and a subsequent combined delivery of RFA + EA. The tissue hydration was necessary to avoid the dryness and consequent rise in tissue impedance that limits RFA and prevents further energy delivery ("roll-off" phenomenon). The results obtained with a straight electrode showed significant larger diameters (RFA = 1.1 ± 0.1 cm; BETA = 3.0 ± 0.2 cm) (65, 66), decreased delivery times, swollen necrotic zones, and non adherence of the electrode to the ablated tissue compared to RFA alone (63). Furthermore the central area of coagulative necrosis was larger (63).

The increased duration of EA treatments has not precluded its evaluation in human studies, in which its safety and feasibility were confirmed and promising short-

term results were obtained (91). However, all clinical data that exists so far are still more a collection of single case studies and the effectiveness of EA has never been evaluated in the long-term or compared to other well-established treatment options like RFA, MTA or palliative chemotherapy alone. A specific field of investigation in which EA could prove particularly useful would be the evaluation of those lesions "awkwardly" positioned (i.e. close to major vessels) that are normally not suitable for the thermal ablation techniques. In this setting the long-term comparison of EA plus chemotherapy with chemotherapy alone would definitely demonstrate any increase in the overall survival and possibly support the use of EA for this particular clinical indication.

Irreversible electroporation

A newer technique that utilizes direct current to create cell necrosis and ablate liver lesions is the irreversible electroporation (IRE) (92). Using this technology, a cell is subjected to a powerful electrical field created by high-voltage electrical current to induce irreversible pores in the lipid bilayer of cells and damage the cell's homeostasis mechanism, resulting in cell death (93, 94). Numerour experiments have been conducted in porcine livers (95-98). The technique seems safe close when performed close to major vessels and does not seem influenced by the "heat-sink" effect because of the lack of thermal energy (94, 97). Although the clinical experience available on liver tumors is based on short-term follow-ups, these two settings represent specific indications for IRE (small tumors abutting a major vascular structure or tumors abutting a major portal pedicle where "heat-sink" effects could be significant) (94). For these reasons IRE is the

current technique for tumours close to major blood vessels while RFA (with or without chemoembilization) would treat the remaining ones.

Immunoregulatory effects of liver ablation therapies

Compared to liver resection where the portion of liver parenchyma affected by the disease is removed, ablative techniques leave the treated zones *in situ*. Tumour debris produced by the disruption of cancerous cells are presented to the immune system and elicit specific responses by the organism that may prove valuable in the post-treatment surveillance for potential recurrences. Changes evoked in the immune system, including those on the local and systemic inflammatory response as well as modifications of immune cells and serum proteins, have been extensively investigated for almost all the ablative techniques available. Results obtained confirmed that the *in situ* presence of debris from the tumour elicits a complex and well-orchestrated response at all levels of the immune system and, even more interestingly, showed that important differences are present among ablative techniques for the immune stimulation produced.

Changes in immune cells

Potentially, *in situ* tumor destruction may present the immune system with large amounts of antigen for the induction of antitumor immunity. Following the thermal ablation of a hepatic lesion, coagulative necrosis occurs where the local temperatures are higher than 60-65°C. While apoptotic cell death is a physiologic phenomenon not recognized as harmful by the immune system, necrotic cell death is often seen as a result of dangerous events (Matzinger's "danger" model of immunity) (99, 100). This is

because necrosis is usually accompanied by the release of peculiar proteins called "danger signals". Such signals are presented to the immune systems via the antigen presenting cells and trigger adequate T cell responses. An increased synthesis and cell surface expression of Heat Shock Proteins (HSP) are effective "danger signals". These substances are normally involved in the mechanisms of cell repair playing an important anti-apoptotic effect. When released HSP bind to dendritic cells (DCs), specialized and pivotal APC, are internalized by endocytosis and activate them. DCs activated by HSPs can cross-present antigenic peptides, generating a cytotoxic T lymphocyte response against cells producing these peptides. HSP have been experimentally demonstrated after RFA of HCC (101, 102). Moreover, large amounts of tumor debris derived from tumor cells necrosis may undergo phagocytosis by immature DCs surrounding the area and only subsequently are activated by HSP and other inflammatory mediators released at the same site (103), thus favoring maturation and migration to the afferent lymph nodes. Finally, in conjunction with the generation of thermally-altered tumor antigens, the non specific inflammatory stimulus induced by necrotic cells following RFA might help to overcome immune-tolerance or anergy towards the transplanted tumor, configuring it as an "in-vivo tumor vaccination" (104). All these hypotheses are supported by sporadic cases of spontaneous regression of metastases and reduced number of secondary deposits following RFA treatments (104).

Preclinical studies in pigs and rabbits revealed an influx of immune cells in the periphery of the coagulated area after RFA, together with an increased T-cell proliferation (105, 106). In tumour free domestic pigs RFA was usually followed by a

marked local inflammatory response with a dense T-cell infiltrate in the liver (105), and in the livers of rabbits implanted with epithelial tumours there were similar findings (106). The local inflammation consisted of a lymphocytic and plasma cell infiltrates and was located around the necrotic centre in the hemorrhagic rim, which is believed to be a crucial area for the recruitment and activation of tumor-specific T lymphocytes (105). Den Brok et al. demonstrated that a weak but detectable immune response is present after RFA. The immune response elicited results in a delay in the outgrowth of tumor cells and the protection of 20% of mice when re-injected with cancer cells (107). The stimulation of T cells is usually driven by DCs (108). After RFA up to 7% of DCs present in regional lymph nodes contained tumour antigens (109). Expression of co-stimulatory molecules, lymph node homing chemokine receptor, antigen presentation, and cytokine secretion were enhanced by incubation with HCC treated tissue as compared with untreated HCC and normal liver tissue. Moreover, HCC-specific T-cell responses could be induced by monocytes activated with GM-CSF and incubated with thermally ablated HCC tissue (110).

The demonstration of a specific T-cell response was also suggested by clinical studies on circulating cells. Changes in circulating DCs were extensively analysed by Ali et al. (108). Myeloid DCs displayed the characteristics of immature cells prior to RFA. Following RFA a transient decrease in myeloid DCs was observed 7 days from treatment. Subsequently, DCs acquired a more mature phenotype with an increased ability to stimulate CD4+ T cells. The decreased number of circulating cells observed at 7 days

from treatment was probably due to their sequestration in lymphoid organs for the maturation and the antigen-presenting process (108).

Zerbini et al. have also suggested that RFA could trigger a specific anti-tumor T cell response in HCC patients (111). Using an IFNγ –ELISPOT assay they found that before RFA, and upon stimulation with HCC cell lysate, 3 out of 20 patients showed a specific T cell response, while none was observed in HCC patients stimulated with an autologous non-malignant liver lysate. Importantly, 4 weeks after RFA, the fraction of HCC patients showing a specific T cell response against HCC protein lysate rose up to 9 HCC patients, which was significantly higher than that detected before RFA. However, a T cell response against non HCC liver protein lysate was also observed after RFA in 2 HCC patients. Given to the protein composition of the HCC lysate, CD4+ T cells were preferentially stimulated while the involvement of CD8+ T cells was minor. In HCC patients the proportion of T cells among the overall lymphocyte pool, as well as the proportion of CD4+ and CD8+ subsets among T cells, were not significantly altered. Similar results were also obtained for naive and memory CD4+ T cells and for naive and memory CD8+ T cells (111).

Similar results were demonstrated by Hansler et al. in metastatic and hepatocellular carcinoma (HCC) patients (Table 2) (104). Authors found that HCC and colorectal cancer cells produced a 5-6 fold rise in the number of tumor-specific circulating CD4+ and CD8+ T cells and a 300 fold rise in their cytotoxic activity following RFA (104). Clinically, patients with local recurrences displayed a lower cytotoxic activity against cancer cells compared to patients without recurrences, suggesting that patients presenting with a tumor recurrence were those that produced a

poor immune response to the cancer cells (104). Finally, the proliferative response of circulating B cells was also strongly stimulated by RFA in metastatic cancer patients (112).

Taken together, all these observations support the hypothesis that heat shock delivery and massive necrotic cell death produced by RFA favours the presentation of otherwise cryptic antigens and the subsequent immune activation, thus inducing a tumor specific T-cell response by means of stimulation with DCs. Unfortunately, these effects seemed to confer no protective effect on tumor recurrences as were not sufficient to prevent HCC relapses (111). To date, there are several questions that still remain unanswered: 1) what is the nature of the HCC antigens contained in the protein tumor lysate? 2) Are these proteins unique tumor associated antigens? 3) are these antigens constitutively expressed in HCC cells or their expression could be induced by RFA? 4) What is the role of HCV and or HBV antigens in RFA dependent T cell stimulation?

Changes in cytokines and in acute phase proteins

All invasive surgical procedures induce the release of a variety of cytokines that lead to a general inflammatory stress. This stress response may be implicated in positive processes, like the healing of injured tissues, but could also result in the stimulation of tumor cell growth (113). Following RFA, Interferon γ (IFN-γ) (112), C-reactive protein (CRP) (113) and Vascular-Endothelial Growth Factor (VEGF) levels (113) markedly increase compared to controls. Contrasting results were obtained for Tumor-Necrosis

Factor α (TNF-α), which remained unchanged in two studies (113, 114) and increased in one (108), Basic Fibroblast Growth Factor (bFGF), decreased (115) or did not change (113), Interleukin 1 (IL-1), increased (108) or remained the same (114), Interleukin 6 (IL-6), increased (113) or was unchanged (115), and Hepatocyte Growth Factor (HGF) increased (113) and decreased (115). Tumor Growth Factor β (TGF-β), Interleukin 8 (IL-8) and Interleukin 10 (IL-10) did not show significant variations following RFA (113, 114) (Table 3). Finally, heat shock proteins were released *in vivo* after RFA in HCC patients, and enhanced cell-mediated immune responses by activating the natural immunity and by augmenting HCC-specific cytotoxic T-cell responses (101, 102, 116).

Author	Year	Technique	Subjects	No. of subjects	Neutrophils	Monocytes	Dendritic Cells	T cells			NK	B cells
							$CD1^+ CD11^+$	$CD3^+$	$CD4^+$	$CD8^+$	$CD3^- CD16^+ CD\ 56^+$	$C3^- CD19^+$
Rughetti et al. (117)	2003	RFA	Mets. patients	8	↑	↑						
			HCC patients	4	=	↑						
Ali et al. (108)	2005	RFA	HCC patients	8			= ↓					
Zerbini et al. (111)	2006	RFA	HCC patients	11				=	=	=	↑	
Hansler et al. (104)	2006	RFA	Mets. patients	6				↑	↑	↑		
			HCC patients	6				↑	↑	↑		
Napoletano et al. (112)	2008	RFA	Mets. patients	13				↓	↓	=	=	↑
			HCC patients	4				=	=	=	=	=

Table 2[3]

[3] Results of studies presenting changes of circulating immune cells after the different ablative techniques. Mets.: Liver metastases.

Author	Year	Technique	Subjects	No. of subjects	IFN-γ	TNF-α	bFGF	IL-1β	IL-6	IL-8	IL-10	HGF	VEGF	TGF-β	IGF-1	MIP-2	CRP	SAA
Chapman et al. (118)	2000	RFA	Murin model	19		=										=		
Schell et al. (114)	2002	RFA	Mets and HCC patients	17		=		=	=	=	=							
Ng et al. (119)	2004	RFA	Porcine model	23		↑		↑										
Ali et al. (108)	2005	RFA	HCC patients	8		↑		↑										
Ng et al. (120)	2006	RFA	Murine model	160		↑			↑									
Evrard et al. (113)	2007	RFA	Mets patients	10		=	=		↑			↑	↑	=			↑	
Meredith et al. (115)	2007	RFA	Mets murine model	70			↓					↓						
Napoletano et al. (112)	2008	RFA	Mets and HCC patients	17	↑													
Teague et al. (121)	2004	Electrolytic	Porcine model	16		=		=									↑	

Table 3[4]

[4] Results of studies presenting changes of circulating immune cells after the different ablative techniques. RFA= Radiofrequency ablation. Mets.: Liver metastases.

Histological changes after radiofrequency ablation

RFA is one of a range of thermal ablative therapies that are minimally invasive and provide an effective, predictable and controllable method of producing localised tissue destruction. Image-guided, percutaneous RFA has been used in most parts of the body, but the most widely accepted applications are for the treatment of liver tumours including hepatocellular carcinoma (HCC) in early cirrhosis, local control of inoperable colorectal liver metastases, inoperable renal cell carcinoma and inoperable metastatic lung tumours (122). There is a considerable body of evidence to support its use in the treatment of unresectable small HCC, recurrent small HCC (as a bridging therapy before liver transplantation), and as a primary treatment in competition with partial hepatectomy for resectable small HCC (123). Furthermore, RFA seems more effective than other types of local therapy and particularly the previously widely used percutaneous alcohol injection (124).

The formation of the thermal ablation zone that follows RFA (or with any thermal ablative technique) is a complex combination of energy absorption, heating and conduction and possible tissue water evaporation, condensation and movement. While many studies have not only examined the macroscopic and histological findings immediately following RF ablation but also the evolution of the resulting lesions over time, none of them specifically examined the reasons for the zonal nature of the changes. A detailed analysis of the histological and cellular changes following RFA could help in understanding the results obtained in a clinical setting and provide the basis for future

research to overcome the limitations of the delivery systems and the production of zones (shells) which contain significant numbers of viable cells.

Macroscopic changes

Numerous factors influence the final volume of the ablated zones. The correlation between duration of the RFA and diameter of the ablated area is logarithmic, with the greatest increase observed during the first 30 minutes of application (39, 40). Modifications in the design of RF electrodes (internally cooled straight electrodes, parallel clustered internally cooled straight electrodes or multi-needles expandable electrodes) and energy delivery systems influence the shapes and the volumes produced (44). Different shapes have been described including spherical, ellipsoid, conical, inverted conical, cross-shaped, teardrop-shaped, tongue-shaped, mushroom-shaped, butterfly-like or even three separate ovals (4, 48, 125, 126). Patent intrahepatic vessels close to the periphery of the ablated area also have more influence on the volumes and shapes than with others ablative techniques (Table 4) (10, 127). When RFA is conducted in close proximity to large vessels the area obtained usually becomes asymmetric and with a defect adjacent to the vessel itself, thereby limiting the ablation extent and increasing the possibility of residual tumour (38, 39, 118, 128-131). As a consequence, peripheral or surface ablation zones are more likely to be complete spheres than those deep within the liver due to the relative lack of large vessels near the surface (38). To minimize this distortion, higher temperatures, multi-electrode arrays, double ablations or

Pringle's manoeuvre (temporary occlusion of the liver vascular inflow) have all been evaluated (Table 4). Results confirm that ablations conducted with these methods extend up to but do not include the vessel wall (38, 49, 125, 132, 133). On the contrary, non-perfused tissue ablated when a Pringle's manoeuvre has been applied is more likely to induce thrombosis and endothelial thermal damage of vessels larger than 6 mm because they are no longer protected by the blood flow within them. Consequently, the risk of infarction or segmental bile duct injury is increased (38, 125, 134, 135). Post-procedure venography demonstrates a 7% rate of complete thromboses and a 14% rate of partial thromboses (129).

After ablation, and in the first post-ablation week, gross examination of the ablated area presents a core of ablated tan to charcoal grey tissue ("white zone") with a surrounding narrow dark rim ("red zone"), the whole being encompassed by normal parenchyma (38, 41, 126, 131, 136-138). The white zone has a colour gross appearance similar to the normal tumour tissue, rendering more difficult the gross evaluation of the ablation obtained (139). Central areas of darker tissue are observed within the white zone probably due to the intense charring of the severely desiccated tissue (41). Kuromatsu was the only author that described a more complex situation than merely the two zones of ablation and included from the center to the periphery, four different concentric areas: a brown area, light red area, dark red area and a red area with rough demarcation margins (140). No macroscopic differences of the ablated zones have been cited to the differing animal models and disease states (e.g. metastatic tumours vs. hepatocellular carcinomas).

One week following RFA, the gross and histological appearance evolves with the central area becoming brown, the peripheral area light brown and the development of

clearly demarcated margins (140). At this stage the entire ablation is usually smaller than immediately following the RFA treatment (141).

Overall microscopic changes

The standard histologic examination of the ablated area in the first week post-ablation demonstrates three concentric zones or shells. A zone of coagulative necrosis (CNZ) with microcavitation phenomena (also called "necrotic zone" or "zone 1") corresponded to the white zone observed on the gross examination. A surrounding zone known as the hemorrhagic rim (HRZ; also called "transitional zone", "ischemic zone" or "zone 2") corresponded to the red zone. Finally, the normal parenchyma (NP; also called "non-ablated zone" or "zone 3") encompassed the previous ones. All these zone or shells represent reducing levels of thermal injury down the outward temperature gradient (Table 5) (38, 41, 126, 131, 138, 139, 142-144). The zonal changes also correspond to a decrease in the intensity of tissue fluorescent emission as evaluated with real-time light-based tissue spectroscopy (143, 145, 146), a technique able to distinguish between tissue types and evaluate changes between thermally-damaged and normal tissues (147-149). *In vivo* optical properties reflect tissue structure (cell shape and number), tissue composition (concentration-dependent chemical absorbance), and tissue function (hemoglobin, myoglobin, and cytochrome oxygenation states). The spectroscopic examination accurately defines the advancing edge of ablation for the HRZ and the CNZ during the procedure (145).

The three classic histological zones depicted have been obtained with a "static" analysis of tissue sections fixed in formalin after RFA. A more accurate and "dynamic" *in vivo* assessment used a video microscopy technique on exteriorized rat livers provides a detailed insight into the functional changes that occur in the microvascular flow during RFA (i.e. blood redistribution, hyperaemia, and stasis). Using this technique five different anatomo-functional zones can be identified: coagulative necrosis, cellular edema, sinusoidal stasis, parenchyma shunting and normal liver. The histological characteristics of each zone were dependent on the tissue temperature (Table 6) (150). Furthermore, as the electrode temperatures increased the zone adjacent to the electrode progressively extends out in a radial manner with similar outward displacement of the surrounding zones, with all of them retaining their original histological characteristics (150).

One week following the RFA treatment the HRZ was thicker and the CNZ smaller than during the acute phase. The overall result was of a general decrease in dimensions of the ablated area (141).

Coagulative Necrosis Zone

Histological analysis shows that complete coagulative necrosis is present in only 40% of the specimens and that although this generally corresponds to disrupted cell outlines, there is also preserved nuclear staining, prominent nucleoli and increased cytoplasmic eosinophilia (139). Granular and amorphous debris with artefactual aggregation are also present (126, 136, 151, 152). Subcellular organelles are generally completely destroyed, chromatin clumping is present at the nuclear margins and nuclear

membranes are extensively disrupted (143). The outlines of cell walls is barely perceptible and the periphery of hepatocytes is ragged (152). Apoptosis or expression of Heat-Shock Protein 70 (HSP-70) has never been found in the CNZ, confirming the necrosis as the main mechanism of cell death for this zone (142).

Incomplete ablations are partly explained by the close proximity to a vessel greater than 3 mm of diameter that allowed the tissue to be protected by the "heat-sink" effect of the blood flow within the vessel (139, 153). In fact large blood vessels, and bile ducts to a lesser degree, appear to be relatively protected from thermal injury justifying the clinical observations that the liver parenchyma distal to an ablated area is generally not significantly damaged by RFA treatment. For portal and hepatic veins, the patency rate of vessels smaller than 3 mm in diameter decreased with subsequent reduction in the caliber, whereas vessels larger than 3 mm were routinely patent (153, 154). All vessels (large and small) contiguous to the ablated parenchyma showed blood clot formation and endothelial injuries such as loss of endothelium, deformation of nuclei and acidophilic changes of the cytoplasm (154). The extent of vessel wall injury decreased with increasing diameter for vessels greater than 3 mm (153). When vessels smaller than 3 mm were present within the RFA area, abrupt termination was present at the margin of, or shortly after entering, the ablated zone (153). These small vessels showed transmural degeneration on the side exposed to the RFA heat and degeneration of smooth muscle cells where RFA heat failed to reach. Intramural fibrin thrombi were also noticed (126). Small bile ducts also demonstrated coagulative necrosis as these were not protected by the heat-sink effects of adjacent vessels. Large bile ducts were intact due to the preservation of blood flow in large vessels that remained patent (38). In specimens in

which some morphologically intact cells (25%) or definitive normal tissue (35%) were present (155), hepatocytes still exhibit significant changes including a homogenous eosinophilic staining of their cytoplasm and a dense homogenous basophilic staining of their nuclei (38, 152). Rarely they are elongated, with spindleform nuclei and a streaming cytoplasm (49). Haemolysis is present in both the sinusoids and the vessels. Erythrocytes are ruptured and in some veins compressed against the vessel wall by a bubbles of gas (152).

Coagulative necrosis is a phenomenon that evolves progressively over a relatively short (hours to days) time. Within the first 24 hours the hepatocytes show a shrunken cytoplasm and some of them appear as acidophilic bodies. By the third day cellular lysis is present, on the sixth day the acidophilic degeneration of cells is complete and the nuclei have disappeared altogether. By day nine the eosinophilic homogenization of the necrotic area is total and after one month the entire area is in advanced state of fibrosis (48). In some reports the CNZ adjacent to the electrode was not present until 3 days after the RFA treatment (48, 49, 140, 156), while other experimental studies found coagulative necrosis even within (38, 48) and immediately after the first 24 hours (141).

The severity of the endothelial injury correlated with the re-endothelization process and the overall long-term patency of the vessel involved. Between one and three weeks following RFA intimal thickening below the endothelium is found in vessels greater than 1 mm but not in vessels with diameters less than 1 mm (154). This change corresponded to the re-endothelization process and the subsequent patency of the vessel involved. After 3 weeks vessels that lacked the initial intimal thickening had an absent re-endothelization and remained not patent (154).

Transitional Zone

Dilatation and congestion of the sinusoids with extravasation of blood cells are the features of this zone (41, 126, 141, 152, 156) while small and large vessels are usually unaffected (139). Sinusoidal endothelial cells are separated from the hepatic cords (140). Hepatocytes are vacuolated (128), they lack recognizable subcellular organelles, their nuclear membrane is disrupted to varying degrees and chromatin clumping is present (143). The outer area of the HRZ shows only congestion of the sinusoids. Between the boundary of HRZ and NP a mild sinusoidal dilatation is present with endothelial cells normally adhering to the hepatic cords (140). Apoptosis is present in the HRZ but the amount very much depends on the time elapsed between the RFA and the tissue removal. Specimens removed within one hour contain few apoptotic cells compared with those collected and examined later (131, 142). A similar pattern of expression is found for HSP-70 and although specimens collected half an hour following RFA do not show any significant differences compared with the normal parenchyma for HSP-70 expression, after a few days HSP-70 is definitively present (142).

The HRZ, as the CNZ, demonstrates evolution over time. The HRZ is more evident in specimens removed 3 to 7 days following RFA treatment (49). After one week granulomatous and inflammatory changes with an initial fibrosis appear on the external margins of the HRZ, with the fibrotic tissue being clearly separated from the normal parenchyma (140). After one month a definitive fibrotic capsule surrounds the ablated

area while sinusoidal congestion and extravasation of blood cells have completely disappeared (137, 156).

Viability assessment

Haematoxylin and eosin staining as a method to assess viability relies only on the morphological examination of the cell membranes and intracellular structures. This technique gave inconsistent results when performed on cells within 24 hours of the RFA (42). Definitive evidence of irreversible cellular damage requires histochemical assays (lactate dehydrogenase activity, maleate-dehydrogenase and nicotinamide adenine dinucleotide – NADPH - diaphorase activity, intracellular ATP measurements) and immunohistochemical stainings (Ki-67 antibody – a nuclear marker of cell proliferation). Lactate-dehydrogenase activity is a marker for cytosolic glycolytic enzyme functionality that, when absent, suggests a disorder within the cell. Maleate-dehydrogenase and NADPH-diaphorase activity indicate the intracellular mitochondrial viability of cells based on the presence of cell respiration, the concept being that a cell that is not respiring is not viable.

Cells that appeared morphologically normal from both the CNZ and the HRZ have been tested for viability and the CNZ was composed of dead tissue immediately after the ablation in the majority of cases (38, 41, 49, 137, 144, 156). When vessels were present, cells around the vessel remained viable on the opposite side from the ablation source (126) increasing the risk of residual tumor in those areas (157). Viability staining of veins revealed massive loss of endothelial cells when the portal vein was occluded and

endothelial cell viability was inversely related to the degree of closure (158). In the HRZ, the cytosolic enzyme activity is normal but the mitochondrial enzyme activity is reduced or even absent, suggesting that a progressive loss of cell viability is occurring (156). Although the same intracellular concentrations were found in the HRZ and the NP (144), the HRZ lacks mitochondrial cell respiration and is in a state of "necrobiosis" leading to apoptosis (41, 49). After one month all cells of the HRZ are completely dead (156).

Comparison with radiological findings

On ultrasound (US) monitoring during RFA, ablated zones appear as hyper-echoic areas that surround the electrode tip and progressively increase in diameter (40, 127, 136, 159, 160). The hyper-echoic areas usually produce an acoustic shadow that prevents recognition of the posterior margin of the ablation (40, 136). Small (1 to 2 mm), round, hyper-echoic foci are present within the zones ablated during RFA corresponding to micro-bubbles of gas (nitrogen) produced by the heating of tissue (38, 40). On live microscopy these bubbles are first visible 2 minutes after exposure to temperatures of 95°C, and within 20 seconds they coalesce into larger aggregates within patent sinusoidal lumens (150). Their presence renders irregular the borders of the hyper-echoic area and corresponds to the hyper-echoic linear streaks radiating into the surrounding liver parenchyma (40, 136). Bubbles can be seen to track away from the probe (through necrotic tissue) into patent adjacent sinusoids (Table 6) (150), portal and hepatic venules, adjacent hepatic veins and peripheral subcapsular locations but never into the inferior vena cava (40, 139, 150).

A few minutes following the ablation a relatively hypoechoic area surrounds the electrode tip and a central echogenic nidus appears (40, 136). As the area cools, the ablation develops a pattern of white charring and air along the applicator path, a darker homogeneous area of necrotic tissue, and a surrounding rim of heterogeneity thought to represent marginal edema (38, 136). At the conclusion of the RFA the ablated zones have a variable size (0.5–5.0 cm) that usually decreases over the next 15–30 minutes (49, 159).

Computed tomography (CT) and Magnetic Resonance Imaging (MRI) scans demonstrate sharply demarcated hypo-dense, non-enhancing regions around the electrode tract as early as 15 minutes after ablation (49, 132, 136, 156). Contrast-enhanced CT obtained immediately after RF ablation shows regions of hypo-attenuation or hepatic parenchymal enhancement surrounded by a variable hyperemic rim on arterial phase images, portal venous phase images, or both (49, 136, 156). The hypo-attenuation always corresponds to the CNZ (136) while the hyper-attenuation is ascribed to the HRZ (156) or the NP (136). A 1-cm hyperdense central area is observed along the electrode tract in the centre of the treated area corresponding to regions of greater cellular disruption (49). On unenhanced images, the lesions appear hypodense with variable internal homogeneity and hyperdense regions, the latter likely to indicative hemorrhagic products (136). Differentiation of treated regions from untreated hypo-attenuating tumours is obtained with delayed (> 5 minutes) post-contrast images. Treated tissues have a persistent attenuation and images obtained 1 to 3 days following RFA are sharper than those obtained within four hours of ablation (49). One month after RFA, CT images show demarcated regions of hypo-attenuation but loss of the surrounding ring enhancement. Ablated zones at 1 and 6 months after follow-up are smaller than those measured

immediately after RFA (156). For the detection of residual untreated tumour tissue after RFA residual vascularity diagnosed by contrast-enhanced CT findings 4 weeks after ablation correlates well with histopathological confirmation of residual tumor viability (156).

MRI of ablated tissue showed a concentric "target-like" appearance of heterogeneous signal on both T1- and T2-weighted images. After contrast administration treated areas did not enhance (49, 138). Differences in signal intensities correlated with the histopathologic zones of ablation, and sequential tissue changes over time corresponded to equivalent modifications (Table 7) (141).

A complete and spherical ablation zone on US corresponded to an incomplete non-spherical ablation at the gross examination in 23 % of cases (38). Furthermore, the hyper-echogenicity observed during RFA did not accurately correspond to the actual extent of coagulative necrosis at histologic analysis (38, 40, 49, 136, 159, 160), although post-procedural imaging yielded better results due to the peripheral dissipation of micro-bubbles (136). After ablation, no discernible variation in flow was observed between the ablated and the viable tumour when conventional, non-enhanced colour Doppler techniques were used. The use of a US contrast medium highlighted the coagulative necrosis as a region devoid of contrast enhancement after RFA that prior to the ablation had an intense acquisition of the medium (137, 159). Areas devoid of perfusion after RFA were also found at contrast-enhanced CT and MRI and corresponded within 2 mm to measurements of the pathologically observed regions of coagulative necrosis, providing more accurate results than US (136, 152). Unenhanced CT had the best correlation to pathologic size followed by contrast-enhanced CT and US. Contrast-

enhanced CT correlated most accurately with the lesion shape, but slightly overestimated the size because of ischemic areas peripheral to the ablated zone (152). Again, in all cases the most accurate predictor of induced coagulative necrosis was the identification of a previously enhancing region of tumour lacking contrast enhancement after ablation therapy. Altered densities (CT) or intensities (MRI) were not predictive of the extent of the CNZ (49).

Author	Year	Experimental model	Number of subjects	Parameter investigated	Volumes obtained	Mean % of volume variation
Patterson et al. (125)	1998	*In vivo*, porcine livers	2	No occlusion Pringle	6.5 cm^3 (1.7-14.1) (no occlusion) vs. 35.0 cm^3 (20.7-48.9) (Pringle)	+ 538% (Pringle vs. no occlusion)
Chinn et al. (128)	2000	*In vivo*, porcine livers	6	No occlusion, HA occlusion, PV occlusion, Pringle	4.3 ± 1.0 cm^3, 7.6 ± 2.9 cm^3 (HA), 8.6 ± 3.8 cm^3 (PV), 12.6 ± 4.8 cm^3 (Pringle)	+ 77% (HA vs. no occlusion), + 200% (PV vs. no occlusion), + 293% (Pringle vs. no occlusion)
Chang et al. (161)	2002	*In vivo*, porcine livers	8	No occlusion, HV occlusion, Pringle, Complete (HA, PV, HV) occlusion	4.9 ± 1.5 (No occlusion) 14.4 ± 2.6 (HV) 19.2 ± 5.9 (Pringle) 28.6 ± 3.4 cm^3 (Complete occlusion)	+ 294% (HV vs. no occlusion) + 392% (Pringle vs. no occlusion) + 584% (Complete vs. no occlusion)
Shen et al. 2003 (162)	2003	*In vivo*, porcine livers	10	Peripheral no occlusion, Peripheral Pringle, Sites adjacent to PV and HV	4.9 cm^3 (2.2–8.7) (Peripheral no occlusion), 10.6 cm^3 (3.6–17.5) (Peripheral Pringle), 6.4 cm^3 (1.2–6.6) (adjacent PV) 5.6 cm^3 (0.9–27) (adjacent HV)	+ 216% (Peripheral Pringle vs. Peripheral no occlusion) + 130% (adjacent PV vs. Peripheral) + 114% (adjacent HV vs. Peripheral) + 114% (adjacent PV vs. adjacent HV)
Bangard et al. (163)	2006	*In vivo*, porcine livers	10	Sites adjacent to PV vs. HV	7.5 ± 4.1ml (adjacent PV) vs. 16.0 ± 5.5 mL (adjacent HV)	- 53% (adjacent PV vs. adjacent HV)

Table 4[5]

[5] Studies investigating the effects of the hepatic vasculature on the dimensions of the ablated zones obtained with RFA. HA = Hepatic Artery. PV= Portal Vein. HV= Hepatic Vein. Pringle = Pringle manoeuvre (both HA and PV occlusion). Peripheral = ablation conducted on a peripheral site, far from the major vessels.

Characteristics	Coagulative Necrosis Zone (zone 1)	Hemorrhagic Rim Zone (zone 2)	Normal parenchyma (zone 3)
Temperature	>60°C	40-60°C	Physiologic
Effects	Denaturation of cellular proteins, dissolution of the membrane lipid bilayer, drive of extracellular and intracellular water out of tissue/cells	Microvessel spasms and thrombosis leading to ischemia, ischemia-reperfusion injury (later)	Normal
Consequences	Coagulative necrosis	Inflammation	Normal
Gross appearance	Core of tan to charcoal gray with central areas of darker tissue	Narrow dark rim	Normal
Hepatocytes:			
• Hematoxilin and Eosin	Disrupted cell outlines, eosinophilic staining of cytoplasm, dense basophilic staining of nuclei	Vacuolation	Normal
• Viability (Ki-67, enzyme activity)	Mostly dead tissue, few specimens with viable cells	Momentarily viable but committed to death	Normal
• Apoptosis (TUNEL, caspases)	Absent	Present	Absent
• HSP-70 expression	Absent	Present	Absent
Sinusoids and vessels	Hemolysis	Sinusoid dilation and congestion	Normal

Table 5[6]

[6] Characteristics of the histological zones. TUNEL = terminal deoxynucleotidyl transferase-mediated dUTP nick and labeling. HSP = Heat Shock Protein.

Zone	41-44°C	45-49°C	50°C	51-90°C	> 90°C	Correspondence with histological zones
1 = Tissue coagulative necrosis	-	-	-	Cellular coagulative necrosis and vaporization. No normal cell structures. No microvascular flow	Microbubble formation	CNZ
2 = Cellular edema/necrosis	-	Cell edema, hepatic cord thickening (↑) and reduction of sinusoidal diameters, centrifugal shunting of blood towards sinusoids of zone 3 and 4	Hepatic cord thickening (↑↑). Collapsed and effaced sinusoids, flow stasis	Hepatic cord thickening (↑↑↑)	Microbubble formation (proximal part to the tip). Hepatic cord thickening (↑↑↑↑), obliterated sinusoids	CNZ / HRZ
3 = Sinusoidal stasis	Centrifugal shunting of blood towards sinusoids of zone 4	Distended hepatic cords (↑), sinusoidal stasis. Centrifugal shunting of blood from zone 2. Reversal of stasis when cooling down associated with increased endothelial permeability	Distended hepatic cords (↑↑). Stasis of sinusoidal flow. No reversibility	Distended hepatic cords (↑↑↑).Stasis of sinusoidal flow. No reversibility	Microbubble moving from zone 1 and 2 to patent sinusoids. Distended hepatic cords (↑↑↑↑). Stasis of sinusoidal flow. No reversibility	HRZ
4 = Parenchyma shunting	Centrifugal shunting of blood from zone 3. Increased sinusoidal flow	Centrifugal shunting of blood from zone 2	Peripheral hyperemia, increased sinusoidal flow	Endothelial leakiness	Microbubble moving from zone 1 and 2 to patent sinusoids.	NP
5 = Normal liver tissue	Normal hepatic anatomy and flow	Normal hepatic anatomy and flow	Normal hepatic anatomy and flow	Normal hepatic anatomy and flow	Normal hepatic anatomy and flow	NP

Table 6[7]

[7] Individual anatomico-functional zones with in-vivo live microscopic analysis of exteriorized rat livers during the radiofrequency ablation. Modified from Kruskal et al. (150. Kruskal, J. B., Oliver, B., Huertas, J. C., and Goldberg, S. N. Dynamic intrahepatic flow and cellular alterations during radiofrequency ablation of liver tissue in mice. *J Vasc Interv Radiol* **12**: 1193-1201, 2001.). CNZ = Coagulative Necrosis Zone. HRZ = Hemorrhagic Rim Zone. NP = Normal Parenchyma.

	Acute Phase (1 day)		Subacute Phase (2-6 days)		Chronic Phase (7 days)	
	MRI appearance	**Histopathology**	**MRI appearance**	**Histopathology**	**MRI appearance**	**Histopathology**
Electrode tract	Low intensity on T1 High intensity on T2	Tissue loss	Normal intensity on T1 High intensity on T2	Tissue loss	Normal intensity on T1 High intensity on T2	Tissue loss
CNZ	High intensity on T1 Low intensity on T2	Coagulative necrosis	Normal/High intensity on T1 Low intensity on T2	Coagulative necrosis	Normal/High intensity on T1 Low intensity on T2	Coagulative necrosis
HRZ	Normal intensity on T1 High intensity on T2 Enhancing rim on T1	Sinusoidal congestion	Low intensity on T1 High intensity on T2 Enhancing rim on T1	Inflammatory infiltration	Low intensity on T1 High intensity on T2 Enhancing rim on T1	Fibrous tissue

Table 7[8]

[8] Correlation between Magnetic Resonance Imaging (MRI), histopathologic findings and temporal modifications. Modified from Lee et al. (141. Lee, J. D., Lee, J. M., Kim, S. W., Kim, C. S., and Mun, W. S. MR imaging-histopathologic correlation of radiofrequency thermal ablation lesion in a rabbit liver model: observation during acute and chronic stages. *Korean J Radiol* **2**: 151-158, 2001.). CNZ = Coagulative Necrosis Zone. HRZ = Hemorrhagic Rim Zone.

Histological changes after electrolytic ablation

Liver experimental studies

Nordenstrom and Samuelsson were the first authors to use electrolysis to ablate the liver (62, 67), although their studies were mainly based on lung ablation and the liver was only used as a comparison (62). It was not until 1998 that specific investigations on the hepatic tissue started systematically (Table 8-11) (73, 74). Initial results showed that EA resulted in small insignificant increases in the local tissue temperature (73, 87) and in transient elevation of the liver function tests (70, 164-168). EA proved immediately to be very safe in terms of morbidity and mortality (73, 74, 164-167), and veins and bile ducts directly adjacent to EA lesions were usually left undamaged (70). In the experimental "worst-case scenario" of intravascular electrode placements (89), and provided that low currents (50 mA) were used (169), electrodes placed immediately adjacent or directly into large hepatic veins did not alter the liver parenchyma surrounding the veins and did not occlude the vessels involved, exception made for one asymptomatic case (Table 8) (89).

Macroscopically, ellipsoidal zones of hepatic necroses are created around the electrode tips (89). A linear dose–response correlation was described in rats but in larger lesions (e.g. those obtained in pigs) the destruction curve becomes more logarithmic because of the increased dilution of the pH-gradient as the lesion progresses (Table 8-11) (81). Separated electrodes (2 cm apart) produce larger lesions because when the electrodes are very close the cytotoxic gases generated from each of them mix, cancelling out their respective effects (70, 74). Increased zones of ablation may also be obtained with multiple electrodes and by the use of a Pringle manoeuvre (88). Lesions usually appear black as the hemoglobin is transformed into hemin due to the acidification of the local enviroment (81). The lesion at the anode is usually harder and firm, while the lesion at the cathode is usually oedematous and larger (84). Specific macroscopic characteristics are present in

rats (70). Small blood vessels (less than 1 mm) are thrombosed for a short distance (0.5-1.0 mm) surrounding the central necrotic zone (70) and this occlusion sometimes produce an infarction in the hepatic parenchyma peripheral to the ablated zone, often described as an "electrolytic segmentectomy" (60, 74, 164). This derives from the high ratio present between the relatively large ablated zone and the physically small volume of the lobes in the rat liver.

Microscopically the ablated zone was always sharply demarcated from the adjacent parenchyma (68-70, 73, 74, 76, 84, 87, 164, 165, 170). At both electrodes, the central cavity corresponding to the electrode is surrounded by cellular debris and necrosis. Numerous microvascular thrombi frame the ablated zones from the normal tissue while a transitional 1-mm thick congested zone is usually present (81). Anodic lesions characteristically become well demarcated and hepatocytes in this area have a pycnotic nucleus with little or absent cytoplasm (69, 75, 80, 81). Conversely cathodic lesions attract water and show generalized oedema (69, 75, 80, 81), hepatocyte nuclear and cytoplasmic swelling and occasional disruption of the plasma membranes (69, 81). A few days after ablation, fibroblasts, biliary proliferation and white-cell infiltration are present around the necrotic zone (68).

Using electron microscopy different cellular changes can be demonstrated depending on the distance from the anode. Adjacent to the electrodes abnormalities of mitochondria, peroxisomes, granular endoplasmic reticulum, cytoplasm, glycogen and nuclear chromatin were present. In the intermediate zone changes affected only the mitochondria and the peroxisomes, while at the border with the normal parenchyma no alterations were found (81). At the cathode the distribution of toxic features was uneven and no correlation could be made with the distance from the electrode (81).

Comparison with other ablative techniques

The comparison of EA and RFA for the experimental ablation of tumors demonstrates similar lesions with electrodes that are surrounded by necrosis with both techniques (171). After

RFA the cell membranes disappeared but the nuclei were still intact, whereas after EA these structures were completely disrupted and the necrotic area was often surrounded by infiltrating lymphocytes. This inflammatory reaction was not apparent after RFA (171). A second study compared EA (80 C/cm^3) with laser induced interstitial thermotherapy (LITT; 2 Watts, 5 to 10 min) for the ablation of colorectal tumor metastases in a rat model (172). Both modalities were effective in reducing the tumor growth with similar complete (21-22%) and partial (77-78%) response rates (172), but EA did not significantly increase the tissue temperature compared to LITT.

Combination with other ablative techniques

Recently, combination of EA with RFA has been investigated by Cockburn *et al*. in a modality called "BETA"(Bimodal Electric Tissue Ablation) (Table 10) (63). The BETA modality consisted in an initial application of EA to hydrate the tissue (using the electrode as a cathode and inserting the other – anode – subcutaneously) and a subsequent combined delivery of RFA + EA. The tissue hydration was necessary to avoid the dryness and consequent rise in tissue impedance that limits RFA and prevents further energy delivery ("roll-off" phenomenon). The results obtained with a straight electrode showed significant larger diameters (RFA = 1.1 ± 0.1 cm; BETA = 3.0 ± 0.2 cm), swollen necrotic zones, and non adherence of the electrode to the ablated tissue compared to RFA alone. Furthermore the central area of coagulative necrosis was larger and surrounded by a wider livid rim of swollen tissue, although the hyperemic rim was of similar thickness compared to RFA alone (63). Similar results were confirmed in two other studies (BETA = 3.0 ± 0.3 cm and 2.5 ± 0.1 cm) (65, 66). Larger diameters were achieved with a LeVeen electrode and, even in this case, those obtained with the combined BETA modality were significant larger than with RFA alone (RFA = 2.9 ± 0.3 cm; BETA = 5.0 ± 0.3 cm) (64, 173).

BETA lesions had the same temporal evolution as EA alone with a proliferation of fibroblasts and bile ducts progressively replaced the necrotic zones (65). The fibrous reaction

started at the edges of the necrotic tissue and, at two weeks, was associated with a variably intense mononuclear inflammatory cell infiltrate and bile duct proliferation. Foreign body type giant cells ingested the necrotic debris (65) and at two months post-ablation the fibrous capsule sent septa into the necrotic zone which was subject to an intense reorganization into a scar tissue. At four months most of the lesion had changed into a contracted scar and evidence of perilesional regeneration was present (65).

The only complication observed with the technique was the development of skin necrosis and subsequent subcutaneous abscesses at the positive electrode site (a scalpel blade placed under the skin in the subcutaneous tissues) (65). The very small surface area probably contributed to the morbidity and the increase of the surface area of the positive electrode obtained with a grounding plate decreased the risk of damage (66). However, in this case, lesions obtained were smaller than those measured when the positive electrode was connected to the subcutaneous scalpel blade probably because of the increased resistance of the pig outer skin that reduced the current flow (66).

Liver clinical studies

A large number of studies have been conducted on animals but relatively few have involved patients so far (Table 11). The first clinical study has been reported by Chinese authors on the treatment of 388 liver cancers with EA between 1987 and 1992 (174). However, data presented were highly heterogeneous for numerous clinical variables and results could not lead to any definitive conclusion about the effectiveness of the technique (174). Other Chinese authors later presented a high rate of tumor destruction in patients affected by large (3-20 cm.) hepatocellular carcinomas (HCC) (175, 176). Even these articles were biased by the heterogeneity of numerous clinical variables, were only empirical with no consideration given to defined assessment factors (e.g. dose-finding experimental preliminaries or strictly defined assessment parameters) and had no adequate statistical analysis (175, 176).

EA data were not confirmed by any other similar clinical study until 2000, when Berry *et al*. reported the first case of successful EA on a single 3-cm colorectal liver metastasis at one year of follow-up (91). Two years later, EA was used in conjunction to liver resection for patients with unresectable hepatic disease (90). The patients underwent formal resection of hepatic metastases, followed by EA of those that could not be resected surgically. Two patients with EA of lesions adjacent to the inferior vena cava had the tumor mass ablated without vascular damage, confirming the lack of significant temperature increase and the technique's safety close to major vessels (90). EA has also been used for the palliative treatment of a 4 cm HCC. However, in this case peripheral enhancement was seen after 3 months of follow-up, which led to the suspicion of tumor recurrence (177). This suggests that tumor diameter is an important prognostic factor for the local recurrence rates similar to the other techniques of thermal ablation (53, 55, 57, 58).

Pancreas experimental studies

Inoperability of pancreatic cancer often results from proximity to, or encasement of large blood vessels that are anatomically close to the tumor (178). Theoretical advantages of EA over more frequently used thermal ablation modalities is the relative safety of this procedure when used close to major blood vessels (89). To date six studies have investigated the use of EA in pancreatic tissue (Table 12). Animals died in both the control and the ablation groups but usually from complications related to the anesthesia (178, 179), or from postoperative gastric distension and bleeding ulcers (180). Macroscopically, the ablation zone breached the capsule and was associated with small periglandular fluid collections after two weeks (179, 180). This findings were present in 70% of the specimens (7/10 pigs) when 50 Coulombs were delivered at 50 milliAmpere, and in 40% (2/5 pigs) for 25 Coulombs at 25 milliAmpere (181). Peripancreatic fluid collections derived from both the capsule breach and by an impaired drainage of the electrolytic products and necrotic debris from the pancreatic duct, especially because the EA was conducted in the splenic lobe that is

12 cm distant from the duodenum (180). The authors concluded that in the clinical situation the use of a pancreatic stent and sphincterotomy after EA would help maintain the patency of the duct and reduce the incidence of complications.

In all studies two main ablated zones were observed: one centrally in which coagulative necrosis was the main feature, and a peripheral transitional zone, in which inflammation was present (infiltration of neutrophils and lymphocytes) (178, 179, 182). This localized zone of pancreatitis around the site of coagulative necrosis corresponded to the inflammatory transitional zone observed in the liver experiments. It was small, well demarcated from the normal parenchyma and did not produce any significant change in the amylase or glucose blood levels (179, 180, 183). No generalized pancreatitis or inflammatory cytokines changes were observed (182-184). After two weeks, an abscess formation at the site of EA was noted, possibly resulting from the poor drainage of the pancreatic debris (180). In addition there was a marked inflammatory infiltrate, extensive fat necrosis, predominantly sublobular parenchymal necrosis, and moderate intrapancreatic hemorrhage (180, 181). After two months, a scar replacement was observed and all peripancreatic fluid collections had reabsorbed (180, 181, 183). No damage to the vessels was ever demonstrated, even when the ablation was conducted close to the wall (180, 181).

In five studies EA was applied perductally and not transperitoneally (Table 12). This makes a major difference compared to EA for the treatment of liver metastases, as the perductal approach holds promise for palliative care with local tumor control via endoscopic treatment. However, it is also important to point out that despite the first experimental studies in animals there is still no description in the literature of an application of EA for the treatment of pancreatic tumors in patients, while RFA has been recently used in a patient affected by pancreatic insulinoma (185). This data raise concerns whether pancreatic EA is suitable for the clinical use.

Author	Year	Experimental model	Dose delivered	Ablation time per lesion	Ablations per liver	EA morbidity and mortality	Findings
Griffin et al. (60)	1995	30 rats ; 30 abl.	10-15 C/cm^3, 1-5 mA, 1-16 V	10-90 min.	One ablation	-	Gold electrodes Dose-response correlation C - volume Anode greater ablated volume Necrotic coagulative necrosis + “electrolytic segmentectomy” Fibrosis and repair over time
Baxter et al. (73)	1998	16 rats; 9 abl.	4 C, 2-4 mA	18-32 min.	Rats = two lobes	None	Evaluation of temperature changes ↑ 0 - 4.2°C at the end of treatment
Robertson et al. (74)	1998	50 rats, 42 abl.	1-5 C, 1-5 mA	10-90 min.	One ablation	None	Dose-response correlation C - volume ↑ ablated volume for electrodes 2 cm apart Coagulative necrosis surrounded by variable vascular occlusion and infarct (relatively large lesion for small lobes) Necrosis sharply demarcated from normal liver
Wemyss-Holden et al. (164)	2000	58 rats; 40 abl.	5 C, 10 mA	10 min.	One ablation	None	Long-term follow-up (6 months) ↑ ablated volume for electrodes 2 cm apart Replacement of necrosis with normal scars
Turler et al. (87)	2000	25 rats; 15 abl.	60-80 C/cm^3, 10 mA, 5-25 V	-	One ablation	None	Implanted colorectal liver mets. ↑ 3.9°C at the end of treatment Tumor destruction similar to parenchyma Necrosis sharply demarcated from normal liver
Turler et al. (76)	2000	24 rats; 17 abl.	80 C/cm^3, 10 mA, 5-25 V	-	One ablation	None	Implanted colorectal liver mets. 5 weeks follow-up ↓ tumor progression Necrosis sharply demarcated from normal liver
Wemyss-Holden et al. (166)	2000	55 rats; 46 abl.	4 C, 3 mA	-	One ablation	None	Implanted colorectal liver mets. Tumor destruction similar to parenchyma ↑ ablated volume for electrodes 2 cm apart
Von Euler et al. (69)	2001	25 rats, 25 abl.	5-10 C, 1-5 mA		One ablation	-	No differences of ablated diameters between the liver and the mammary tissue
Von Euler et al. (81)	2003	30 rats; 27 abl.	5-10 C, 1-5 mA	19-85 min.	One ablation	None	Dose-response correlation C – volume Ultrastructural changes according to the distance from the electrodes No changes in venous blood gases

Table 8[9]

[9] Liver studies on small animals. Abl. = ablated animals; C = Coulomb; mA = MilliAmpere; Mets = metastases.

Author	Year	Total animals used; number of animals ablated	Dose delivered	Ablation time per lesion	Ablations per liver	EA morbidity and mortality	Findings
Samuelsson et al. (62)	1980	15 rabbits	2.5-40 C, 6-12 mA, 6-12 V	-	-	-	Dose-response correlation C - volume
Li et al. (75)	1997	1 dog	124 C, 30 mA, 8.5 V	69 min.	One ablation	-	3-cm electrodes separation Tissue samples from anode, cathode, between them and normal liver Hydration around cathode, dehydration around anode Na^+ and K^+ higher around the cathode, Cl^- around the anode Protein precipitations around electrodes
Baxter et al. (73)	1998	5 pigs; 2 abl.	20-50 mA	10 min.	One ablation	None	Evaluation of temperature changes ↑ 0 - 4.2°C at the end of treatment
Berry et al. (167)	1999	16 pigs; 12 abl.	100-1000 C	-	One ablation	None	Lesions up to 6.5 cm with multiple electrodes
Wemyss-Holden et al. (165)	2000	16 pigs; 16 abl.	100 C, 50 mA	10 min.	3 ablations	None	Long-term follow-up (4 months) ↑ ablated volume for electrodes 2 cm apart Replacement of necrosis with normal scars
Wemyss-Holden et al. (89)	2000	6 pigs; 6 abl.	100 C, 50 mA	10 min.	One ablation	One thrombotic occlusion (asymptomatic)	Ablation near and within a major HV No changes in venous blood gases
Lin et al. (84)	2000	*Ex-vivo* livers	11-88 C, 6-43 mA, 10 V	-	-	-	Local injection of saturated saline (liquid electrode) Increased currents, charge delivered and ablated volumes with higher saline concentrations
Finch et al. (184)	2000	25 pigs	-	-	-	Transient rise of LFTs	IL-8 and TNF-α levels unchanged
Finch et al. (186)	2000	38 pigs	25-1000 C, 80 mA	-	-	-	Doubling electrodes (2 and 4) increases the volume ablated
Finch et al. (187)	2000	25 pigs	-	-	-	-	Real time monitoring of the correlation of pH values and necrotic changes
Wemyss-Holden et al. (70)	2002	21 pigs	25-300 C, 30-80 mA	8-100 min.	2 ablations	One thrombotic occlusion (asymptomatic)	Dose-response correlation C - volume Increased variability for > 75 C 300 C = 2.2 cm diameter ↑ ablated volume for electrodes 2 cm apart
Finch et al. (68)	2002	14 pigs; 4 abl.	80 mA	20 min.	3-6 ablations	None	Δ pH effective real-time monitor of the ablation extent All ablations completely were necrotic for pH < 6 or > 9 Homeostatic effect by surrounding vessels during ablation
Von Euler et al. (81)	2003	4 dogs; 4 abl.	25 mA, 90 C	60 min.	One ablation	None	1-2 pairs of electrodes used Dose-response correlation C – volume Ultrastructural changes according to the distance from the electrodes No changes in venous blood gases
Berry et al. (88)	2004	28 pigs; 28 abl.	80 mA, 50-1000 C	-	One ablation	None	Two electrodes, Pringle manoeuvre Dose-response correlation C - volume

							Larger lesions for two electrodes vs. one Larger lesions for Pringle manoeuvre
Berry et al. (168)	2004	17 pigs; 14 abl.	80 mA, 50-800 C	-	One ablation	Transient rise of LFTs	IL-8 and TNF-α levels unchanged
Finch et al. (85)	2004	8 pigs; 8 abl.	80-100 mA, 100-200 C	22-44 min.	9-12 ablations	None	Local injection of acetic acid or normal saline (liquid electrode) No significant advantages
Teague et al. (121)	2004	20 pigs; 16 abl.	200 mA, 0-1000 C	35-90 min.	One ablation	Transient rise of LFTs Transient platelets reduction (400 and 800 C)	No significant differences of TNF-α and IL-1β wth controls
Metcalfe et al. (169)	2007	6 pigs; 6 abl.	50-100 mA, 100 C	17 min.	One ablation	Six pigs suffered cardiac electromechanical dissociation at 100 mA (autopsy = gas embolism)	Ablation within 5 mm of large veins and within the IVC 78% ablations encased the veins 22% of ablations touched the veins 78% complete necrosis up to the vessel wall All vessels = intimal damage and mural thrombosis
Hinz et al. (171)	2008	6 pigs: 3 RFA vs. 3 DC	80 mA, 150 C	31 min.	Six-seven ablations	None	EA ablation compared with RFA RFA shorter times (4 min.) Similar diameters obtained and complete tissue destruction for both Mild inflammation and minimal transitional zone after DC No inflammation and larger transitional zone after RFA

Table 9[10]

[10] Liver studies on large animals. Abl. = ablated animals; C = Coulomb; mA = MilliAmpere; HV = hepatic vein. Δ = differential; LFTs = Liver Function Tests. DC = Direct Current. RFA = Radiofrequency ablation. W = Watts.

Author	Year	Total animals used; number of animals ablated	RFA Dose delivered	RFA ablation time per lesion	DC Voltage applied	DC polarization time per lesion	BETA ablation time per lesion	Ablations per liver	EA morbidity and mortality	Findings
Cockburn et al. (63)	2007	6 pigs: 3 RFA vs. 3 BETA	20 W	4 min.	9 V	0-15 min.	<20 min.	Eight ablations	-	DC followed by RFA+DC (BETA) Larger diameters for BETA compared to RFA alone Dose-response correlation C – volume
Dobbins et al. (173)	2007	-	-	-	-	-	-	-	Transient rise of LFTs	Larger diameters for BETA compared to RFA alone
Dobbins et al. (64)	2008	4 pigs (same pig with RFA and BETA lesions)	80 W	4 min.	9 V	15 min.	19 min.	Six-eight ablations	-	Standard 35-mm Le Veen electrode Larger diameters for BETA compared to RFA alone
Dobbins et al. (65)	2008	8 pigs (all BETA lesions)	20 W	-	9 V	5 min.	-	Six ablations	Transient rise of LFTs Skin abscesses of the positive electrode site (subcutaneous scalpel blade)	Diameters = 3.0 ± 0.3 cm.
Dobbins et al. (66)	2008	6 pigs (same pig with RFA and BETA lesions)	80 W	0.5 min.	9 V	15 min.	1.2-1.7 min.	Six ablations	Full-thickness burn with scalpel blade, none with grounding plate	Positive electrode connected to grounding plate vs. scalpel blade Smaller ablations for grounding plate

Table 10[11]

[11] Studies describing the results obtained with the "BETA" modality (combination of Radiofrequency with Electrolytic Ablation). LFTs = Liver Function Tests. CRP = C-Reactive Protein.

Author	Year	Number of patients	Type of tumor	Lesion diameter	Dose delivered	Treatment duration	EA morbidity and mortality	Findings
Xin et al. (174)	1994	388	Liver cancer (not specified)	3-13 cm	8-10 V, 40-80 mA, 100 C/cm^3	25 min/100C	Heterogeneous group of patients, results not easily applicable	Heterogeneous group of patients, results not easily applicable Number of electrodes according to tumor side
Wang et al. (175)	1994	74	HCC	3-20 cm	8-13 V, 40-80 mA, 400-1000 C (cumulative)	3-5 hours	Postop. fever 15% symptoms localized peritonitis	Number of electrodes according to tumor side 33.3% survival at one year follow-up Curative effects poor for lesions > 9 cm.
Lao et al. (176)	1994	50	HCC	3.5-21 cm	6-10 V, 50-100 mA, 300-1000 C (cumulative)	1.5-4 hours	Postop. fever Intraop. mild bleeding	Number of electrodes according to tumor side 69.0% survival at one year follow-up
Berry et al. (91)	2000	1	Colorectal metastasis	3 cm	-	-	None	No clinical or histological recurrence at one year follow-up
Wemyss-Holden et al. (170)	2002	5	Colorectal metastases	-	60 mA, 100 C	35 min.	Transient rise of LFTs	One metastasis ablated before resection Complete necrosis
Fosh et al. (90)	2002	9	Colorectal metastases	0.5-3 cm	200-1000 C (cumulative)	1-3.5 hours	Transient rise of LFTs and WCC	EA adjunct to resection 66.6% survival at 9 months median follow-up 17 months median survival after the procedure
Fosh et al. (177)	2003	1	HCC	4 cm	1500 C	Almost 5 hours	Transient rise of LFTs Postop. pulmonary atelectasis with small pleural effusion.	Liver cirrhosis (Hep.B) Area of peripheral enhancement at 3 months follow-up

Table 11[12]

[12] Liver clinical studies. C = Coulomb; mA = MilliAmpere; HCC = hepatocellular carcinoma; LFTs = Liver Function Tests; WCC = White Cell Count.

Author	Year	Total animals used; number of animals ablated	Approach used	Dose delivered	Ablation time per lesion	Ablations per pancreas	Follow-up	EA morbidity and mortality	Findings
Fosh et al. (178)	2001	10 rats; 8 abl.	Transperitoneal EA	8 mA, 2-10 C	-	One ablation	3rd p.o. day	One control rat and one in the EA group died for the anaesthesia	No changes in glucose or amylase levels Central coagulative necrosis and peripheral transitional inflammation
Wemyss-Holden et al. (179)	2003	12 pigs; 6 abl.	Perductal EA (after duodenotomy)	50 mA, 50 C	23 min.	One ablation	3rd p.o. day	One control pig died for the anaesthesia Two pigs in each group had a delayed return to normal activity	Mean ablated diameter 1.5 cm Central coagulative necrosis and peripheral transitional inflammation No differences among groups for amylase, glucose, calcium, urea, and electrolytes
Morrison et al. (183)	2003	8 pigs; 8 abl.	Perductal EA (after duodenotomy)	50 mA, 50 C	21 min.	One ablation	2 weeks and 2 months	None	No significant modifications of IL-1β or TNF-α Histological scar by the 2 p.o. month
Morrison et al. (180)	2004	8 pigs; 8 abl.	Perductal EA (after duodenotomy)	50 mA, 50 C	21 min.	One ablation	2 weeks and 2 months	Three pigs died within the third p.o. day for acute gastric distension and bleeding ulcer	Mean ablated diameter 2.4 cm Localized necrosis, inflammation and abscess at two p.o. weeks Histological scar by the 2 p.o. month Transient p.o. increase of amylase and CRP. No differences for glucose, calcium, urea, and electrolytes
Teague et al. (182)	2004	12 pigs; 6 abl.	Perductal EA (after duodenotomy)	50 mA, 50 C	17 min.	One ablation	3rd p.o. day	None	Mean ablated diameter 1.5 cm Central coagulative necrosis and peripheral transitional inflammation No significant modifications of IL-1β or TNF-α
Morrison et al. (181)	2005	15 pigs, 10 abl.	Perductal EA with endoscopic retrograde approach (after enterotomy)	25 mA, 25 C	10 min.	One ablation	2 weeks and 2 months	None	Localized necrosis, inflammation and abscess at two p.o. weeks Histological scar by the 2 p.o. month Inflammation and scarring of the pancreatic segment distal to the ablation Significant increase of WCC and CRP compared to controls No differences among groups for amylase, glucose, calcium, urea, and electrolytes

Table 12[13]

[13] Pancreas studies. Abl. = ablated animals; C = Coulomb; mA = MilliAmpere; EA = Electrolytic Ablation; P.O. = postoperative. WCC = White Cell Count. CRP = C-Reactive Protein.

Experimental models of liver ablation

The development of any new hepatic ablative therapy is a process that requires a detailed understanding of the basic physical and chemical properties of the ablative modality. Identifying methods of assessing tissue response to ablation is the first step to optimise treatment monitoring. Local and systemic effects, the safety and efficacy of the technique, local changes into tissue temperatures, modifications close to large vessels (188, 189), the effects of vascular occlusion (Pringle manoeuvre) (188, 190, 191), the creation or appropriate dose-response curves needs to be experimented on appropriate preclinical models. Over the years various models have been adopted, the most common are *ex-vivo* non-perfused models (hepatectomy specimens), *in-vivo* models (live animal experiments) and, more recently, *ex-vivo* perfused models.

Ex-vivo non-perfused models

The most commonly used model for the study of hepatic ablation is the liver explanted from animals (hepatectomy specimens). Livers from large animals such as bovine and porcine specimens are frequently used because of their similarities with human ones. Advantages are the possibility to build a dose-response curve, to assess the effects of different antennas shapes and to conduct multiple ablations (192-195). Disadvantages derive from the lack of perfusion, which makes impossible to evaluate the effects of the Pringle maneuver of "heat-sink" effect, the lack of respiratory excursions where these are important to be considered (196), and the lack of live cells on which direct thermal effects cannot be evaluated.

In-vivo models

In-vivo animal models have been widely used to overcome the limitations of the hepatectomy specimens. Data generated from these studies are very reliable and closely similar to results observed in humans. Due to the presence of blood they can be used to investigate the consequences of the "heat-sink" effect and the Pringle maneuver on ablations. Furthermore, the presence of live cells allows the investigation of the effects of thermal ablations on them. Results generated from *in-vivo* models are directly transferable to clinical practice and represent the current gold standard for pre-clinical experimental studies of hepatic ablation. Specific disadvantages include the costs that involve *ad-hoc* dedicated animal facilities, laboratories, anesthetists and theatres especially for experiments involving large animals. While small animal models (rats or mice) are less expensive and easier to handle, their organs have significant differences in size, function and anatomy compared to the human liver and the number of ablations that can be performed is limited.

Ex-vivo perfused models

The isolated perfused *ex-vivo* model theoretically would have most the advantages of both previous models. A normothermic liver perfusion system using autologous blood maintains physiological and metabolic functions as well as the hemodynamic changes close to those of *in-vivo* models with good preservation of liver architecture (197-199). This should permit the histological study of lesions generated by thermal ablation, real-time monitoring of the evolution of the lesions, close monitoring of the effects of "heat sink" or Pringle maneuver. One peculiar advantage of *ex-vivo* perfused models would be the absence of other interacting organs that may affect the extent of systemic responses and therefore are ideal for the investigations of the organ physiology without any additional confounding factors (autonomic nervous systems response, hormones, cytokines). Finally, the model would be relatively inexpensive compared to *in-vivo* studies because does not need dedicated anesthetists and theatres. The use of organs collected from dead animals would also

avoid ethical problems or licensing. The main limitation is the limited lifespan of the organ perfused and the interaction of blood with non-biological surfaces of the perfusion circuit that might activate biological pathways of inflammation.

History

The *ex-vivo* organ perfusion started with Carrel in the first half of the 20th century that used normothermic oxygenated acellular perfusates (serum) (200). Experiments continued with cold oxygenated acellular perfusates until 1963 when, for the first time, cold autologous blood was used an *in-vivo* isolated perfusion of the liver (201, 202). In an attempt to mimick as close as possible the physiological environment, pulsatile perfusions were introduced in 1967 using cold acellular perfusates on kidneys (203). Liver pulsatile perfusions were technically more challenging for the dual vascular supply but were considered indispensable to dilate peripheral vessels and supply oxygenated whole blood to the entire organ. Research in this field gradually introduced pulsatile perfusions of the hepatic artery with cold acellular perfusates (204), pulsatile perfusions of both the hepatic artery and portal vein with a cold 50% mixture of autologous blood and acellular perfusate (205) and pulsatile perfusion of the hepatic artery and continuous perfusion of the portal vein with cold acellular perfusates (206). Further advances allowed the successful perfusion of animal livers for 24 hours (207) and 72 hours (208).

Current models

Ex-vivo perfused models have been used for research on liver physiology, pharmacology and toxicity as well as for support of liver failure, organ preservation (normothermic perfusion), and viability assessment (209-211). Current models differ with respect to the perfusates used (acellular, autologous blood) (198, 212-214) and temperatures adopted (normothermic, hypothermic perfusion) but most of them use standard cardiopulmonary circuits, including a blood reservoir, pump, oxygenator, and a heat exchanging device (215, 216). Three models add significant

differences in their circuits. The Berlin model place the organ in a waterlogged and sealed chamber that mechanically modifies the internal pressures (217). As the fluid transmittes the oscillations to the liver, imitating the intraabdominal pressures, the perfusions of peripheral lobules are significantly improved (217). Additionally, the group has introduced a simultaneous dialysis system to regulate constantly the pH and electrolytes and remove excess toxins ans waste products from the recirculating perfusate (218). Differently, the Japanese model place the organ in a special accommodation device that simulates the intraabdominal arrangement in the pig body, while the liver is supported by a special inferior vena cava tube. The blood flow through the hepatic artery is pulsatile using a diaphragm-type artificial heart (219). Finally, the Oxford model does not use two separate pumps for the hepatic HA and PV but arterial perfusion is pumped directly, whereas the portal vein is perfused via gravity (220, 221).

Aims of the study

Null hypothesis

The null hypothesis (H0) for this study is that there is no difference between EA (the experimental technique of hepatic ablation) and RFA (the current gold standard technique of hepatic ablation) for perfusion, acid base balance, immunologic and histological parameters. The alternative hypothesis (H1) is that EA produced significant differences from RFA. To accomplish this purpose an *ex-vivo* perfusion model using autologous blood perfusate was adopted. This decision was made to avoid a large number of live animals for the experiments with their ethical and economic implications. The *ex-vivo* model selected for the study was the one described by the Oxford group.

Materials and Methods

Circuit preparation

Our *ex-vivo* perfusion is achieved by means of an extracorporeal sterilized circuit similar to those used for cardiopulmonary extracorporeal bypass surgery (Medtronic Inc., Minneapolis, Minnesota - United States; custom pack, cardiac surgery division Europe). It consisted of 1) an atraumatic centrifugal pump (Bio-console 560) that provided the hepatic arterial flows and pressures, 2) an oxygenator, 3) a heat exchanger unit and 4) a portal venous reservoir to simulate the venous flows and pressures. After passage through the liver, the venous blood is collected from the supra- and infra-hepatic IVC into a container simulating the systemic venous reservoir and returned to the centrifugal pump (Figure 2). The only difference of this circuit from physiological hemodynamics and oxygenation was that the blood supplied to the liver through both vessels (including the PV) was fully oxygenated.

The circuit was setup before the organ harvesting and one litre of physiological Normal Saline (Baxter Healthcare Ltd, Liverpool – UK) was allowed to run through the intraluminal and extraluminal compartments. All lines of the circuit as well as the hollow fibre filter were then filled with Normal Saline and kept clamped.

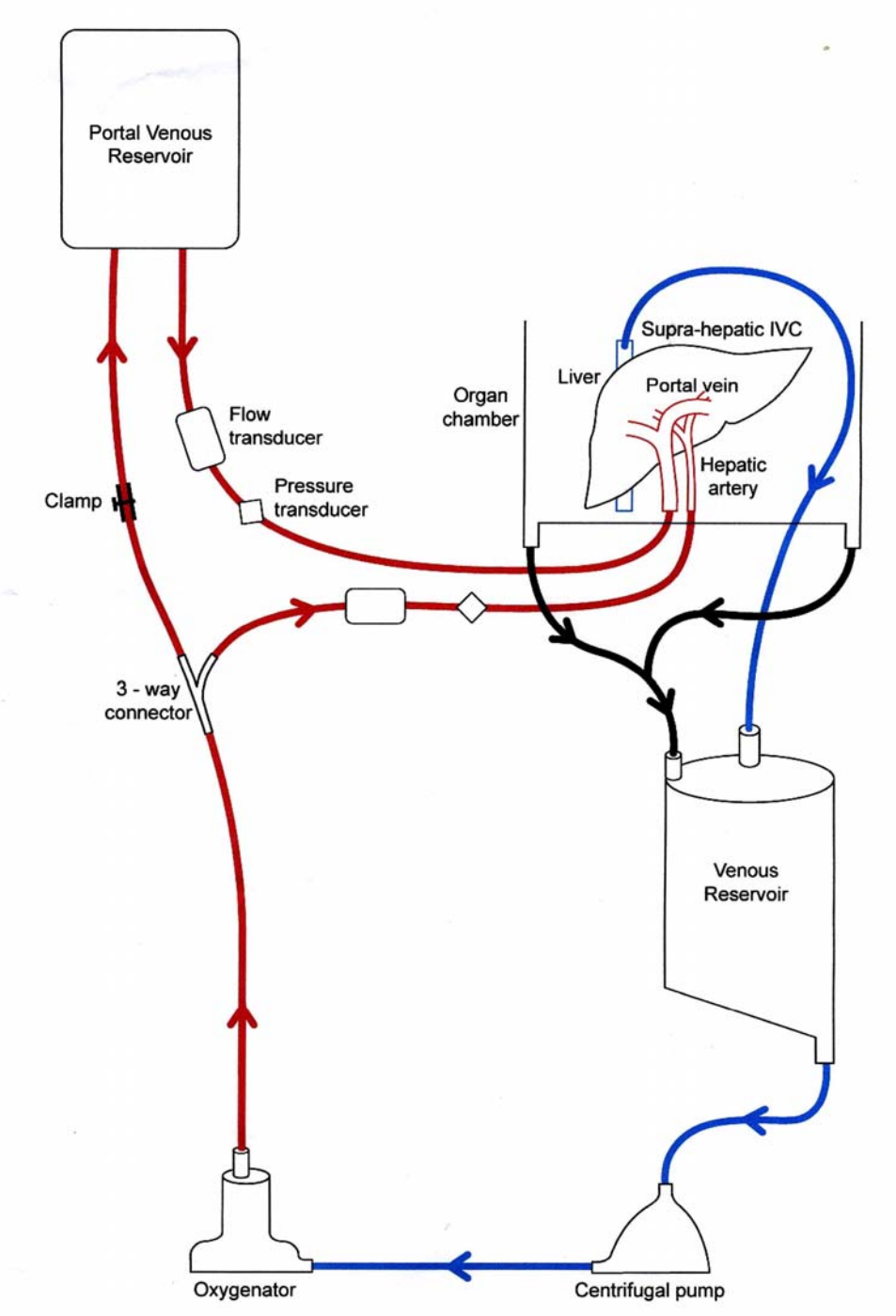

Figure 2[14]

[14] Schematic drawing of the circuit for the ex-vivo perfusion of the liver.

Organ harvesting

The animals used in this study received human care and the study protocols were implemented in accordance with the United Kingdom "Guidance on the Operation of the Animals (Scientific Procedures) Act 1986". Animals were humanely sacrificed in the abbatoir with final exsanguination during the blood-harvesting procedure performed in accordance with Home Office regulations and in a similar manner to all the other pigs entering the food chain process. The animals were initially stunned with electrocution in the abbatoir and the final exsanguination was reached with a cut through the carotid arteries. A pre-heparinised non-pyogenic container with 5000 units of heparin was used to collect the autologous blood. Once the exsanguination was finished and the pig was dead the animal was left on a metal table and received a midline laparotomy. All these initial manoeuvres were conducted by the abbatoir personnel, afterwards the harvesting process was performed by the candidate.

Intact livers were obtained post mortem at the abbatoir from 17 female domestic white pigs weighing 45-60 kg. The candidate has received assistance from a colleague, Mrs. Seok Ling Ong, during the harvesting process and the conduction of his experiments and has provided assistance to her for the organ harvesting and throughout her experiments. Liver tissue and data collected from the controls experiments (n=7) have been shared and used in both thesis (joint control group: Mr. Gianpiero Gravante and Mrs. Seok Ling Ong) while the ablation experiments with RFA and EA have been reported in this thesis only (RFA n=5, EA n=5). Following median laparotomy, the diaphragm and pleurae were divided in order to access the suprahepatic inferior vena cava (IVC) and thoracic aorta (Figure 3). These vessels were isolated, clamped and divided along with the oesophagus (Figure 4). The aorta was lifted and detached from the vertebral column down to the level of the celiac trunk along with a cuff of diaphragm (Figure 5). The gastrocolic omentum was divided and the front of the left pancreatic segment exposed (Figure 6). Dissection between the

inferior border of the pancreas and the right kidney allowed identification of the major retroperitoneal vessels (superior mesenteric vein - SMV, Aorta and IVC; Figure 7). The retroperitoneum was opened, SMV and aorta clamped and divided (Figure 8). Finally, the liver was lifted up, the IVC detached from the vertebral column and any non-vascular attachments freed allowing the liver, stomach, pancreas and spleen to be removed en-bloc.

Figure 3[15]

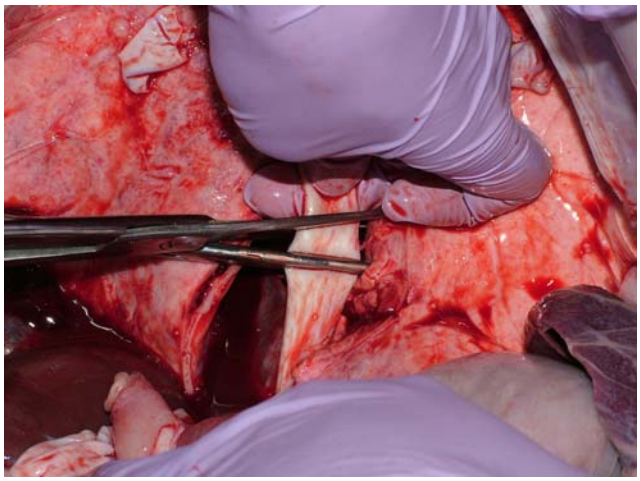

Figure 4[16]

Figure 5[17]

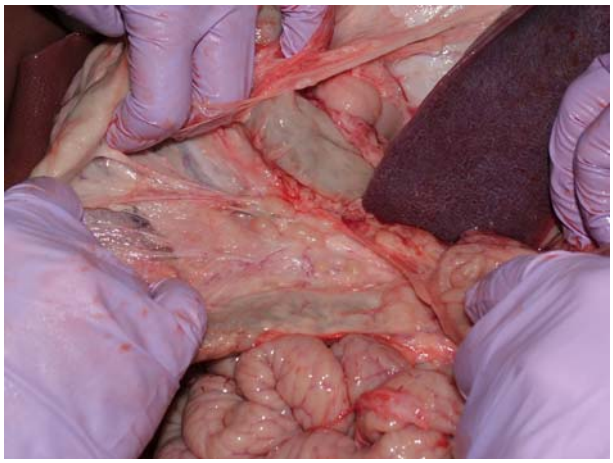

Figure 6[18]

[15] Division of the diaphragm and pleurae.
[16] Clamping and division of the thoracic aorta.
[17] Lifting and detachment of the aorta from the vertebral column.
[18] Division of the gastrocolic ligament.

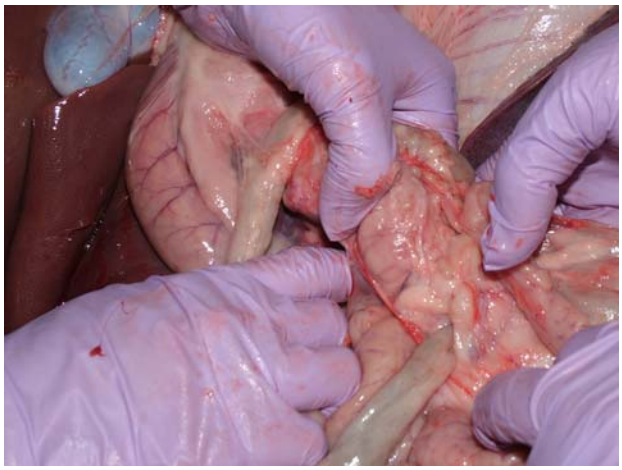

Figure 7[19]

Figure 8[20]

[19] Dissection between the inferior border of the pancreas and the right kidney.
[20] Opening of the retroperitoneum.

Following removal of the liver and its attachments, the portal vein (PV) is isolated in the hepatoduodenal ligament and cannulated with 18FG Nelaton catheter (Astratech, Sweden) (Figure 9). The celiac trunk is identified at its origin from the aorta and the hepatic artery (HA), cannulated with a female catheter (10FG, Penine Healthcare, UK) and ligated with 0 vicryl (Polyglactin 910, Ethicon) (Figure 10). The liver is immediately flushed through (two litres of cold water via the PV and one litre through the HA) to remove any residual blood clots and an initial wedge biopsy is collected (time -2, end of the warm ischemia time). After the spleen has been mobilised and the gastrosplenic ligament divided it is removed (after clamping and ligating the splenic vessels). The superior mesenteric artery (SMA) is carefully isolated and ligated. The gastroduodenal ligament is freed from any connective tissue and fat in order to isolate, clamp and ligate the right gastric artery, and at this point the stomach is removed (Figure 11). The pancreas is carefully dissected from the splenic artery and pancreatic branch(es) of the HA are freed and ligated. The liver is then again flushed but this time with three litres of cold Soltran preservation solution (Baxter Healthcare Ltd, Liverpool – UK), again two litres through the PV and one litre via the HA. The liver is then stored under sterile conditions in ice for the transport to the laboratory.

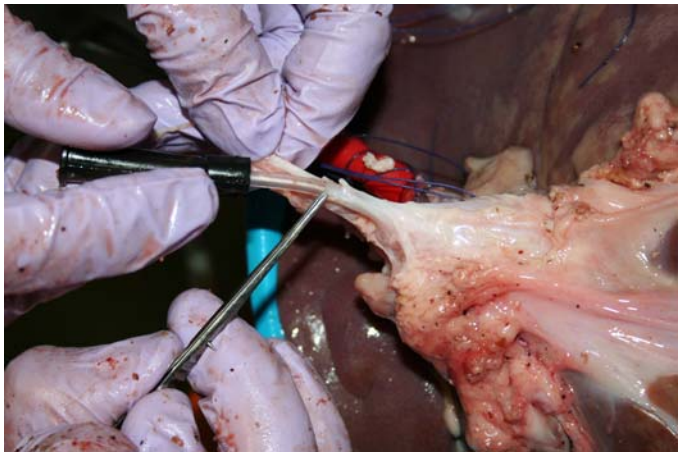

Figure 9[21]

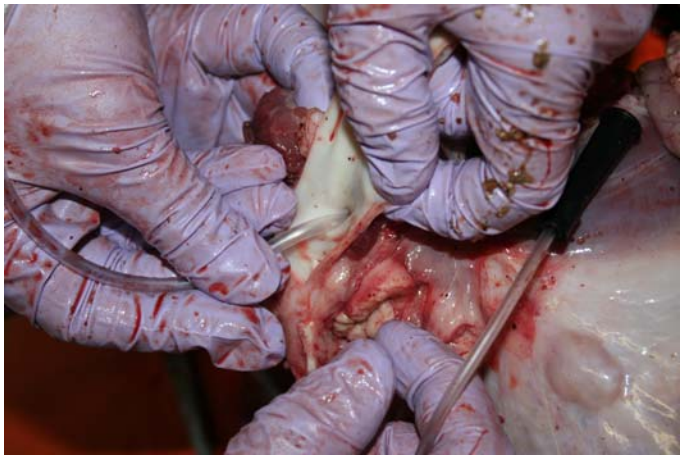

Figure 10[22]

Figure 11[23]

[21] Cannulation of the portal vein.
[22] Cannulation of the hepatic artery from the origin of the celiac trunk.
[23] Gastroduodenal ligament opening.

Circuit priming

A hematocrit of approximately 20% has been suggested to provide the optimum combination of blood and oxygen-carrying capacity at physiologic flows and pressures (222-224). Because the porcine baseline physiologic hematocrit is 40%, on reaching back to the perfusion laboratory 1000 ml of heparinised autologous porcine blood was diluted by the addition of 1000 ml of Normal Saline (1:1) in a sterile beaker. This diluted blood was added to the systemic venous reservoir of the circuit during the backbench preparation and was used as the perfusate for *ex-vivo* liver. To this perfusate one bolus of sodium bicarbonate, Calcium chloride, Cefuroxime, and vasodilating prostacyclins (Epoprostenol) was added (Table 13). Continuous infusions of insulin, sodium bicarbonate, prostacyclins and sodium taurocholate were also started to mimic as closely as possible normal physiological conditions.

Drug	Manufacturer	Dosages
One time boluses:		
• Epoprostenol sodium (Flolan)	Glaxo Smith Kline	20 ml (500µg in 50 ml of diluent, diluted with 200ml of N/S)
• Sodium Bicarbonate 8.4%	Polyfusor, Fresenius Kabi Ltd	40 ml
• Cefuroxime sodium (Zynacef)	Glaxo Smith Kline	750 mg in 10ml of water
• Calcium Chloride 14.7%	Martindale pharmaceuticals	10 millimoles in 10 ml
• Heparin		25000 U
• Adrenaline (Epinephrine)		10 ml (1mg in 1 ml of diluent, diluted with 100 ml of N/S) *if loss of resistances*
Infusions:		
• Epoprostenol sodium (Flolan)	Glaxo Smith Kline	20 ml/hr (500µg in 50 ml of diluent, diluted with 200ml of N/S)
• Sodium Bicarbonate 8.4%	Polyfusor, Fresenius Kabi Ltd	35-40 ml/hr titrated according to ABG
• Sodium taurocholate	Sigma-Aldrich	10 ml/hr (2% w/v, 2 g in 100 ml of N/S) i.e 200 mg/hr
• Insulin (Actrapid)	Novo Nordisk	100U/hr (10U/ml given at a rate of 10 ml/hr)
• Adrenaline (Epinephrine)		30-45 ml/hr titrated according to HA pressures and flows (1mg/100 ml: 1mg in 1 ml of diluent, diluted with 100 ml of N/S) *if loss of resistances*

Table 13[24]

[24] Substances added during the perfusion.

Sodium bicarbonate was added to the circuit for all the experiments in the same way and doses: immediately before the organ reperfusion as a single bolus of 35 ml, and during the experiment at a fixed rate of 35 ml/hour. This was necessary to maintain the pH within physiologic ranges after reperfusion for the acidotic changes derived from the ischemia-reperfusion injury, and during the experiment for the continuous spillage of lactic acid in the circulation.

The perfusate is allowed to prime the centrifugal pump under the effect of gravity. Any air bubbles are tapped out towards the venous reservoir. Biomedicus BP560 is started at a pump speed of 1200 rpm to prime the remaining part of the circuit with the perfusate. A mixture of Oxygen (95%) and Carbon Dioxide (CO_2; 5%) is supplied to the oxygenator at a rate of 2 litre/min. An oxygenator is also connected to the water bath / heat exchanger pre-set at a temperature of 39ºC (physiological temperature of pig). To prime the portal venous limb of the "liver circuit", the hepatic arterial limb had to be clamped. The pressure transducer lines were also primed. After about 45 minutes of priming the circuit, the pressure-measuring device on the Bioconsole BP560 was zeroed to air. To zero the flow, both the inlet and outlet into the flow transducer were fully clamped.

Priming was carried out for one hour and during this time the organ was prepared for perfusion. Once all the lines were fully primed and perfusate optimized, samples were taken for full haematological, bio-chemical and blood gas analysis.

Backbench preparation of the liver for the perfusion

Once the priming of the circuit was begun the organ was removed from the bag in the icebox. Following this period of cold ischemia, a second wedge biopsy of hepatic tissue was taken (time -1, end of the cold ischemia time). Cannulation of the common bile duct (CBD) after ligating the cystic duct, supra- and infra-hepatic inferior vena cava (IVC) was carried out. This was necessary to accurately measure the bile production during the experiment as an indirect measure of liver viability without having interferences from the bile already present in the gallbladder. At the same time the gallbladder was simply excluded from the main bile flow by closure of the cystic duct and not surgically removed from the liver in order to avoid any minimal traumatism to the liver parenchyma of the gallbladder bed that could have altered some of the biochemical parameters measured (transaminases).

A 30-cm length of quarter inch Medtronic tubing with perforated end was used to cannulate the suprahepatic IVC. Purse string suture with 2-0 Prolene (Polypropylene, Ethicon) was used to secure the cannula to the central tendon of diaphragm. The cannula tip was placed at the entry point of the three hepatic veins. The position of the tip was crucial in ensuring adequate venous drainage from the liver. The infrahepatic IVC was cannulated with 20-cm of quarter inch Medtronic tubing, secured with 2-0 Prolene and keep it clamped during the perfusion unless the outflow from suprahepatic IVC was compromised.

Before connecting the liver to the circuit, 1 litre of warm 0.9% Normal Saline solution (Baxter Healthcare Ltd, Liverpool – UK) was perfused through the PV and 500 ml through the HA to flush out the Soltran solution and remove air from the organ and the cannulae. The choice to use a crystalloid and not the preservation solution to flush the liver prior to the connection with the circuit was conducted in accordance to the protocol presented by the Oxford group (223). During this process, any leaks or unligated vascular branches, which might bleed during perfusion, were

identified, clipped and ligated with 2-0 vicryl. The organ was then weighed (Ohaus compact scales, USA), placed in a non-pyogenic perfusion container (Figure 12) and connected to the extracorporeal circuit.

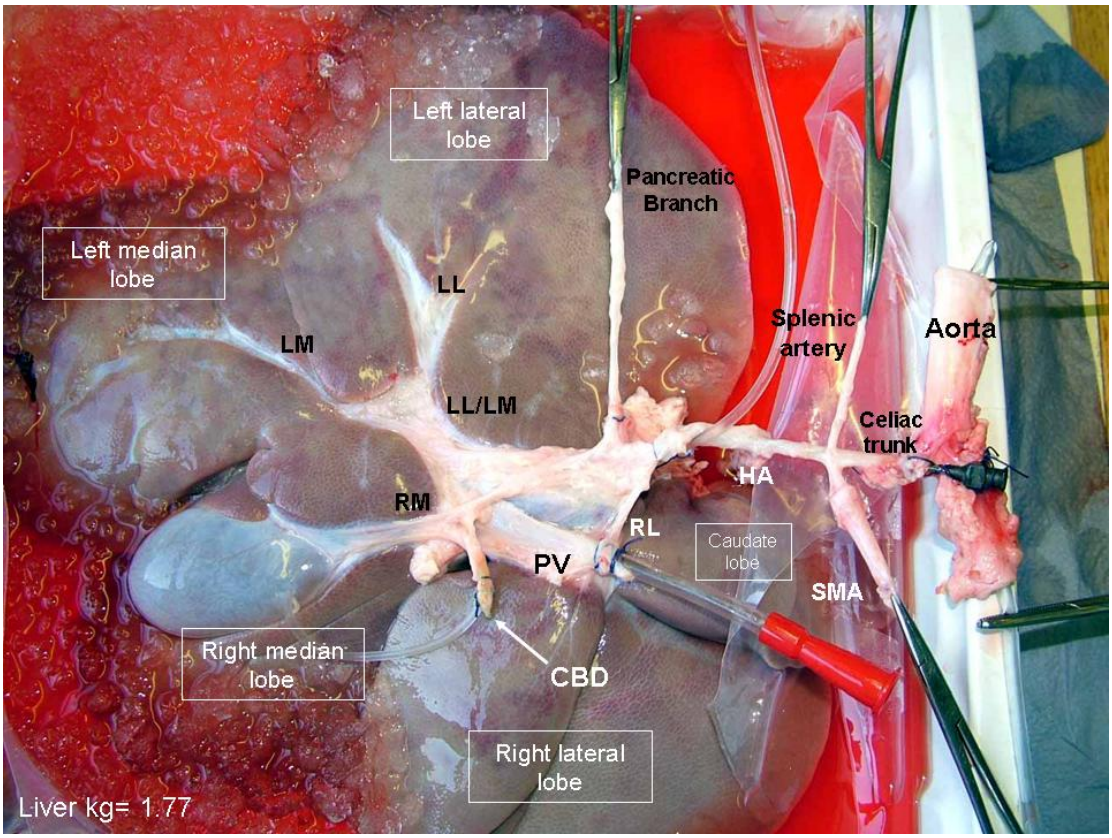

Figure 12[25]

[25] Porcine liver immediately before perfusion. HA = hepatic artery; PV = portal vein; SMA = superior mesenteric artery; CBD = common bile duct; LL = vascular branches to the left lateral lobe; LM = vascular branches to the left medial lobe; LL/LM = vascular branches to the left lateral and left medial lobes; RM = vascular branches to the right medial lobe; RL = vascular branches to the right lateral lobe.

Ex-vivo liver perfusion

Before adding the organ to the extracorporeal circuit, the acid base balance of the perfusate was ensured to be in the physiological range. The pump speed was then increased to around 2000 rpm and, taking standard bypass precautions, the HA, PV and IVC cannulas were connected to the respective lines of the circuit temporarily excluded from the blood flow. Following the connection of the hepatic vessels to the circuit the clamps were released. This allowed the blood pumped out from the centrifugal pump to split between the blood flowing into the HA and that to the portal reservoir. A targeted pressure-based perfusion of the liver was performed using an adjustable vascular clamp aiming to maintain the HA pressure between 80-100 mm Hg. The PV pressure was set at 20-30 mm Hg, values higher than the normal physiologic range. This decision was based on our perfusate, that involved diluted blood to a target hematocrit of 20%, and on previous studies using simple oxygenated acellular buffer solutions. These solutions require higher flows and pressures for an adequate oxygen delivery compared to normal physiologic hematocrit values (225-227).

Two pressure-flow transducers were used to measure blood pressures and flows from the HA and PV cannulas immediately before their entry into the liver (Figure 2). Since the resistance in the portal system is very low as compared to the arterial channel, a second clamp was applied on the inlet tubing of the portal reservoir to control its inflow. Perfusion through the PV was controlled by adjustments of the clamp to the portal reservoir and by the gravity-dependent mechanism through modifications of the vertical height difference between the portal venous reservoir and the organ itself (Figure 13). The vascular clamp of the portal reservoir had both an effect on the PV and the HA pressure and flow. Tightening the portal reservoir clamp decreased the in-flow to the portal reservoir and increased the flow and pressure in the HA. When the clamp was loosened, the in-flow into portal reservoir increased and the flow and pressure in the HA decreased.

Perfusion was maintained within set values of arterial and venous flows and pressures by altering the pump speed, adjusting the resistance of the vascular clamps and altering the height difference between the portal reservoir and the organ. The flows through the HA and PV were controlled to be in the ratio of 1:4 as seen in a live animal.

Figure 13[26]

[26] Circuit during an experiment.

During the first hour of perfusion the flows improved and stabilized with the perfusate being warmed to physiological temperatures. At the same time, the circuit compliance progressively improved (Figure 14). The EA and RFA ablation experiments were conducted after the first hour of perfusion when the hemodynamic parameters became stable. The perfusions were ended after six hours.

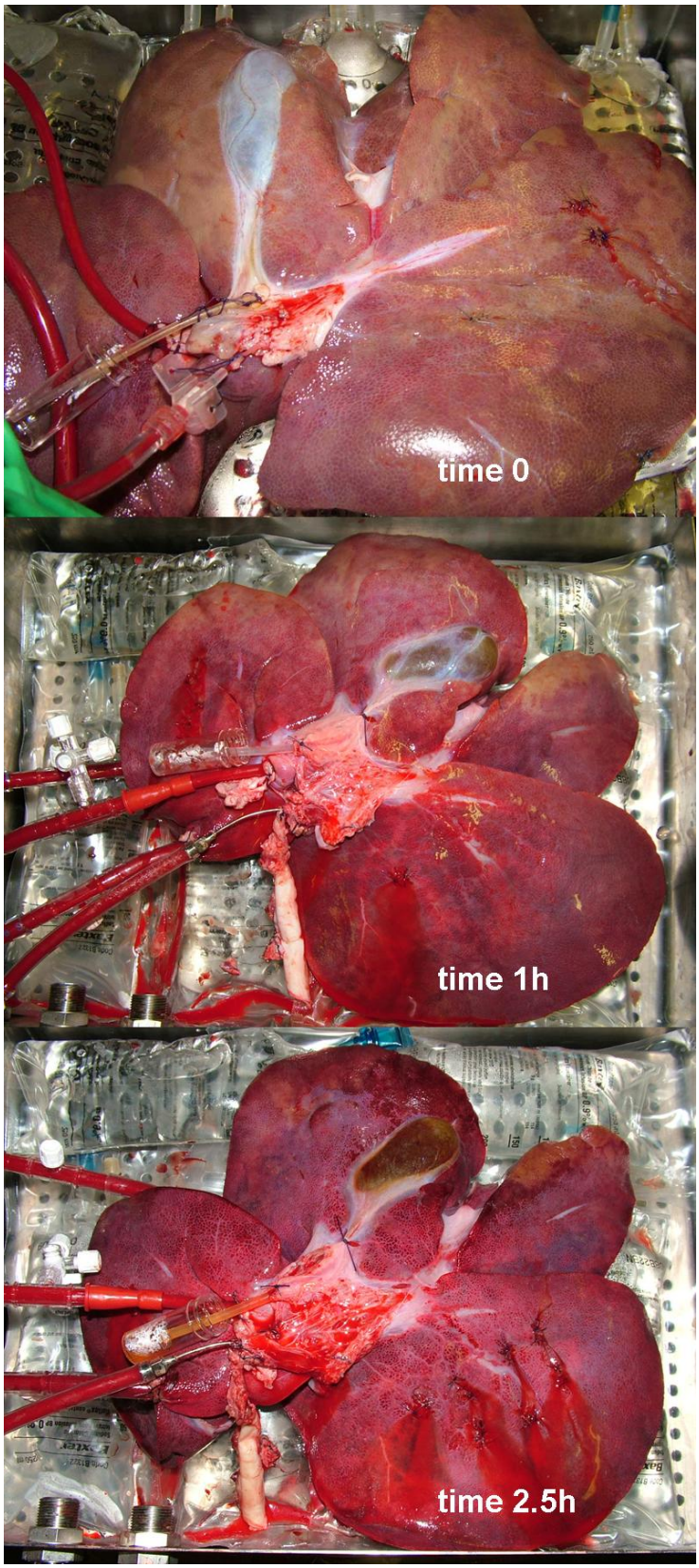

Figure 14[27]

[27] Liver perfusion at different time points: immediately after reperfusion (time 0 – *upper panel*), one hour (*middle panel*) and two hours and a half later (*lower panel*).

Liver ablations

The final target of liver ablations was to achieve ablated zones of approximately 2cm of diameter distant enough not to interfere each other. The ablated diameter was therefore the selected standardised parameter common to both ablative techniques used. The diameter measured was the one on the surface as the depth was more difficult to measure during the ablations. The choice of 2cm was arbitrary considering an appropriate ratio between the dimensions of the liver lobes (including the caudate that was the smallest) and the diameter of the ablations. In a pilot experiment different RFA and EA settings (time, power) were tested to achieve lesions with this target diameter. The final shape of the ablated zone was a half-sphere with the largest diameter (2cm) on the liver surface.

As the purpose of the experiments was to compare RFA with EA, these were conducted in separate livers using only one technique for each experiment. Therefore, every liver received ablations from one ablative technique only, either RFA or EA. Each liver lobe received one ablation (left medial, left lateral, right medial, right lateral and caudate) plus the largest lobe had an extra one (usually the left lateral). Therefore, a total of six ablations were performed in each liver with the same ablated technique (Figure 17). Before inserting the probe for the liver ablation the target area was selected using an ultrasound probe in the periphery of the lobe to avoid major vessels. This approach was used to avoid any major hemorrhage that could have endangered the experiments. Any minor bleeding from the probe insertion point was controlled by applying the probe to the surface for a further 2-3 seconds.

Electrolytic ablation

A DC generator was designed to deliver a pre-determined "dose" of coulombs at a constant current which could be varied between 1 and 100 milliAmpere (mA; coulombs = current (amperes) x time (seconds)) (ECU 100, Söring GmbH, Justus-von-Liebig-Ring 10, D-25451 Quickborn, Germany) (Figure 15). Automatic voltage adjustments between 1 and 25 V allowed the pre-determined rate of current to be delivered, regardless of alterations in hepatic parenchymal resistance during treatment. Positive (anode) and negative (cathode) electrodes, used to conduct the current, were placed within the substance of the liver. Platinum electrodes were used (Johnson and Johnson, 6 French, 2 mm diameter) with the cathode and anode electrodes 1cm apart (Figure 16). Anode and cathode electrodes were identical and constructed from fine platinum wire (0.5mm diameter), which was electrically insulated using a semirigid plastic sleeve. Two millimetres of uninsulated electrode were exposed at the tip (74).

After the first hour of perfusion the electrodes were inserted 1-cm deep in the hepatic parenchyma. To achieve 2cm diameter of the ablated lesion 100 Coulomb (C) of energy was delivered at 100 mA for 17 minutes. Upon activation of the generator, the current flow "ramped" up to its pre-determined maximum value (milliamps) over the course of 1 minute. Once this had achieved a "steady state", as treatment progressed the voltage required to maintain a steady current flow was varied automatically in order to compensate for any fluctuation in the resistance between the electrodes. After the pre-determined dose of coulombs was delivered, the current returned to zero over a period of 1 min.

Figure 15[28]

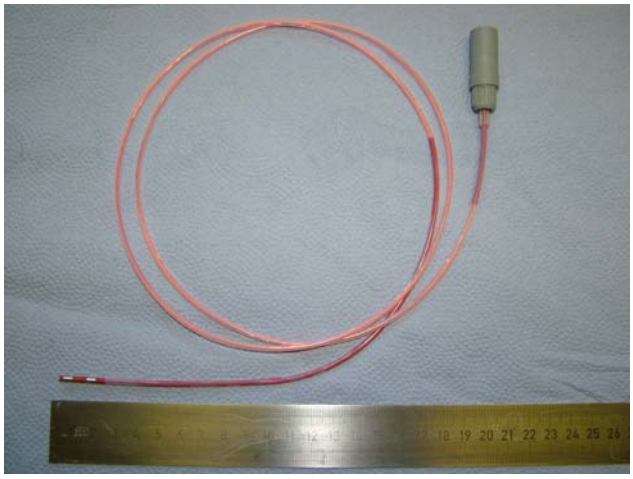

Figure 16[29]

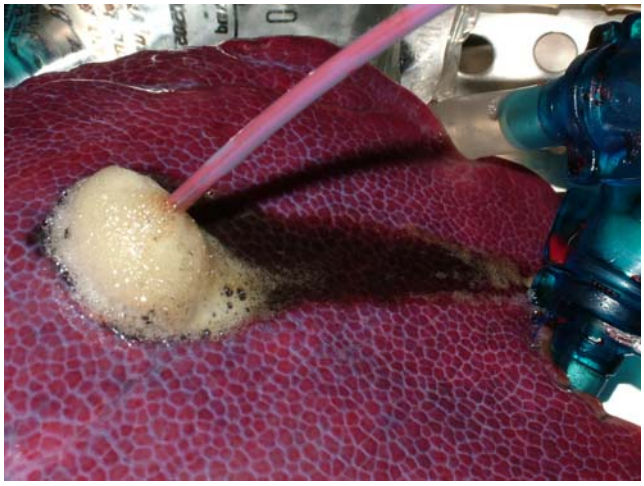

Figure 17[30]

[28] Direct current generator (ECU 100, Söring GmbH, Justus-von-Liebig-Ring 10, D-25451 Quickborn, Germany).
[29] Platinum electrodes (Johnson and Johnson, 6 French, 2 mm diameter).
[30] Hepatic electrolytic ablations.

Radiofrequency ablation

After the first hour of perfusion the applicator was inserted through the hepatic parenchyma. To achieve 2cm diameter of the ablated lesion the RFA generator (Radionics Cool-Tip RF system - Valleylab, CL, United States; Figure 18) was set at a power of 20 Watts, current of 70 Ampere, impedence of 45 Ohms. The 2-mm diameter tip used for the energy delivery was directly inserted 1-cm deep into the hepatic parenchyma (Figure 19). The grounding plate was placed on the liver surface away from the tip insertion on the liver surface opposite to the one where the probe was inserted, so that energy would travel through the liver parenchyma to create the thermal ablation. To achieve 2cm diameter of the ablated lesion each RFA ablation lasted 20 minutes and the temperature generated reached 24°C (Figure 20).

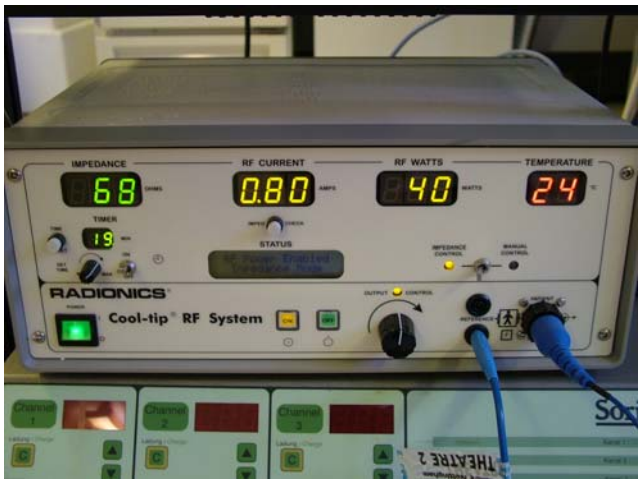

Figure 18[31]

Figure 19[32]

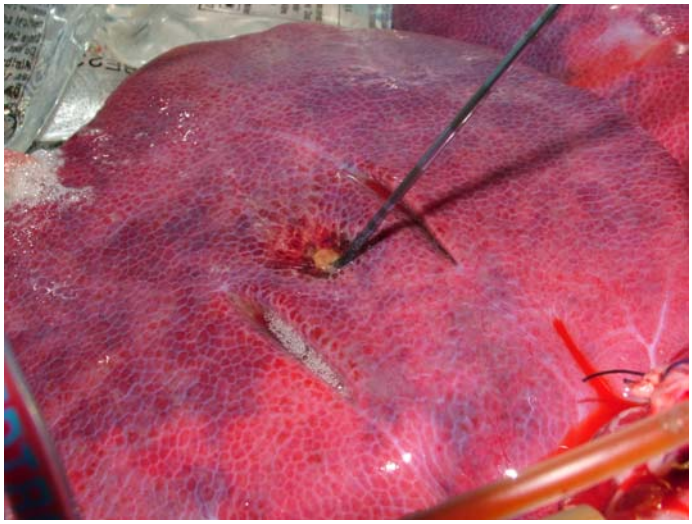

Figure 20[33]

Outcomes evaluated

Different parameters were measured according to the timescale of the experiment (Figure 21).

[31] Radiofrequency generator.
[32] Radiofrequency probe.
[33] Hepatic radiofrequency ablations.

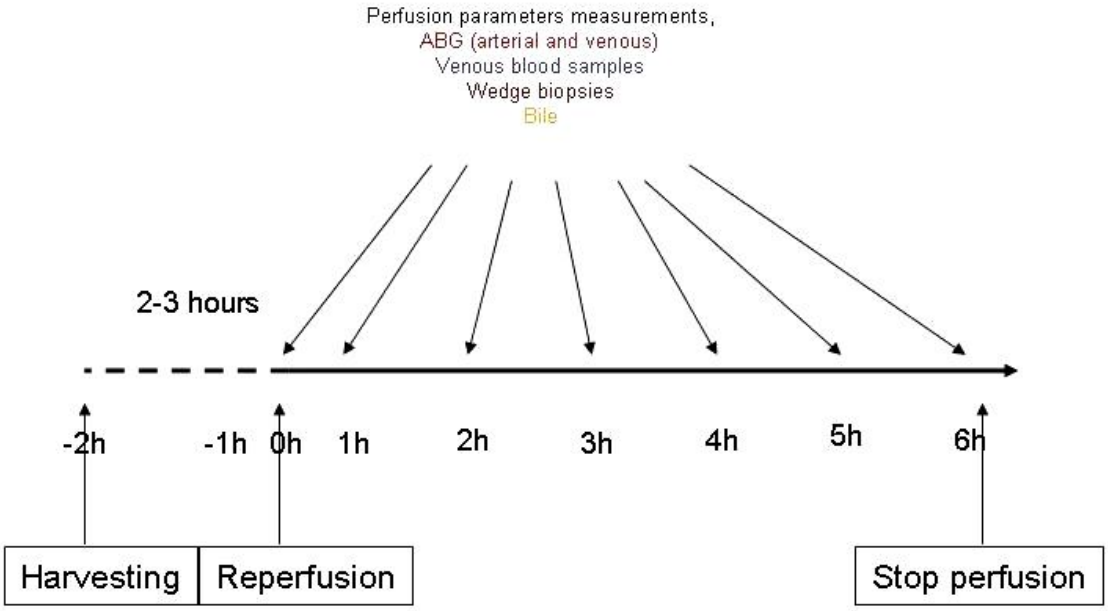

Figure 21[34]

Standard perfusion parameters

Physiological parameters of the organ and of the perfusion were recorded (liver weight, hot and cold ischemia time, hepatic artery - HA - and portal vein - PV - pressures and flows).

Acid base parameters

Arterial blood samples for gas analysis were collected immediately after the reperfusion and hourly until the 6th hour. Samples were immediately analysed using an automated analyzer (ABL800 FLEX; Radiometer Medical ApS, Brønshøj, Denmark). Parameters evaluated were pH, CO_2, Bicarbonate (HCO_3^-), Lactate, Base Excess (BE) and Anion Gap (AG). Venous blood samples

[34] Timescale of the experiments.

for gas analysis were also collected immediately after the reperfusion and hourly until the 6th hour, and immediately analysed using the automated analyzer.

Assessment of liver viability

Rates of drug infusions were titrated according to results obtained from the arterial and venous blood analyses. During the perfusions the organ's viability was checked by assessing three parameters, the arteriovenous oxygen and carbon dioxide extraction ratio and the hourly production of bile (228). The consumption of oxygen and production of carbon dioxide are properties of living cells only and have been associated with the organ's viability during extracorporeal hepatic perfusions (228). The arteriovenous oxygen and carbon dioxide differences were calculated from the arterial and venous blood gases collected hourly during the perfusions. The hepatic metabolic rate for oxygen (HMRO) was calculated by adapting the formula for the cerebral metabolic rate for Oxygen: HMRO = (arteriovenous difference for oxygen x hepatic blood flow) / liver weight (229). Finally, bile production is an indicator of the metabolic performance of the liver and an indirect proof of the viability of liver cells, because only living cells can synthetise bile (221, 228, 230, 231). The bile produced was collected in small containers from the cannulated CBD and measured hourly during the perfusion.

Biochemical parameters

Haematological samples were stored in the appropriate Vacutainer overnight, while biochemical samples were centrifuged and the serum extracted. The Pathology laboratories of the Leicester General Hospital analysed the samples using the Sysmex SF3000 and the Siemens Advia 2120 analysers. Parameters evaluated were pH, CO_2, HCO_3^-, Lactate, BE and AG. Biochemical

parameters such as haemoglobin, number of red blood cells, hematocrit, lactate, glucose, albumin, alanine aminotransferase (ALT), alkaline phosphatase and total bilirubin were also examined. ALT concentrations were used as an index of liver injury, alkaline phosphatase as an index of biliary stasis and albumin as an index of protein synthetic capacity.

Cytokines sample collection

Numerous kits analyse single porcine cytokines but only one, the Searchlight Porcine Cytokine Array® (Thermo Fisher Scientific, Woburn, Massachusetts, United States), simultaneously dose nine cytokines in the same sample of porcine serum. Because no previous studies were conducted on porcine cytokines, especially in an *ex-vivo* liver perfused model, it was decided to use the Searchlight kit that provided the largest number of cytokines dosed with only one sample and to use this kit as a screening tool for the nine cytokines to evaluate differences during the perfusions and among the various ablative techniques. Serum samples for the cytokine assay were collected at different time points: before adding the blood to the perfusion circuit, immediately after the start and hourly throughout the entire perfusion. Blood samples were centrifuged and the serum separated and stored at -70ºC in liquid nitrogen. Once all samples from the various experiments were collected they were sent to the manufacturer in liquid nitrogen (Thermo Fisher Scientific, Woburn, Massachusetts, United States) and were analysed using the Searchlight Porcine Cytokine Array® for Interleukin (IL) -1ß, IL-2, IL-4, IL-6, IL-8, IL-10, IL-12, Interferon (IFN) -γ, Tumor Necrosis Factor (TNF) -α with an ELISA technique.

Histological analysis

All biopsies were gathered from the liver surface at precise time points: immediately before the flushing of the Soltran solution (time -2), after adding the warm Normal Saline to the organ (time -1), 2-3 minutes following reperfusion (time 0) and then every two hours until the end of the experiment (2^{nd}, 4^{th} and 6^{th} hour of perfusion). The specimens were collected and immediately added into formalin. At the end of the experiment specimens were delivered to the Department of Histopathology at the Leicester Royal Infirmary where they were embedded with paraffin and processed for standard Hematoxylin-Eosin and Immunoistochemistry.

The analysis of slides was conducted in a blind fashion, labelling samples with a random generated code. The examiner (G.G.) was not aware of the time point at which biopsies were collected until the code was broken at the end of the statistical evaluation.

Morphologic analysis and ISHAK score

To evaluate the histopathological changes of the liver during the perfusions it was necessary to find a validated and reliable scoring system that could easily be used on the samples collected. After a careful search it became evident that the most validated and used scores were those used for the degree of activity during chronic hepatitis (Table 14) (232). Three scores were initially selected and discussed with the liver pathologist and the statistician: the Knodell Histological Activity Index, the Ishak score (a modification of the Knodell Histological Activity Index), and the METAVIR scoring system (233-235). Parameters evaluated in these scores for necro-inflammatory activity are the periportal, bridging, lobular, confluent necrosis and periportal inflammation. Fibrosis is examined in all scores but it was anticipated that the duration of perfusion was not sufficient to allow any collagen deposition. The ISHAK score can reach a maximum of 24 points, the Knodell only 22 and the METAVIR 13. Furthermore the ISHAK and METAVIR scores evaluate the necro-inflammatory activity with four different parameters, the Knodell score only 3. Combining the maximum possible score with the highest number of parameters available for the necro-inflammatory activity, the ISHAK score was the most reliable and precise for our purpose.

Specimens were immediately fixed in 10% paraformaldehyde and stored in the fridge (-4°C) overnight. The following day they were embedded in paraffin, cut in thin slices (3-5 μm) and stained with standard Hematoxylin-Eosin. Samples were then analysed with the ISHAK score.

Immunohistochemistry

Immunohistochemistry for apoptosis was conducted with the Dako antibody Clone Mib-1 (Dako UK Ltd Cambridge House, St Thomas Place, Ely, Cambridgeshire – United Kingdom) using a dilution of 1:300. Heat mediated antigen retrieval was carried out at high pH using a Dako PT Module. Immunohistochemistry for regeneration was conducted with the Abcam primary Ki67 antibody (rabbit polyclonal) using a dilution of 1:200. Heat-mediated antigen retrieval was carried out at low pH using a Dako PT Module. In both evaluations, immunohistochemistry was carried out automatically on a Dako Autostainer by means of the streptavidin-biotin system (Dako Envision FLEX system) using diaminobenzidine as final chromogen. For both evaluations, the positive control was human tonsil and a negative control was included with the primary antibody omitted.

Apoptotic cells were identified when there was evidence of Caspase-3 positivity. This protease has been implicated as an effector caspase associated with the initiation of the death cascade. Caspase-3 is activated by the upstream caspase-8 and caspase-9, and it serves as a convergence point for different signaling pathways. Therefore, it is an important marker of the cell's entry point into the apoptotic signaling pathway (236).

The apoptotic index was expressed as the ratio of the number of hepatic cells with Caspase positivity out of the total number of nucleated cells in each field (magnification, x400) calculated after counting 25 total microscopic fields for a specific timepoint (5 fields for each slide). Regenerative cells were defined when Ki-67 positivity was evident. The regenerative index was expressed as the ratio of the number of Ki-67 positive cells out of the total number of nucleated cells in each field (magnification, x400) calculated after counting 25 total microscopic fields for a specific timepoint (5 experiments, 5 fields for each slide).

Score	Periportal Necroinflammatory Changes	Bridging and Confluent Necrosis	Focal (Spotty) Lobular Necrosis and Hepatocellular Apoptosis	Portal Inflammation	Fibrosis
0	Absent	Absent	Absent	None	No fibrosis
1	Mild (focal, few portal areas)	Focal confluent necrosis	One focus or less per 10x field	Mild, some or all portal areas	Fibrosis expansion of some portal areas, with or without short fibrous septa
2	Mild/Moderate (focal, most portal areas)	Zone 3 necrosis in some areas	Two to 4 foci per 10x field	Moderate, some or all portal areas	Fibrosis expansion of most portal areas, with or without short fibrous septa
3	Moderate (continuous around <50% of tracts or septae)	Zone 3 necrosis in most areas	Five to 10 foci per 10x field	Moderate/marked, all portal areas	Fibrosis expansion of most portal areas, with occasional portal to portal bridging
4	Severe (continuous around >50% of tracts or septae)	Zone 3 necrosis + occasional portal-central bridging necrosis	More than 10 foci per 10x field	Marked, all portal areas	Fibrosis expansion of portal areas, with marked bridging (portal to portal as well as portal to central)
5		Zone 3 necrosis + multiple portal-central bridging necrosis			Marked bridging with occasional nodules (incomplete cirrhosis)
6		Panacinar or multiacinar necrosis			Cirrhosis, probable or definite

Table 14[35]

[35] ISHAK score.

Sample size estimation

The sample size was calculated using the NCSS 2007 Statistical & Power Analysis Software (Kaysville, Utah, USA). For the calculation we adopted the bilirubin as a gold-standard parameter of the hepatic function. Considering a mean total bilirubin value of 0.60 ± 0.25 mg/dl in adult healthy guinea pigs and an alpha value of 0.05, we obtained a power of 76% with a sample size of 5 livers in each group. Seven livers were perfused without ablation and used as controls, 5 livers underwent EA and 5 RFA. Therefore, 17 experiments were conducted in total.

Statistical analysis

All data were initially inserted into an Excel database (Microsoft, Redmond, Washington – United States) and analysed with the Statistical Package for the Social Sciences Windows version 13.0 (SPSS, Chicago, Illinois, USA). Descriptive statistics used for continuous variables were the mean and standard deviation for continuous parametric variables, median and range for continuous non-parametric variables and frequencies for categorical variables. Normality assumptions were demonstrated with histograms and the Kolmogorov/Smirnov test. For cytokines concentrations, data were normalized after an initial evaluation using a natural logarithmic conversion.

The Friedman test for repeated measures and the ANOVA test for repeated measures were used to assess differences over the hours for non-parametric and parametric variables respectively, including logarithmic normalized data of cytokine concentrations. Correlations were performed

with the Pearson correlation test for parametric variables, Spearman's correlation test for non-parametric variables and with a regression logistic analysis using the stepwise method. The normalized Area Under the concentration-time Curve (AUC) has been calculated for all cytokines using the logarithmic values after correction for the baseline levels. A p value of <0.05 was considered statistically significant.

Results

Standard perfusion parameters

Controls

The mean liver weight was 1709 ± 351 grams, warm ischemia time 19 ± 2 minutes (Table 15), cold ischemia time was 164 ± 22 minutes. The measurement of the HA and PV pressures and flows recorded during the experiments did not evidence any significant differences over the hours (ANOVA test for repeated measures, *p*=NS) (Table 16, Figure 22-25).

Electrolytic ablation

No differences were present between controls and EA for mean liver weight (1709 ± 351 grams vs. 1810 ± 309 grams; Student's t test, *p*=NS), warm ischemia time (19 ± 2 minutes vs. 19 ± 4 minutes; Student's t test, *p*=NS) and cold ischemia time (164 ± 22 minutes vs. 168 ± 35 minutes; Student's t test, *p*=NS). No significant differences in HA and PV pressures and flows recorded during the experiments were present over the hours and compared to controls (ANOVA test for repeated measures, *p*=NS) (Table 16).

Radiofrequency ablation

No differences were present between controls and RFA for mean liver weight (1709 ± 351 grams vs. 1821 ± 343 grams; Student's t test, *p*=NS), warm ischemia time (19 ± 2 minutes vs. 19 ± 3 minutes; Student's t test, *p*=NS) and cold ischemia time (164 ± 22 minutes vs. 169 ± 29 minutes;

Student's t test, *p*=NS). No significant differences in HA and PV pressures and flows recorded during the experiments were present over the hours and compared to controls (ANOVA test for repeated measures, *p*=NS) (Table 16). Concerning the hypothesis of the study, no significant differences were found between EA and RFA for liver weight, warm and cold ischemia times, HA and PV pressures and flows (Student's t test and ANOVA test for repeated measures, p=NS). Therefore the null hypothesis has been true and the alternative hypothesis has been rejected.

Type of experiment	Date	Warm ischemia (min)
Control 1	28/02/2008	16
Control 2	05/03/2008	19
Control 3	06/03/2008	20
Control 4	17/03/2008	22
Control 5	10/04/2008	18
Control6	14/04/2008	22
Control 7	17/04/2008	19
RFA 1	23/07/2008	24
RFA 2	29/07/2008	22
RFA 3	24/07/2008	17
RFA 4	13/11/2008	19
RFA 5	15/01/2009	16
EA 1	22/01/2009	19
EA 2	29/01/2009	14
EA 3	05/03/2009	24
EA 4	12/03/2009	19
EA 5	15/05/2009	19

Table 15[36]

Hour	HA pressure (mmHg)			HA flow (L/min.)			PV pressure (mmHg)			PV flow (L/min.)		
	Controls	EA	RFA	Controls	EA	RFA	Controls	EA	RFA	Controls	EA	RFA
0	89 ± 5	87 ± 8	82 ± 17	0.21 ± 0.11	0.30 ± 0.05	0.35 ± 0.07	28 ± 13	29 ± 8	24 ± 7	0.73 ± 0.42	0.86 ± 0.37	0.81 ± 0.22
1	87 ± 4	94 ± 16	80.1 ± 16	0.34 ± 0.18	0.35 ± 0.09	0.41 ± 0.09	27 ± 6	24 ± 6	25 ± 5	0.73 ± 0.49	1.02 ± 0.32	0.90 ± 0.21
2	86 ± 4	89 ± 10	82 ± 17	0.34 ± 0.17	0.33 ± 0.11	0.42 ± 0.08	31 ± 13	27 ± 4	26 ± 6	0.86 ± 0.28	0.85 ± 0.29	0.80 ± 0.18
3	82 ± 13	89 ± 10	81 ± 16	0.30 ± 0.16	0.36 ± 0.12	0.40 ± 0.08	29 ± 14	26 ± 10	27 ± 7	0.95 ± 0.27	0.87 ± 0.16	0.89 ± 0.19
4	87 ± 4	90 ± 11	80 ± 16	0.26 ± 0.11	0.38 ± 0.14	0.42 ± 0.08	27 ± 12	22 ± 5	28 ± 8	0.94 ± 0.23	0.89 ± 0.23	0.95 ± 0.24
5	85 ± 3	92 ± 13	77 ± 14	0.29 ± 0.09	0.39 ± 0.14	0.34 ± 0.08	22 ± 10	20 ± 7	23 ± 3	1.10 ± 0.13	0.93 ± 0.30	0.91 ± 0.21
6	83 ± 4	85 ± 7	78 ± 18	0.30 ± 0.10	0.37 ± 0.11	0.36 ± 0.07	22 ± 11	22 ± 4	30 ± 8	1.10 ± 0.09	0.93 ± 0.28	0.90 ± 0.20

Table 16[37]

[36] Warm ischemia times for each experiment in the abbatoir.

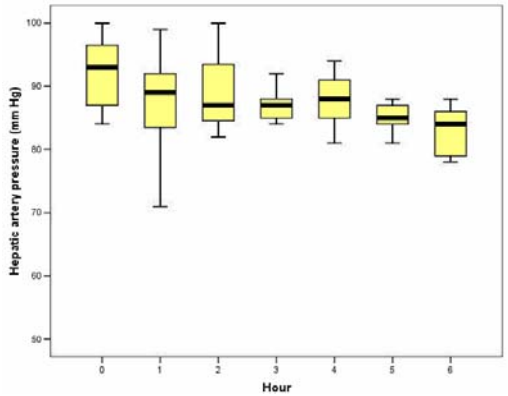

Figure 22

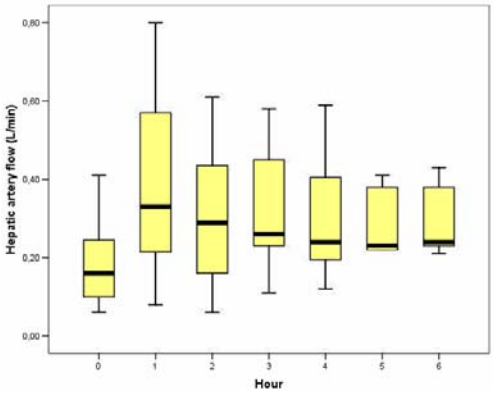

Figure 23

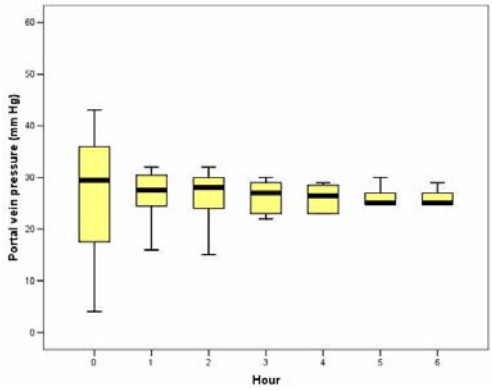

Figure 24

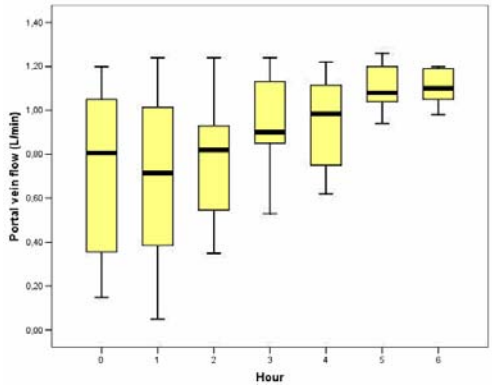

Figure 25[38]

Acid-base parameters

Controls

Acid-base results are shown in Table 17 and Figure 26. No significant changes were observed over time for pH and CO_2 compared to baseline levels (ANOVA test for repeated measures, *p*=NS) (Figure 26). A significant increase of HCO_3^- and AG was present from the second

[37] Physiological parameters of the perfusion. HA = Hepatic artery. PV = Portal vein. Values represent mean ± standard deviation. EA = Electrolytic ablation. RFA = Radiofrequency ablation.
[38] Figure 21-24: Comparison of temporal trends for perfusion hemodynamic parameters. Horizontal lines within the box correspond to the median values, boxes to the 95% confidence intervals and vertical lines to the range of values.

hour, and for BE and lactate from the third hour (ANOVA test for repeated measures, $p<0.001$) (Figure 26).

Electrolytic and radiofrequency ablation

No significant differences were observed between controls and EA or RFA for pH, CO_2, HCO_3^-, BE, lactate and AG (ANOVA test for repeated measures, p=NS; Table 17, Figure 27). With regards to the hypothesis of the study, no significant differences were found between EA and RFA for pH, CO2, HCO3-, BE, lactate and AG (ANOVA test for repeated measures, p=NS). Therefore the null hypothesis has been true and the alternative hypothesis has been rejected.

Hour	PH			CO2 (mmHg)			HCO3- (mEq/L)			Lactate (mmol/L)			BE			AG (mEq/L)		
	Controls	EA	RFA	Controls	EA	RFA	Controls	EA	RFA	Controls	EA	RFA	Controls	EA	RFA	Controls	EA	RFA
0	7.4±0.2	7.3 ± 0.1	7.4 ± 0.1	40.8 ± 6.9	42.2 ± 0.9	41.2 ± 1.5	24.7 ± 7.0	24.5 ± 4.9	27 ± 11.1	3.4 ± 1.7	4.1 ± 0.5	3.7 ± 0.6	0.1 ± 8.3	-0.8 ± 5.7	2.5 ± 11.5	4.4 ± 4.9	6.6 ± 1.2	6.7 ± 0.7
1	7.3 ± 0.1	7.4 ± 0.2	7.4 ± 0.1	45.7 ± 3.5	46.7 ± 9.8	43.5 ± 3.7	23.7 ± 3.4	27.7 ± 6.5	26.3 ± 5.4	4.7 ± 1.0	5.6 ± 2.5	7.5 ± 3.8	-1.4 ± 3.7	2.6 ± 8.3	1.7 ± 5.9	12.5 ± 1.2	12.0 ± 3.4	19 ± 4.3
2	7.5 ± 0.1	7.5 ± 0.1	7.4 ± 0.1	46.0 ± 4.3	47.7 ± 7.5	44.2 ± 4.3	33.6 ± 12.1	34.1 ± 5.9	27.9 ± 3.7	7.4 ± 2.8	9.0 ± 4.4	8.4 ± 5.1	8.8 ± 11.2	10.0 ± 6.9	3.6 ± 4.0	15.0 ± 1.9	17.0 ± 5.2	21.6 ± 5.1
3	7.5 ± 0.1	7.5 ± 0.1	7.4 ± 0.04	47.9 ± 5.8	46.2 ± 7.0	46.5 ± 5.4	37.5 ± 6.6	34.8 ± 5.0	28.5 ± 4.1	9.1 ± 4.9	12.3 ± 6.1	9.6 ± 7.4	13.0 ± 6.6	11.0 ± 5.9	4.0 ± 4.1	16.9 ± 4.4	21.4 ± 6.8	25.3 ± 7.2
4	7.5 ± 0.1	7.5 ± 0.1	7.4 ± 0.02	45.1 ± 4.8	44.7 ± 5.5	46.9 ± 5.4	37.6 ± 6.4	34.2 ± 4.3	29.0 ± 3.8	11.8 ± 5.2	14.1 ± 7.7	10.7 ± 9.4	13.4 ± 6.5	10.5 ± 4.9	4.6 ± 3.5	20.8 ± 4.4	24.7 ± 9.0	28.1 ± 9.0
5	7.5 ± 0.1	7.5 ± 0.1	7.4 ± 0.04	46.3 ± 4.0	44.6 ± 6.6	49.7 ± 8.7	37.1 ± 6.0	34.7 ± 4.9	28.3 ± 4.5	10.5 ± 2.5	14.1 ± 8.0	11.7 ± 12.0	12.9 ± 6.1	11.0 ± 5.1	3.4 ± 4.4	21.0 ± 3.4	24.7 ± 9.3	30.3 ± 11.9
6	7.5 ± 0.1	7.5 ± 0.1	7.3 ± 0.1	48.4 ± 5.1	44.2 ± 5.1	57.4 ± 23.1	35.0 ± 6.2	34.6 ± 5.1	25.7 ± 6.8	12.1 ± 3.9	13.5 ± 8.9	12.8 ± 13.3	10.6 ± 6.6	10.9 ± 5.5	-0.3 ± 6.6	24.2 ± 6.0	26.7 ± 10.3	33.3 ± 15.2

Table 17[39]

[39] Arterial acid-base parameters. CO_2 = Carbon Dioxide. HCO_3^- = Bicarbonate. BE = Base Excess. AG = Anion Gap. Values represent mean ± standard deviation. EA = Electrolytic ablation. RFA = Radiofrequency ablation.

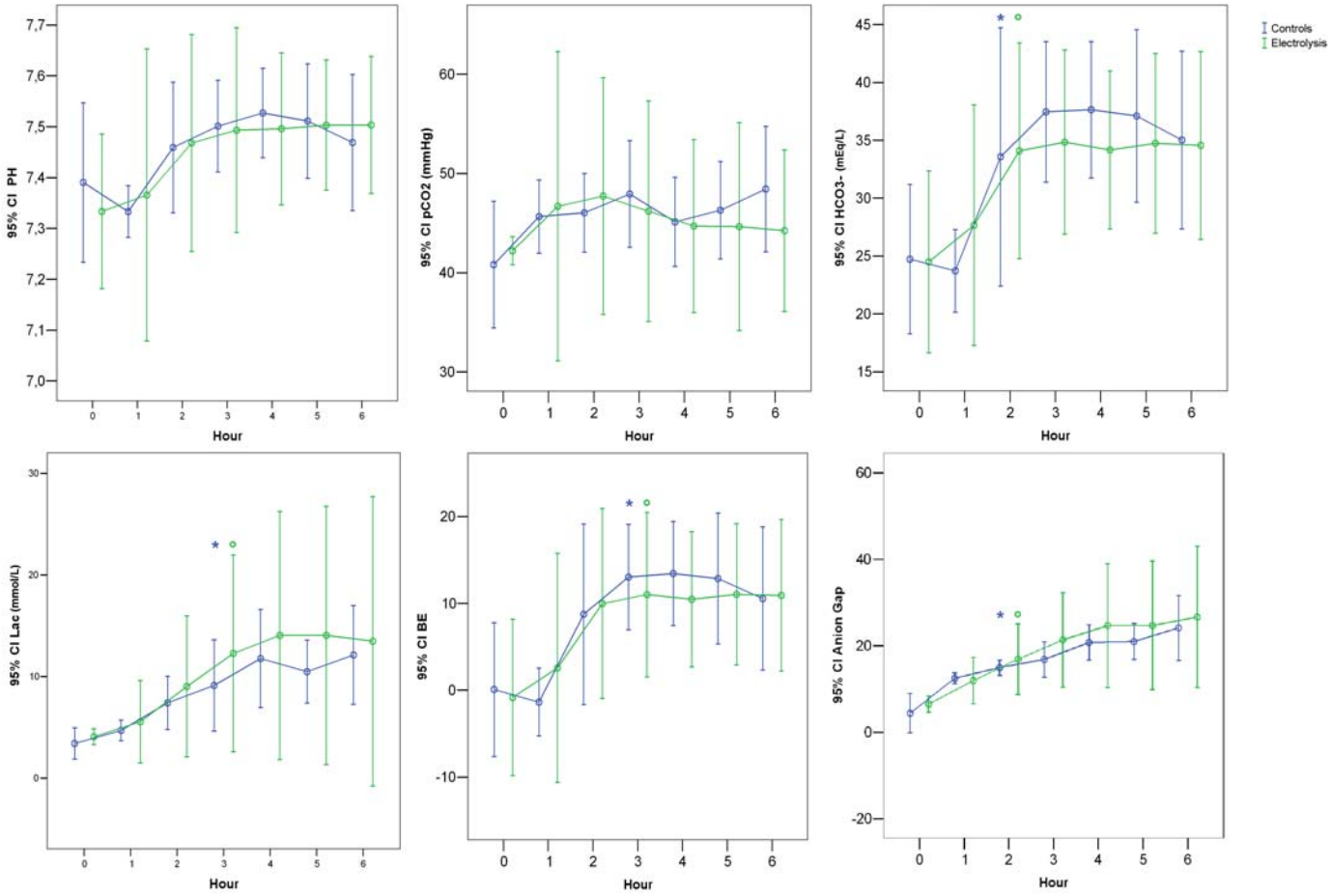

Figure 26[40]

[40] Comparison of temporal trends for pH, CO_2, HCO_3^-, Lactate, Base Excess, Anion Gap (controls and Electrolytic Ablation). Circles represent the median values, error bars the 95% Confidence Intervals.

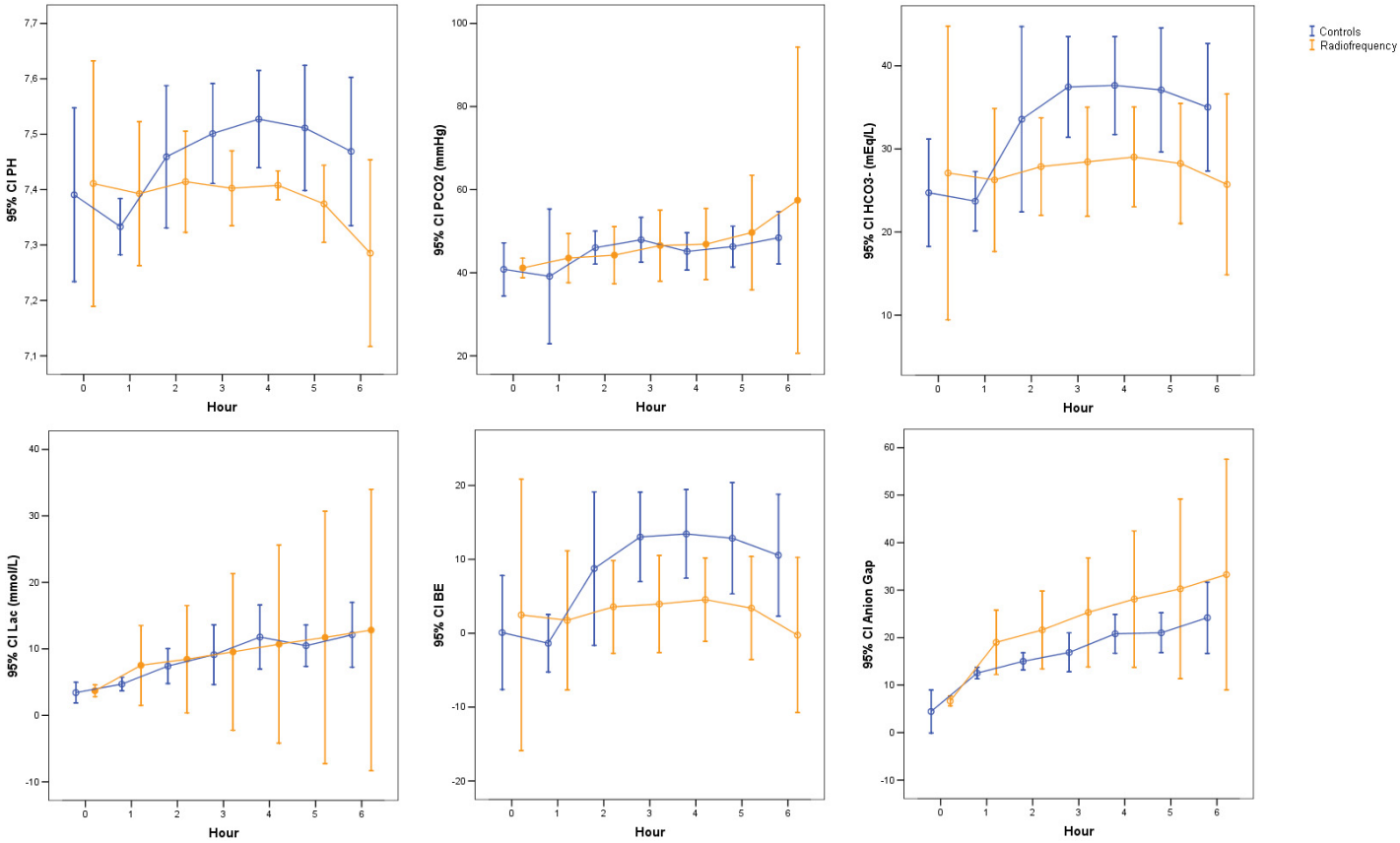

Figure 27[41]

[41] Comparison of temporal trends for pH, CO_2, HCO_3^-, Lactate, Base Excess, Anion Gap (controls and Radiofrequency Ablation). Circles represent the median values, error bars the 95% Confidence Intervals.

Assessment of liver viability

The arteriovenous difference of O_2 and CO_2 showed no significant change over time (Table 18; Figure 28-29). Similar results were obtained for the HMRO (Table 18).

Hour	Arteriovenous O_2 difference (mmHg)	Arteriovenous CO_2 difference (mmHg)	HMRO (mmHgxml/g/min)
0	263 (222-412)	8 (5-14)	41 (24-106)
1	285 (203-334)	7 (3-16)	44 (35-141)
2	281 (144-386)	8 (2-10)	43 (34-109)
3	260 (222-409)	7 (1-10)	44 (23-88)
4	276 (193-318)	7 (4-12)	46 (28-83)
5	241 (208-288)	8 (6-9)	39 (26-62)
6	274 (154-280)	8 (5-12)	39 (29-48)

Table 18[42]

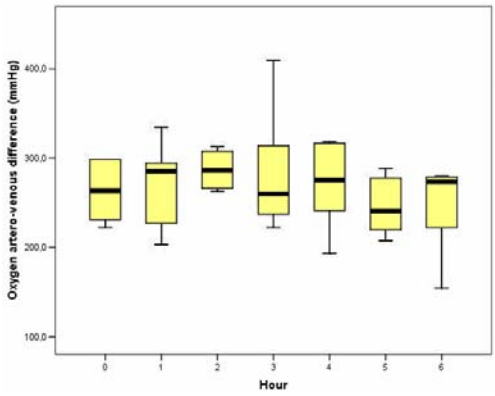

Figure 28

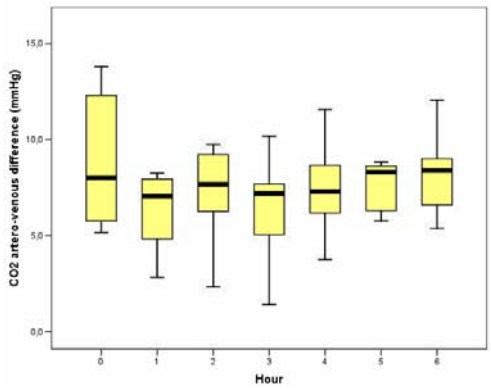

Figure 29[43]

The bile production in all experiments after an initial peak at the second hour of perfusion maintained a stable plateau until the end of the experiment (Table 19, Figure 30). No significant differences were present between controls, EA and RFA (ANOVA test for repeated measures, *p*=NS). Therefore the null hypothesis has been true and the alternative hypothesis has been rejected.

[42] Arteriovenous Oxygen and Carbon Dioxide differences and hepatic metabolic rate for oxygen values. AV = Arteriovenous. O_2 = Oxygen. CO_2 = Carbon Dioxide. HMRO = Hepatic Metabolic Rate of Oxygen. Values represent median (range).

[43] Fig.27-28: Comparison of temporal trends for Arteriovenous O_2 and CO_2 differences. Horizontal lines within the box correspond to the median values, boxes to first and third quartiles and vertical lines to the range of values.

	Bile production		
Hour	Controls	EA	RFA
0	0	0	0
1	16 ± 14	17 ± 11	16 ± 11
2	24 ± 14	23 ± 12	25 ± 14
3	15 ± 4	17 ± 5	16 ± 2
4	15 ± 4	16 ± 6	16 ± 4
5	17 ± 6	16 ± 5	17 ± 5
6	16 ± 6	17 ± 6	15 ± 6

Table 19[44]

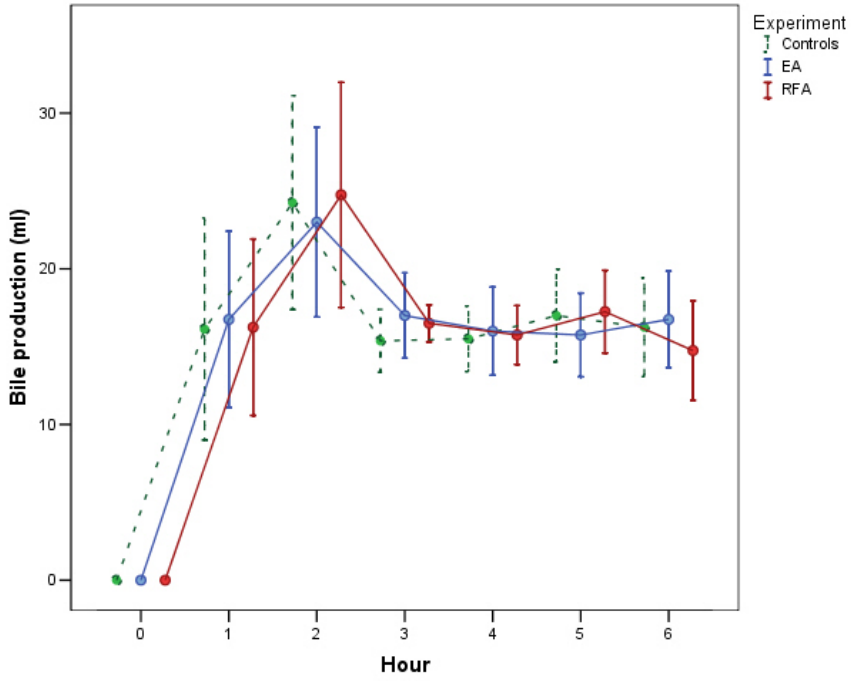

Figure 30[45]

[44] Hourly bile production (ml). EA = Electrolyitic Ablation. RFA = Radiofrequency Ablation.
[45] Error bar graph representing the production of bile according to controls, electrolytic ablation (EA) and radiofrequency ablation (RFA). Circles represent mean, bars one standard error of mean.

Biochemical parameters

Table 20 shows values obtained for hepatic and metabolic parameters investigated. The blood dilution significantly decreased the hemoglobin and the hematocrit to 40% of the original values (Friedman test, $p<0.05$; Table 20, Figure 31). Results demonstrated significantly elevated blood glucose values throughout the experiment compared to basal levels, consistent with a clinical scenario of a severe and prolonged hyperglycemia (Friedman test, $p<0.001$; Table 20, Figure 32).

The synthetic capacity reflected by the albumin synthesis did not significantly change (Friedman test, p=NS), although a trend towards lower values was observed throughout the experiment (Figure 33). A significant increase of alanine transaminase was noted when comparing levels before perfusion with those of the first hour and throughout the rest of the study period, and also between levels immediately after perfusion (time 0) compared with those of the first hour and throughout the experiment (Friedman test, $p<0.001$, Figure 34). No significant differences were observed between values before and immediately after perfusion, although an increased variability was observed in the latter (Friedman test, p=NS; Figure 34). No significant differences were observed for values of alkaline phosphatase (Friedman test, p=NS; Figure 35).

Hour	Hb (gr/dL)	Ht	RBC (10^6 x mm^3)	Glucose (mg/dL)	Albumin (g/dL)	Phosphatase (U/L)	Alanine Aminotransferase (IU/L)	Total Bilirubin (mg/dL)
0	11.6 (10.5-12.2)	0.40 (0.37-0.42)	6.7 (6.0-7.2)	34 (31-36)	12 (7-34)	78 (51-191)	14 (5-65)	<2
1	4.5 (2.9-5.0)	0.16 (0.10-0.18)	2.7 (1.5-3.3)	403 (25-782)	10 (8-11)	62 (53-81)	20 (8-100)	<2
2	4.0 (2.9-4.6)	0.14 (0.10-0.17)	2.4 (1.5-3.0)	709 (394-982)	9 (8-10)	82 (68-118)	98 (52-147)	<2
3	4.0 (2.8-4.5)	0.14 (0.10-0.17)	2.3 (1.5-2.9)	691 (322-1218)	8 (5-10)	88 (41-114)	109 (36-165)	<2
4	3.9 (2.9-4.6)	0.15 (0.11-0.17)	2.3 (1.7-2.9)	636 (173-1054)	9 (3-10)	107 (34-117)	105 (26-178)	<2
5	3.6 (2.8-4.1)	0.13 (0.10-0.16)	2.2 (1.5-2.3)	591 (118-709)	8 (7-9)	105 (67-129)	87 (49-117)	<2
6	4.0 (3.3-4.4)	0.15 (0.12-0.16)	2.3 (2.1-2.8)	564 (509-636)	8 (6-10)	122 (50-127)	108 (43-140)	<2
	3.8 (3.4-4.4)	0.14 (0.12-0.16)	2.2 (2.1-2.8)	545 (454-764)	10 (9-12)	114 (46-121)	117 (49-176)	<2

Table 20[46]

[46] Hepatic and metabolic parameters. Values represent median (range). Hb: Hemoglobin. Ht: Hematocrit. RBC: Red Blood Cells.

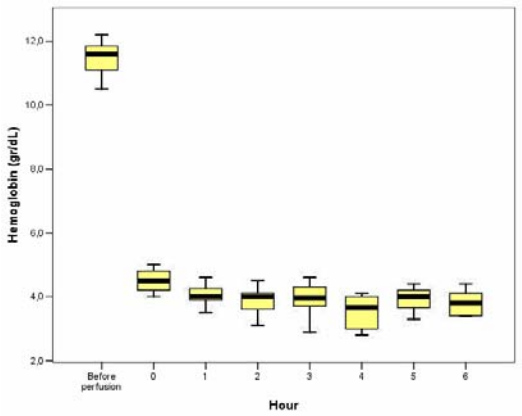

Figure 31

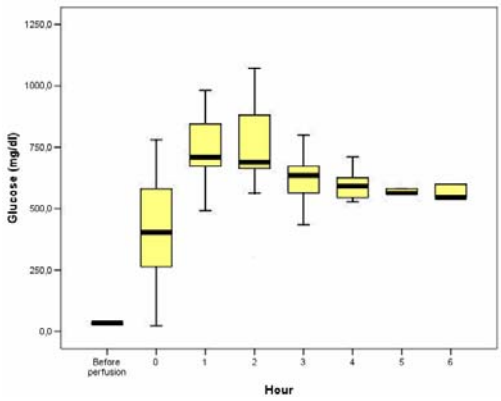

Figure 32

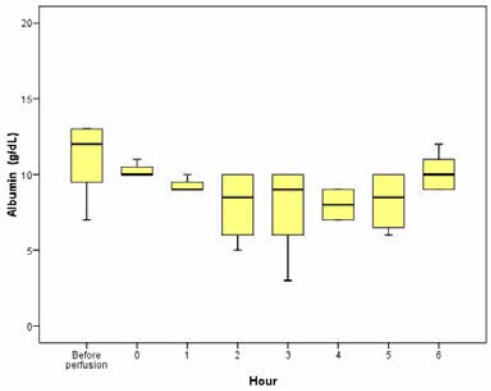

Figure 33

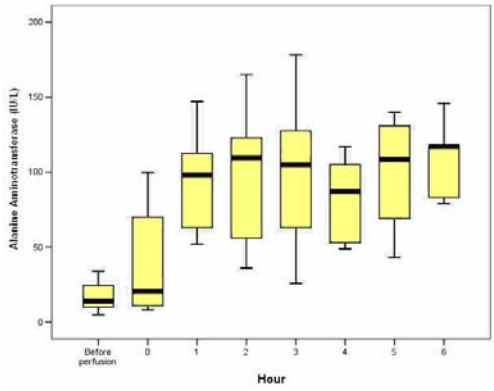

Figure 34

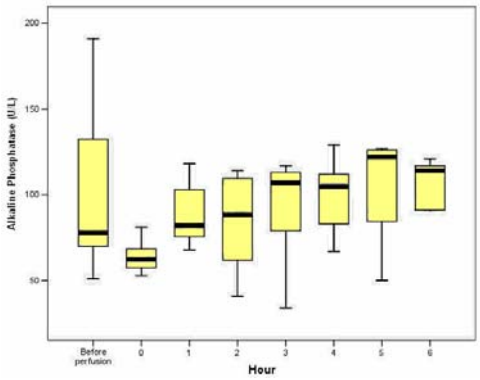

Figure 35[47]

[47] Figure 29-33: Metabolic and hepatic parameters. Horizontal lines within the box correspond to the median values, boxes to first and third quartiles and vertical lines to the range of values.

Cytokines

Controls

After an initial evaluation it was evident that cytokines values had a non-parametric distribution. In order to use parametric tests and avoid non-parametric ones for the statistical analysis, cytokines data were normalized using a natural logarithmic conversion. Cytokines logarithmic data assumed a parametric distribution and therefore parametric tests were used for the analysis.

Normalized logarithmic data obtained for cytokines concentrations are shown in Table 21. Trends over time for each cytokine are showed in Figure 36. The analysis of the Area under the Curve after correction for the baseline levels showed an increase for IL-2, IL-6, IL-8, IL-10 and IL-12 and a decrease for IL-1β, IL-4, IFN-γ and TNF-α (Figure 37). However, only IL-6 and IL-8 had significant changes over time compared to baseline levels (ANOVA test for repeated measures $p<0.001$) while the other cytokines had non significant variations (Figure 36). IL-6 concentration increased significantly from the third hour of perfusion compared to pre-perfusion value and remained significantly elevated (Figure 36). IL-8 concentrations became significantly elevated after the second hour of perfusion compared to pre-perfusion values and continued to rise in the subsequent period (ANOVA test for repeated measures $p<0.001$), and both cytokine concentrations demonstrated a sigmoid increase (Figure 36). No correlation was found between cytokine values and warm, cold and total ischemia time.

Group	Hour	ln IL-1ß	ln IL-2	Ln IL-4	ln IL-6	ln IL-8	ln IL-10	ln IL-12	ln IFN-γ	ln TNF-α
Controls	Before perfusion	3.0 ± 1.1	3.2 ±1.4	4.7 ±1.2	3.3 ±1.2	0.7 ±0.4	4.5 ±1.1	1.1 ±1.5	4.9 ±1.4	4.2 ±1.4
	1	2.7 ±1.1	3.8 ±1.0	4.7 ±1.0	2.9 ±1.0	1.8 ±0.4	4.8 ±0.7	1.2 ±1.0	4.8 ±1.3	4.2 ±1.1
	2	2.6 ±1.1	3.5 ±1.2	4.7 ±0.8	4.7 ±0.3	3.3 ±0.1	5.6 ±1.0	1.5 ±0.6	4.7 ±1.2	5.0 ±1.4
	4	3.2 ±0.6	3.5 ±0.6	4.7 ±0.6	7.3 ±0.2	6.7 ±0.6	5.5 ±1.1	1.8 ±0.4	4.6 ±1.1	4.4 ±1.2
	6	3.2 ±0.6	3.8 ±1.1	4.9 ±0.6	9.0 ±0.7	7.3 ±0.4	5.6 ±1.1	2.2 ±0.6	4.6 ±1.1	4.1 ±1.0
EA	Before perfusion	2.9 ±0.6	3.0 ±0.8	4.5 ±1.1	3.1 ±1.2	0.6 ±1.1	4.2 ±1.1	1.1 ±0.1	4.6 ±1.3	4.1 ±0.7
	1	2.2 ±0.9	2.3 ±1.8	3.9 ±1.5	3.0 ±1.5	2.6 ±1.5	6.7 ±1.0	1.5 ±0.3	3.8 ±1.6	4.6 ±0.5
	2	2.1 ±0.7	2.2 ±1.6	3.6 ±1.3	4.3 ±0.6	5.3 ±0.4	8.3 ±1.7	2.5 ±0.9	3.6 ±1.3	6.3 ±1.7
	4	2.5 ±0.4	2.3 ±1.5	3.6 ±0.9	7.9 ±0.9	6.8 ±0.4	8.6 ±1.8	2.6 ±1.0	4.5 ±1.0	6.3 ±1.7
	6	2.8 ±0.7	2.2 ±1.4	3.5 ±0.9	9.0 ±0.3	7.2 ±0.4	8.8 ±1.7	3.1 ±1.0	4.8 ±1.2	6.2 ±1.6
RFA	Before perfusion	3.1 ±0.4	3.4 ±0.2	4.8 ±0.3	3.6 ±0.2	0.9 ±0.2	4.5 ±0.7	1.3 ±0.1	5.1 ±0.1	4.4 ±0.3
	1	2.8 ±0.4	3.9 ±0.1	4.8 ±0.3	4.2 ±0.2	2.7 ±0.2	6.0 ±0.2	1.3 ±0.4	4.5 ±0.2	4.3 ±0.2
	2	2.8 ±0.4	3.9 ±0.3	4.8 ±0.4	4.6 ±0.1	4.8 ±1.1	7.5 ±0.4	2.0 ±0.2	4.4 ±0.2	5.1 ±0.4
	4	2.8 ±0.3	3.3 ±0.2	4.7 ±0.2	7.9 ±1.0	6.9 ±0.1	7.8 ±0.4	2.2 ±0.2	4.5 ±0.3	5.1 ±0.5
	6	3.0 ±0.2	3.4 ±0.2	4.4 ±0.2	9.2 ±0.4	7.3 ±0.2	7.6 ±0.3	2.4 ±0.3	4.5 ±0.2	4.8 ±0.3

Table 21[48]

[48] Normalized data following the logarithmic transformation from the original concentrations obtained with the cytokine analysis. Values summarise results of controls and ablation pigs and are expressed in log (pg/ml). EA = Electrolytic ablation.

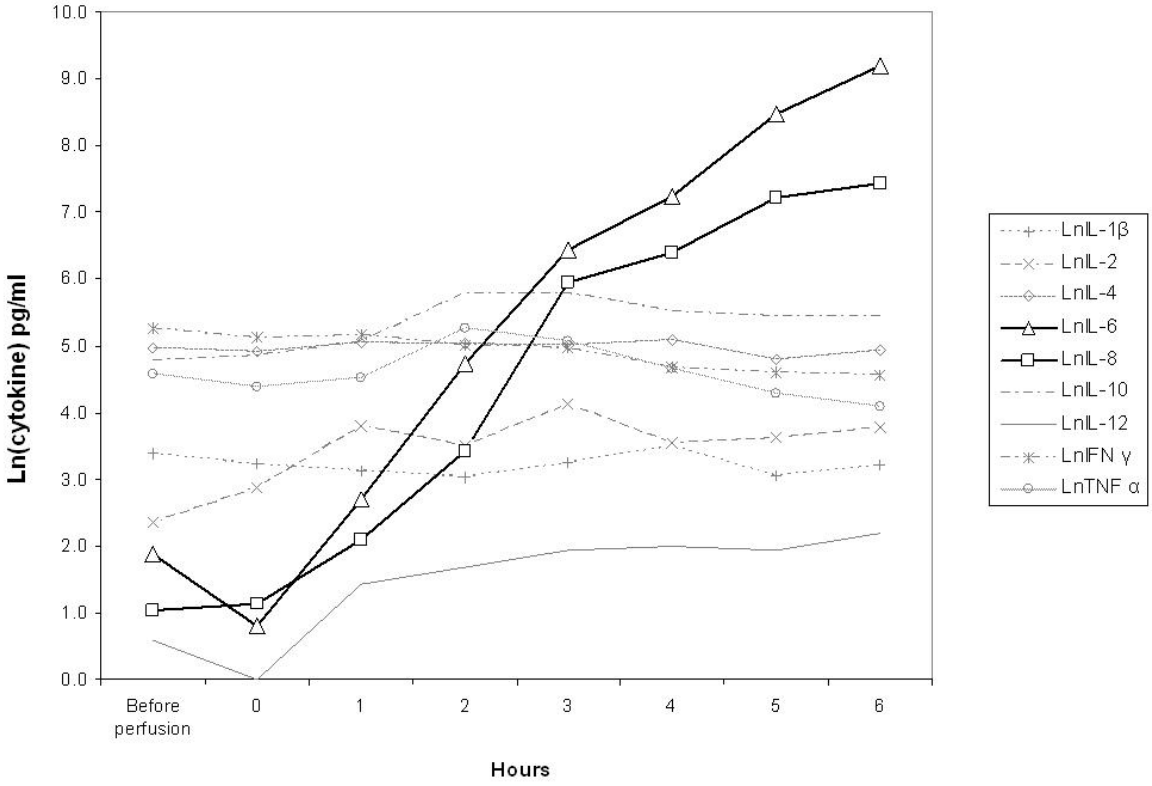

Figure 36[49]

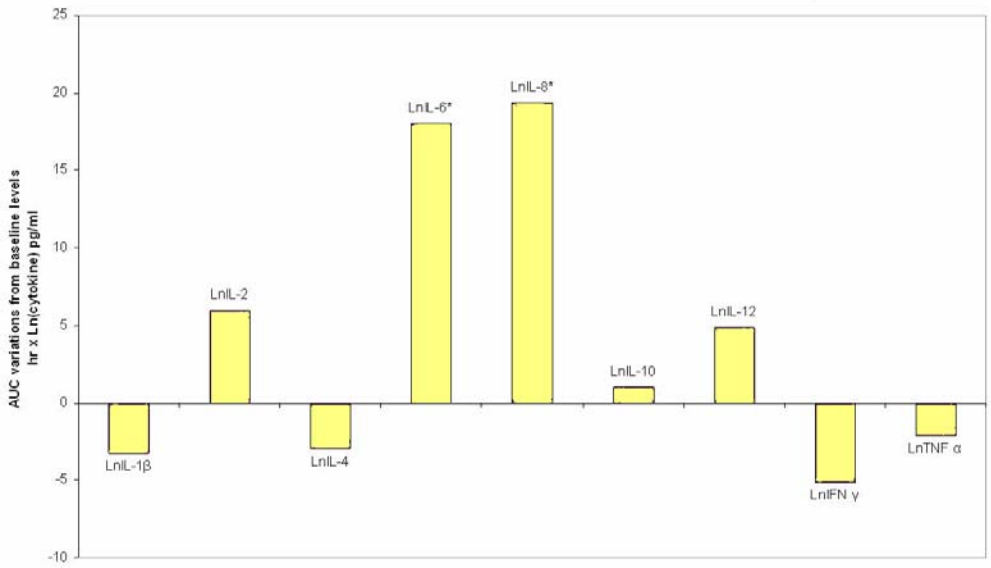

Figure 37[50]

[49] Temporal trends of cytokine values (means). Evidenced (black continue lines) are IL-6 and IL-8 which showed significant modifications over time.

[50] Modifications of the Area Under the Curve (AUC) from the baseline levels for each cytokine. Positive values represent an overall increase in the cytokine concentration, negative values represent an overall decrease. * = significant modification (p<0.05).

Electrolytic ablation

Significant changes were observed in the EA group for log IL-6 after the fourth hour, log IL-8 and log IL-10 after the second hour, and log IL-12 after the sixth hour when compared to baseline levels (ANOVA test for repeated measures, $p<0.001$; Figure 38-40). Significant differences were measured between the control and EA group for log IL-2, IL-4, IL-10 and TNF-α (ANOVA test for repeated measures, $p<0.001$; Figure 40). The log IL-2 and IL-4 were significantly decreased in the EA group when compared to controls, whereas log IL-10 and log TNF-α were increased (Figure 40).

Radiofrequency ablation

Significant changes were observed in the radiofrequency group for log IL-6 and log IL-8 after the second hour, log IL-10 after the first hour, and log IL-12 after the fourth hour when compared to baseline levels (ANOVA test for repeated measures, $p<0.001$; Figure 41-43). Significant differences were measured between the control and RFA group for log IL-8 and IL-10 (ANOVA test for repeated measures, $p<0.001$; Figure 43). In the RFA group the log IL-8 and IL-10 were significantly increased when compared to controls (Figure 43).

With regards to the hypothesis of the study, no significant differences were found between EA and RFA for the various cytokines analysed (ANOVA test for repeated measures, p=NS). Therefore the null hypothesis has been true and the alternative hypothesis has been rejected.

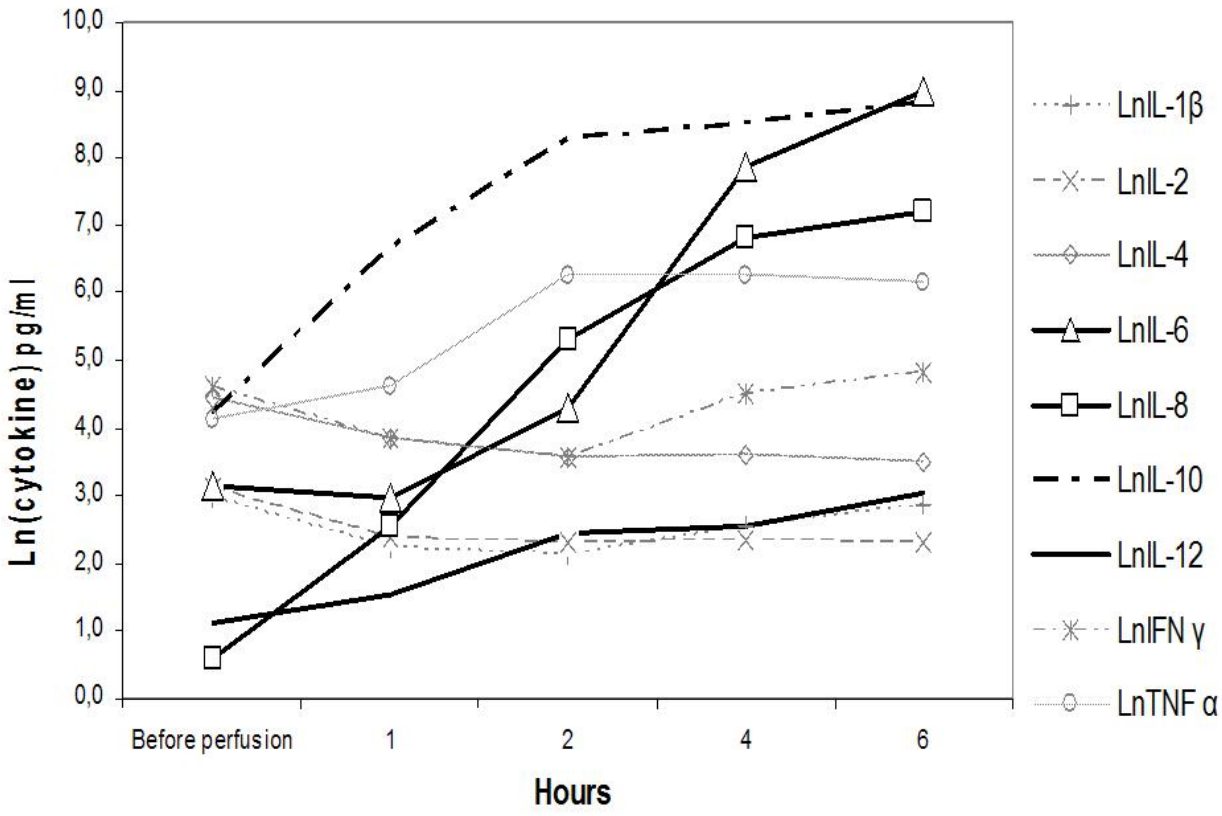

Figure 38[51]

[51] Temporal trends of cytokine values (means) from electrolytic ablations. Evidenced (black lines) are IL-6, IL-8, IL-10 and IL-12 which showed significant modifications over time.

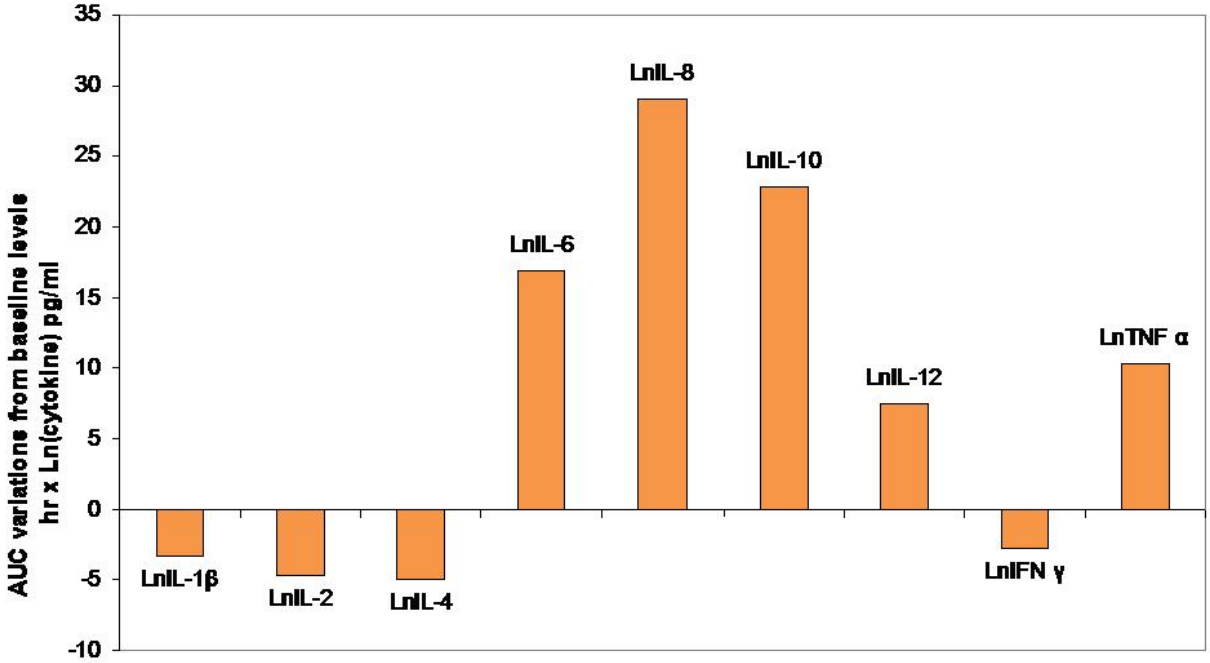

Figure 39[52]

[52] Modifications of the Area Under the Curve (AUC) from the baseline levels for each cytokine from electrolytic ablations. Positive values represent an overall increase in the cytokine concentration, negative values represent an overall decrease.

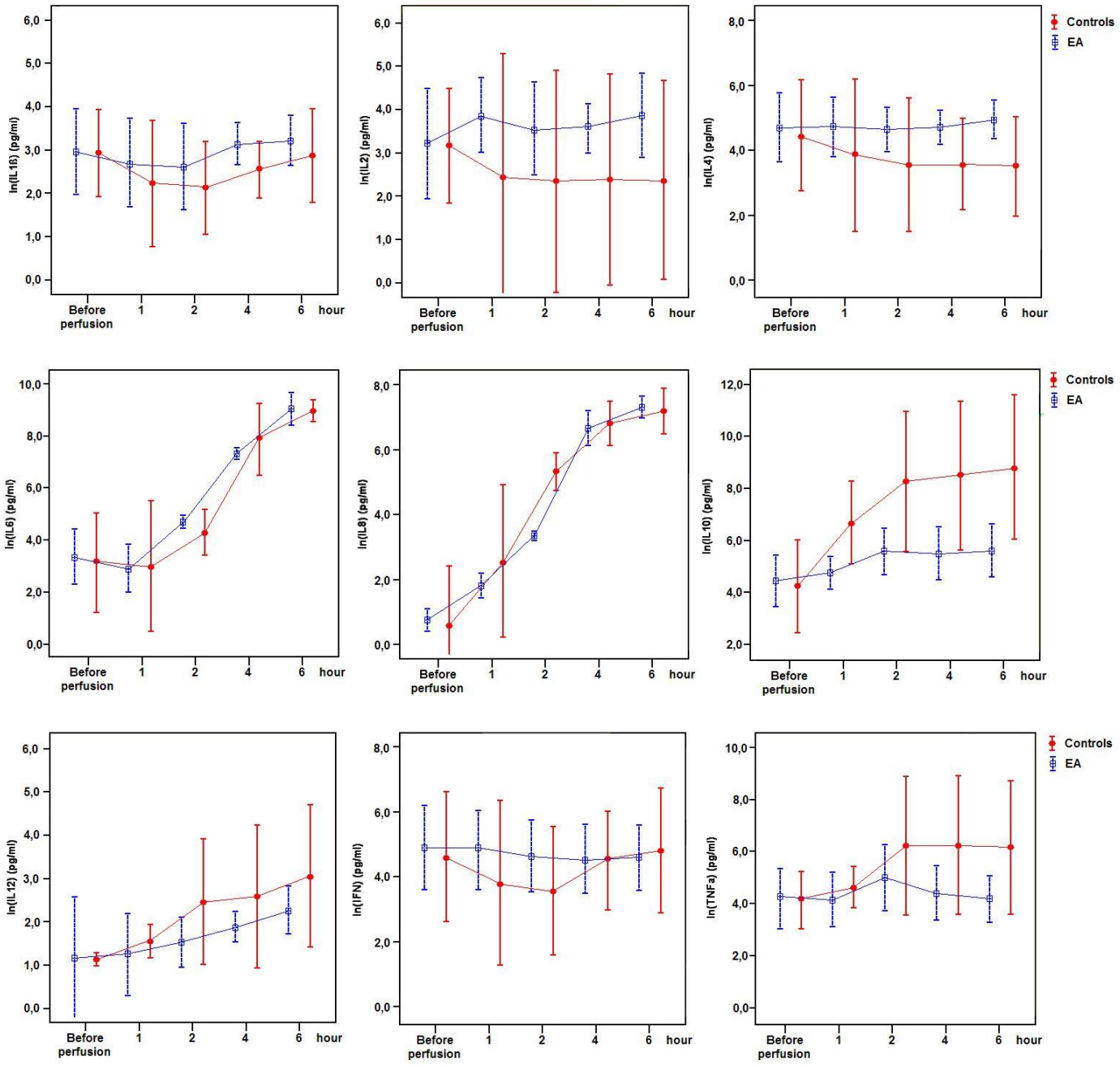

Figure 40[53]

[53] Comparison of temporal trends for each cytokine between controls and electrolytic ablations (EA). Error bars represent 95% Confidence Intervals.

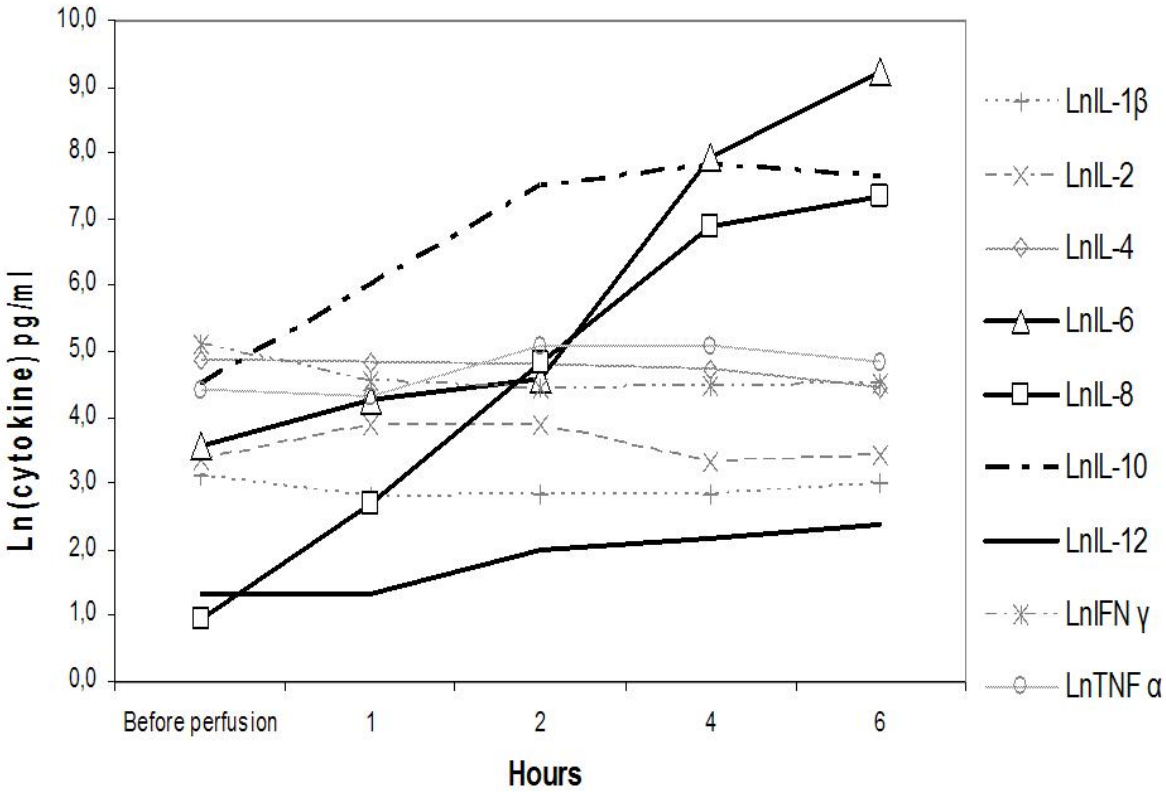

Figure 41[54]

[54] Temporal trends of cytokine values (means) from radiofrequency ablations. Evidenced (black lines) are IL-6, IL-8, IL-10 and IL-12 which showed significant modifications over time.

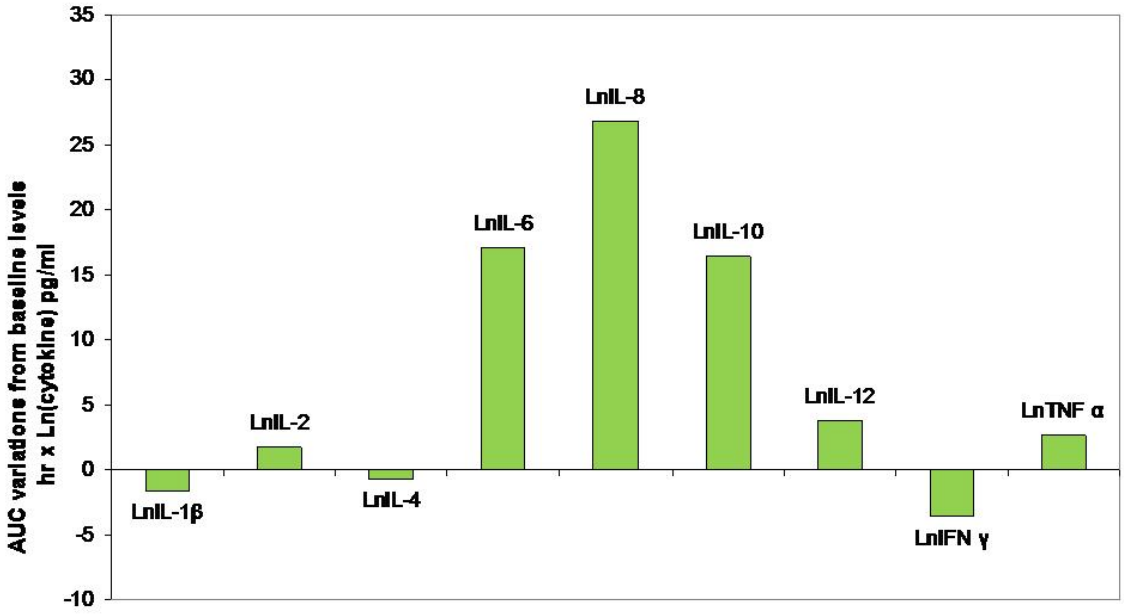

Figure 42[55]

[55] Modifications of the Area Under the Curve (AUC) from the baseline levels for each cytokine from radiofrequency ablations. Positive values represent an overall increase in the cytokine concentration, negative values represent an overall decrease.

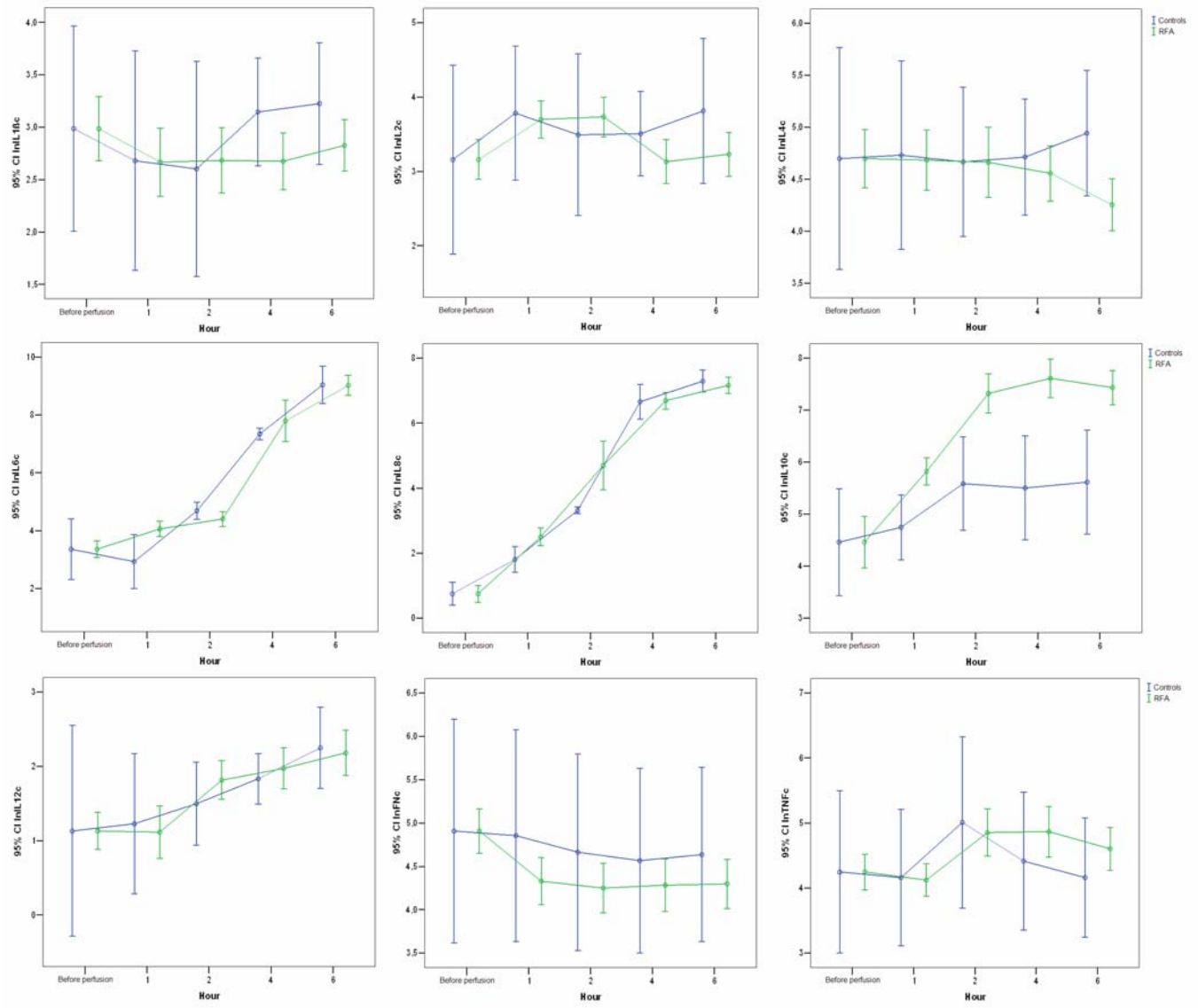

Figure 43[56]

[56] Comparison of temporal trends for each cytokine between controls and radiofrequency ablations (RFA). Error bars represent 95% Confidence Intervals.

Histology

Controls

Morphologic analysis and ISHAK score

Descriptive statistics are presented in Table 22. The ISHAK score showed two peaks of damage immediately before reperfusion and after 4 hours of perfusion, and two recoveries immediately following reperfusion and at 6 hours (Table 22, Figure 44). The ISHAK values after four hours of perfusion were significant different from those recorded at the animal's death and at six hours of perfusion (Friedman's test, $p<0.05$). The first necrotic peak derives from the bridging and confluent necrosis that occurs immediately before reperfusion, then progressively decreases during the next two hours of perfusion and peaks again at four hours. The second peak after four hours of perfusion is a combination of both bridging necrosis and the newly formed focal lobular necrosis that increases between the second and fourth post-reperfusion hours. Periportal necrosis was present to only a minor degree, while periportal inflammation and fibrosis were completely absent (Figure 44). Scattered necroses of single hepatocytes, microvesicular steatotic vacuolization, sinusoidal dilatation, red cell extravasation were observed (Figure 45-50).

	Animal's death	Before perfusion	0 hour	2 hour	4 hour	6 hour
ISHAK score	1.0 (0-4)	3.5 (0-10)	1.6 (0-4)	3 (1-6)	7 (4-10)	0 (0-3)
Apoptotic index (%)	0.5 (0-0.8)	0.2 (0-0.8)	0.7 (0.2-0.9)	0.2 (0-1.2)	0.5 (0.2-0.8)	0.2 (0-0.4)
Regenerative index (%)	2.3 (1.8-3.6)	0.9 (0.9-1.9)	2.6 (0.7-3.3)	2.1 (0.3-7.0)	1.2 (0.7-4.2)	4.1 (1.5-4.5)

Table 22[57]

[57] Values obtained for the ISHAK score, the apoptotic and the regenerative indexes.

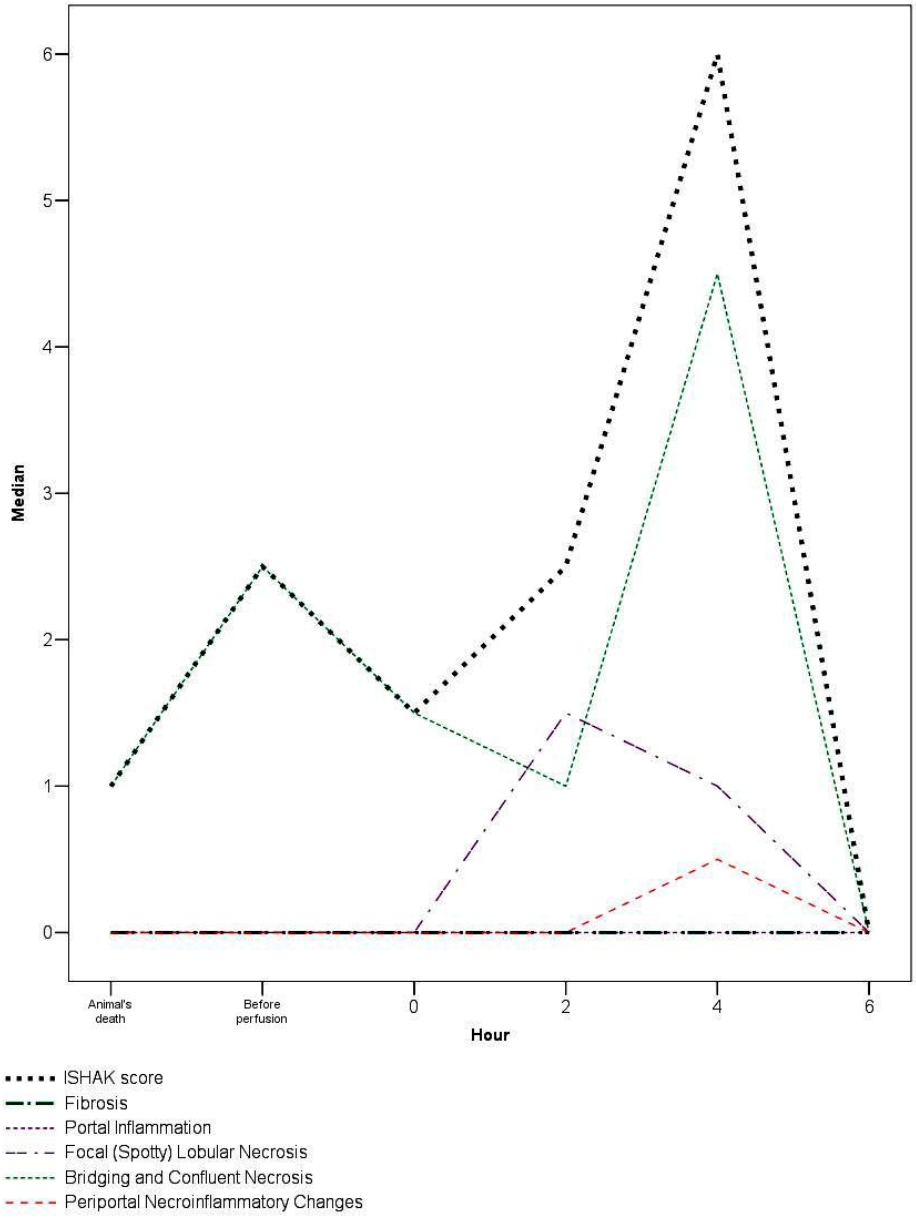

Figure 44[58]

[58] ISHAK score and single parameters assessed throughout the hours.

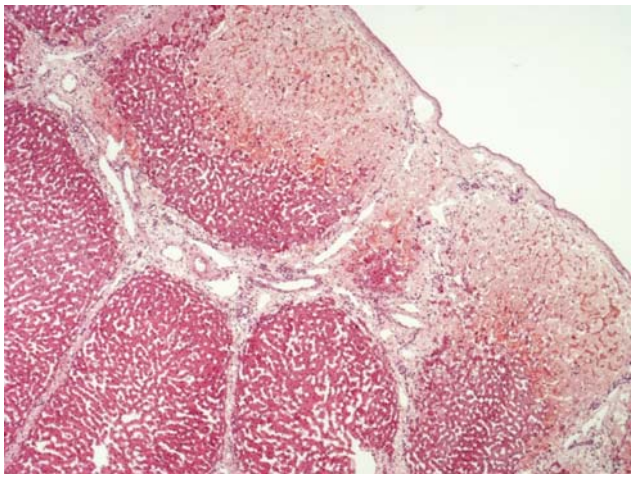

Figure 45[59]

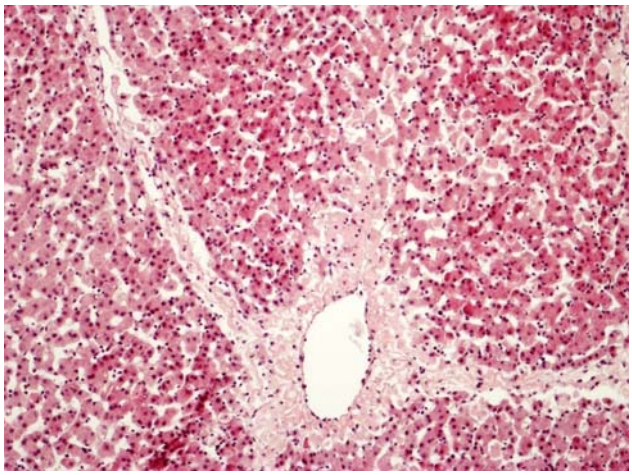

Figure 46[60]

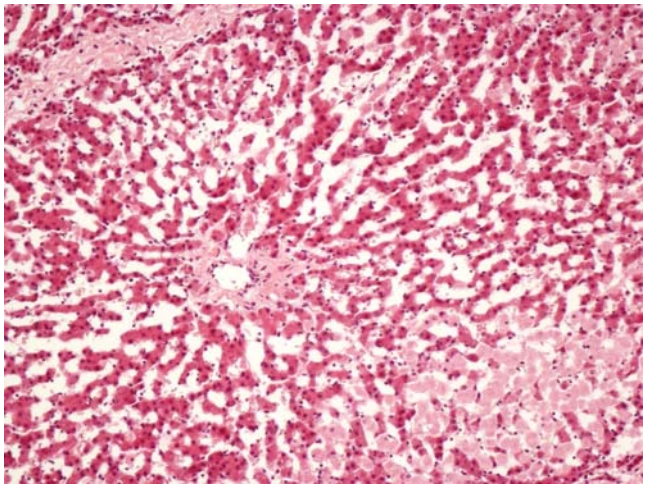

Figure 47[61]

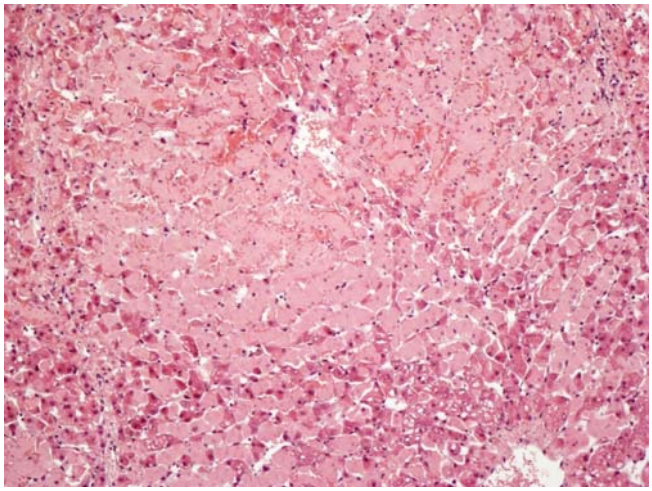

Figure 48[62]

[59] Subcapsular necrosis (4th hour of perfusion; Hematoxylin-Eosin, 40x).
[60] Bridging necrosis (3rd hour of perfusion; Hematoxylin-Eosin, 100x).
[61] Sinusoidal dilatation (4th hour of perfusion; Hematoxylin-Eosin, 100x).
[62] Focal lobular necrosis (5th hour of perfusion; Hematoxylin-Eosin, 100x).

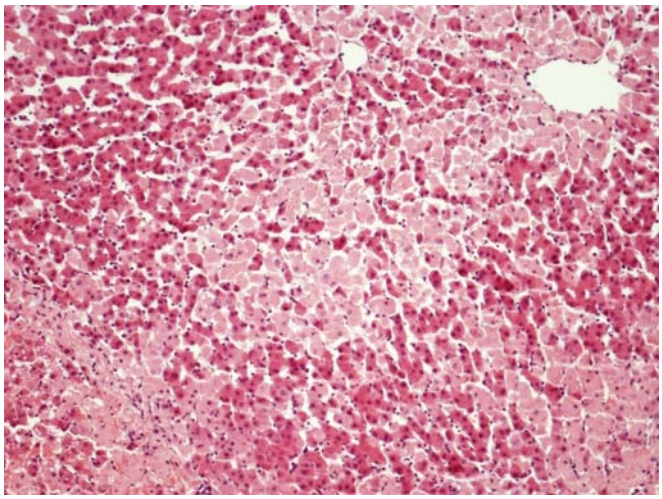

Figure 49[63]

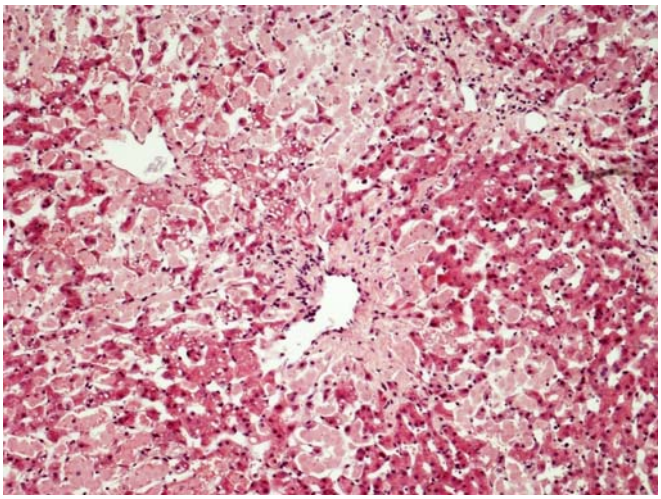

Figure 50[64]

Immunohistochemistry

The apoptotic index had very low values (Table 22) and no significant changes were observed with time (Friedman's test, p=NS, Figure 51). The regeneration index showed the lowest values immediately before reperfusion at the end of the cold-ischemia time and subsequently progressively increased until the sixth hour of perfusion (Table 22). None of these changes however were significant (Friedman's test, p=NS. Figure 52-55). An inverse relationship was present between the regeneration index and the ISHAK score (Spearman r=-0.413, p<0.05).

[63] Bridging and confluent necrosis (4th hour of perfusion; Hematoxylin-Eosin, 100x).
[64] Bridging, confluent necrosis and pericentral adiposis (4th hour of perfusion; Hematoxylin-Eosin, 100x).

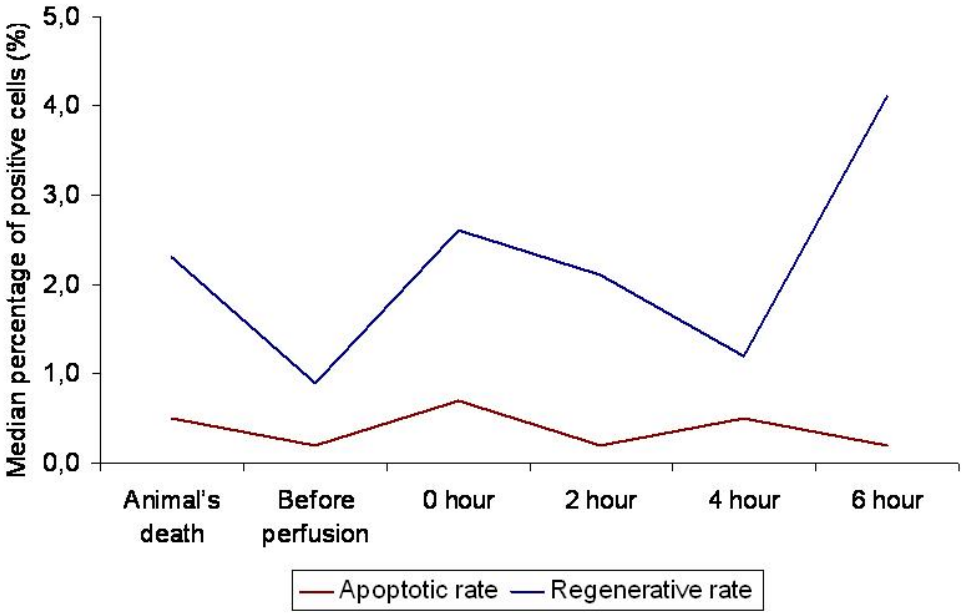

Figure 51[65]

[65] Apoptotic (Caspase) and regenerative (Ki-67) index expressed as percentages of positive cells.

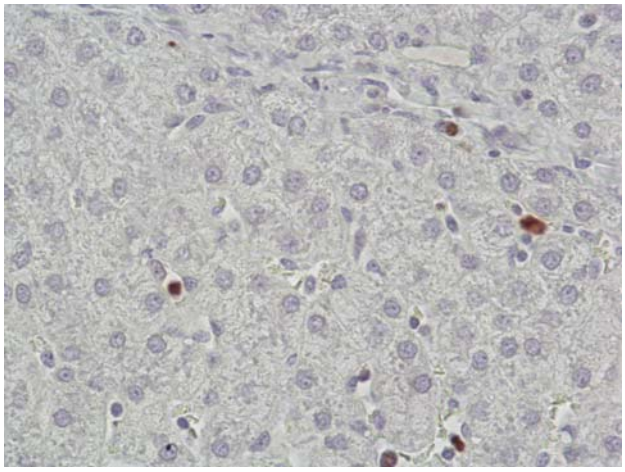

Figure 52[66]

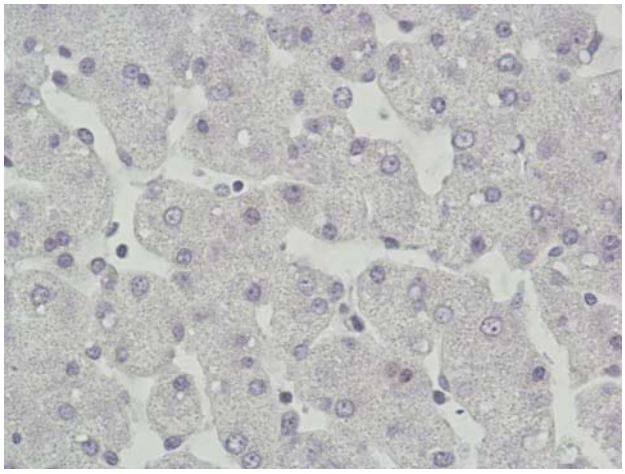

Figure 53[67]

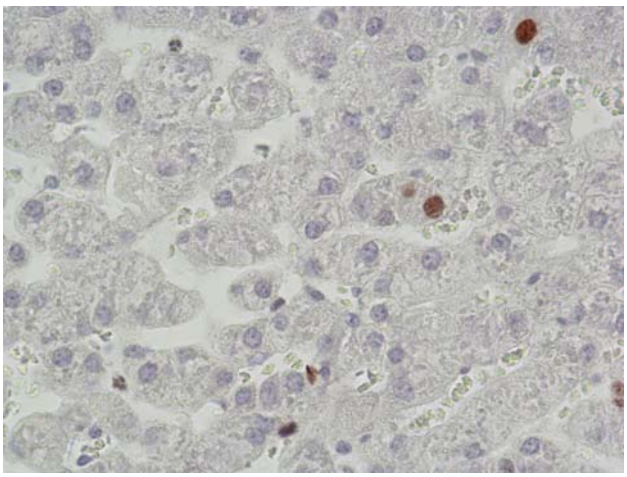

Figure 54[68]

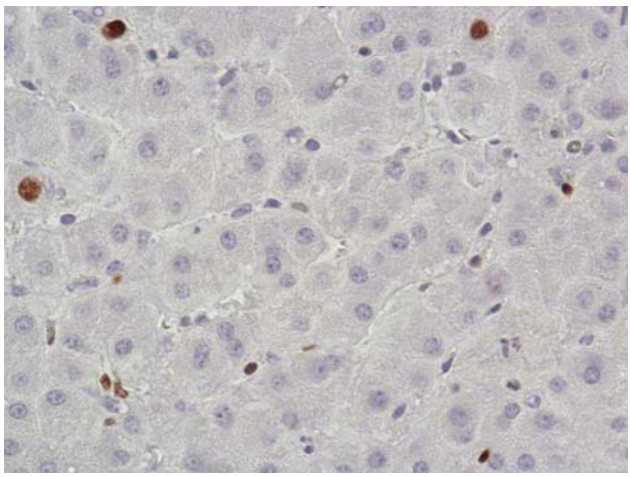

Figure 55[69]

Comparison with the other parameters

Univariate analysis demonstrated no significant correlations with the other parameters investigated and the ISHAK score or the apoptotic index. An inverse relationship was present for the regeneration index with the liver weight (Spearman r=-0.663, p<0.001). The logistic regression

[66] Baseline liver proliferation immediately after the animal sacrifice (time -2; Ki-67 antibody positivity, 400x).
[67] Complete absence of liver proliferation at the end of cold ischemia (time -1; Ki-67 antibody positivity, 400x).
[68] Liver proliferation during the experiment (4th hour of perfusion; Ki-67 antibody positivity, 400x).
[69] Liver proliferation during the experiment (6th hour of perfusion; Ki-67 antibody positivity, 400x).

analysis conducted for factors eventually influencing the ISHAK score demonstrated that the anion gap and the apoptotic index were the only independent variables. The model created with these variables (r=0.76) predicted 57% of the ISHAK variability. Amongst all the factors the anion gap was principally influenced by the lactate and the urea levels, which were able to predict 84% of the anion gap variability (r=0.92). The logistic regression analysis also found that none of the factors investigated had a significant influence on the apoptotic index, while the liver weight had a significant influence on the regenerative index. The model created with this variable (r=0.67) predicted 45% of the regenerative variability.

Electrolytic ablation

Morphologic analysis

Macroscopically the ablated area was black and sharply demarcated from the adjacent parenchyma by a whitish rim (Figure 56). Diameters and radii of the lesions produced are reported in Table 23.

	1st surface diameter (coagulation zone)	2nd surface diameter (coagulation zone)	1st surface diameter (coagulation + transitional zone)	2nd surface diameter (coagulation + transitional zone)	depth (coagulation zone) - cm	depth (coagulation + transitional zone)
EA	1.46 ± 0.06	1.62 ± 0.36	2.00 ± 0.16	2.4 ± 0.27	0.73 ± 0.03	1 ± 0.08
RFA	1.46 ± 0.05	1.44 ± 0.05	2.00 ± 0.16	2.04 ± 0.06	0.72 ± 0.03	1 ± 0.03
Total	1.46 ± 0.05	1.53 ± 0.26	2.00 ± 0.15	2.23 ± 0.27	0.73 ± 0.03	1 ± 0.05

Table 23[70]

[70] Diameters and radii measured for the electrolytic ablations (EA, radiofrequency ablations (RFA) and overall ablations. Measurements were conducted from the border of the probe/electrode at the liver surface (surface diameters) or from the tip of the probe/electrode (depth). RFA probes and EA electrodes were inserted for 1 cm deep in the liver parenchyma before starting the ablations. Depths reported do not include the 1cm of the probe/electrode inserted in the liver. Results are expressed in centimetres with mean and standard deviations.

The normal parenchyma outside the surrounding rim was apparently unaffected (Figure 57). Microscopically the black area corresponded to a necrotic zone where most of the lobules were affected by various histological changes. These consisted of coagulative necrosis, sinusoidal dilatations and hemorrhages (Figure 58-63). A peculiar morphologic pattern was present in most specimens. The coagulative necrosis and hemorrhages affected mainly the peripheral area of the lobule (around the portal triads and septae). Central areas surrounding the centrilobular vein were relatively unaffected (Figure 58-63), although in few specimens the centrilobular area was more involved. Differently, sinusoidal dilatations were more present in the centrilobular area (Figure 60-61). All these histological changes were present to different degrees of severity (Figure 62-63).

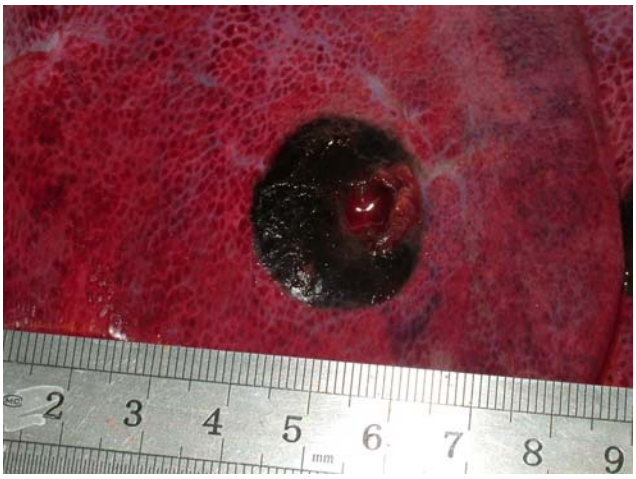

Figure 56[71]

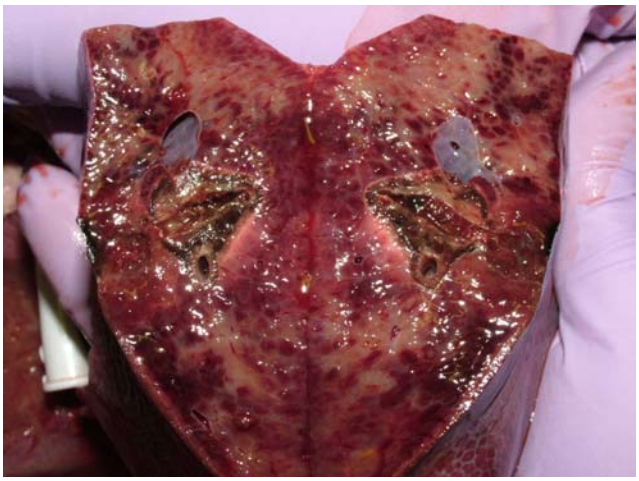

Figure 57[72]

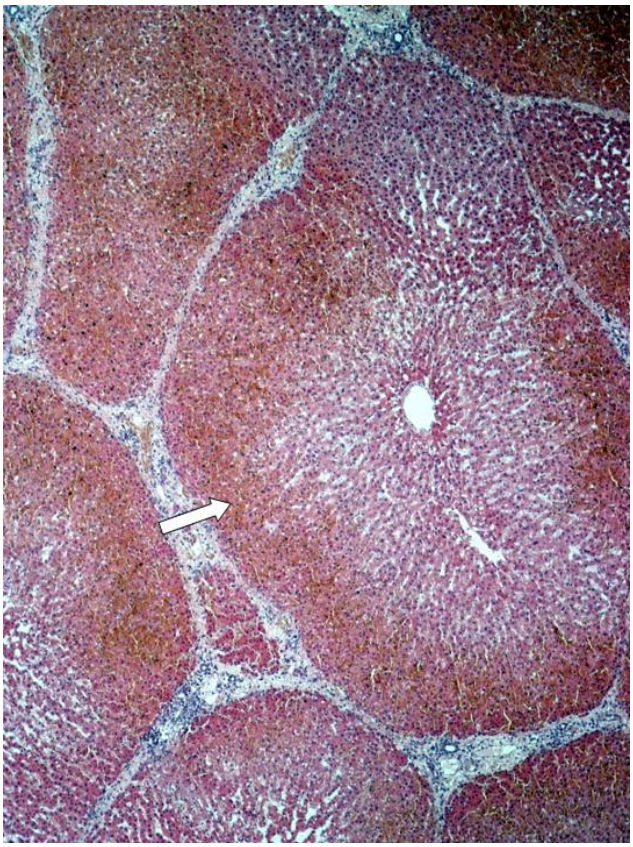

Figure 58

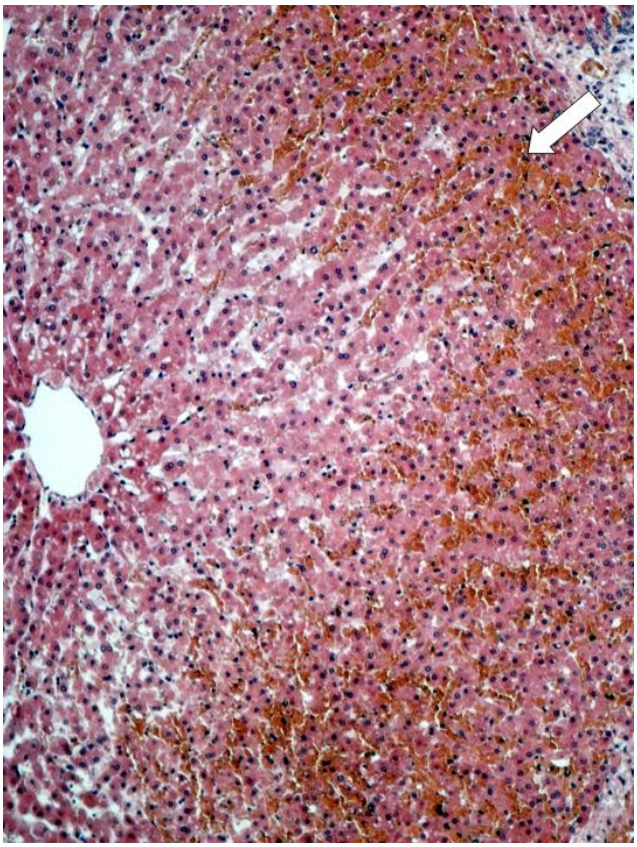

Figure 59[73]

[71] Macroscopic appearance of the electrolytic ablated lesion. The colour black derives from the transformation of the hemoglobin into hemin due to the acidification of the local environment 81. von Euler, H., Olsson, J. M., Hultenby, K., Thorne, A., and Lagerstedt, A. S. Animal models for treatment of unresectable liver tumours: a histopathologic and ultra-structural study of cellular toxic changes after electrochemical treatment in rat and dog liver. *Bioelectrochemistry (Amsterdam, Netherlands)* **59**: 89-98, 2003..

[72] The transitional zone is usually less than 1 mm (white arrows) and produces a sharp demarcation between the ablated zone and the normal parenchyma.

[73] Figures 56-57: Coagulative necrosis and hemorrhages (white arrows) involving the peripheral areas of the lobule around the portal triads and septae (*Fig.56: 40x, Fig.57: 100x*).

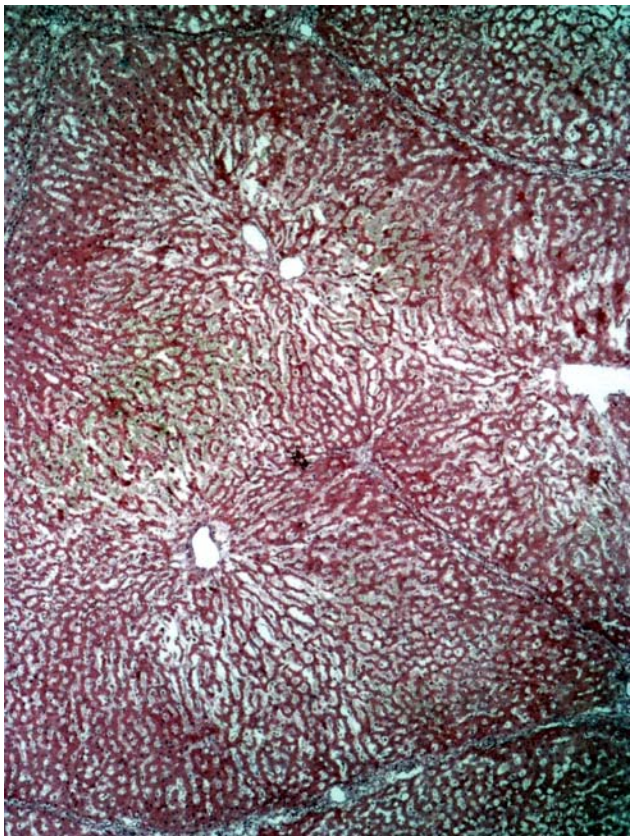

Figure 60

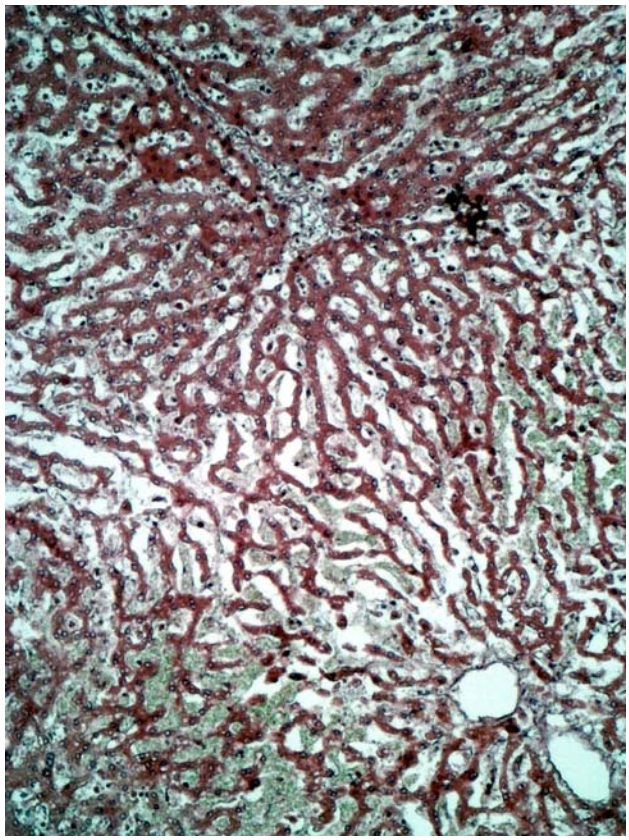

Figure 61[74]

[74] Figures 58-59: Sinusoidal dilatations in the centrolobular area (*Fig.58: 40x, Fig.59: 100x*).

Figure 62

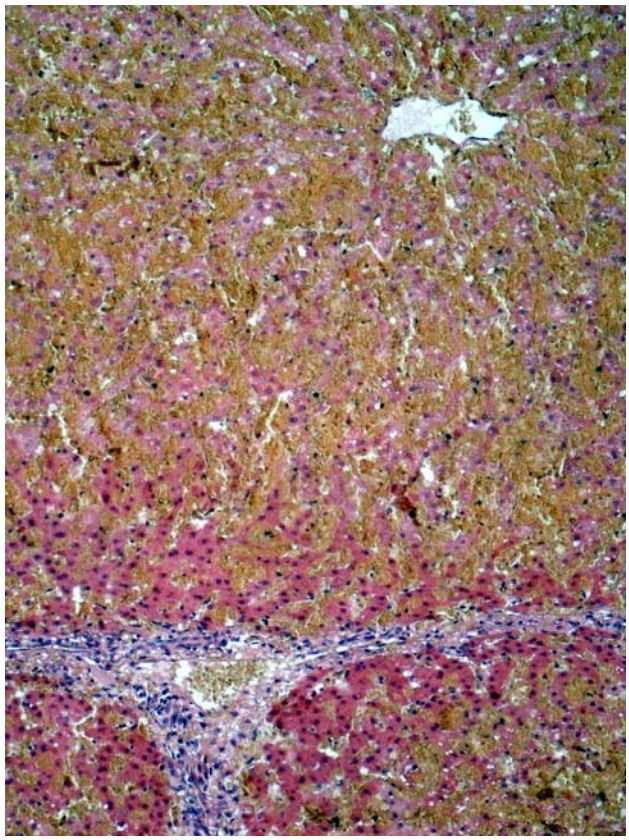

Figure 63[75]

Immunohistochemistry

No significant changes of the amount of apoptotic and regenerative cells were observed over the controls and no peculiar morphologic patterns were present (Figure 64-65). Apoptotic and regenerative cells were present in both the necrotic areas as well as the non-affected zones.

[75] Figure 60-61: Hemorrhages involving the hepatic lobule. Different degrees of severity between the left and right panel (*both figures: 100x*).

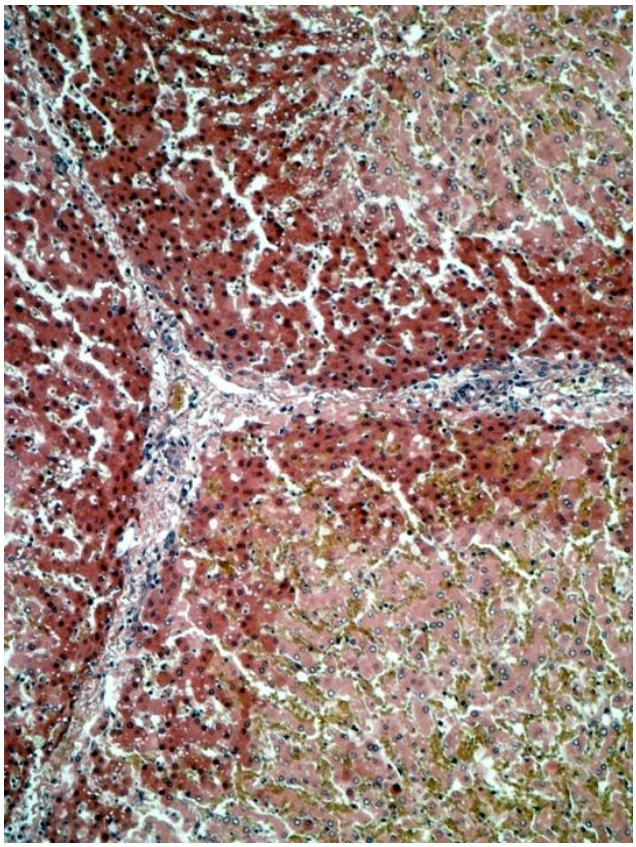

Figure 64

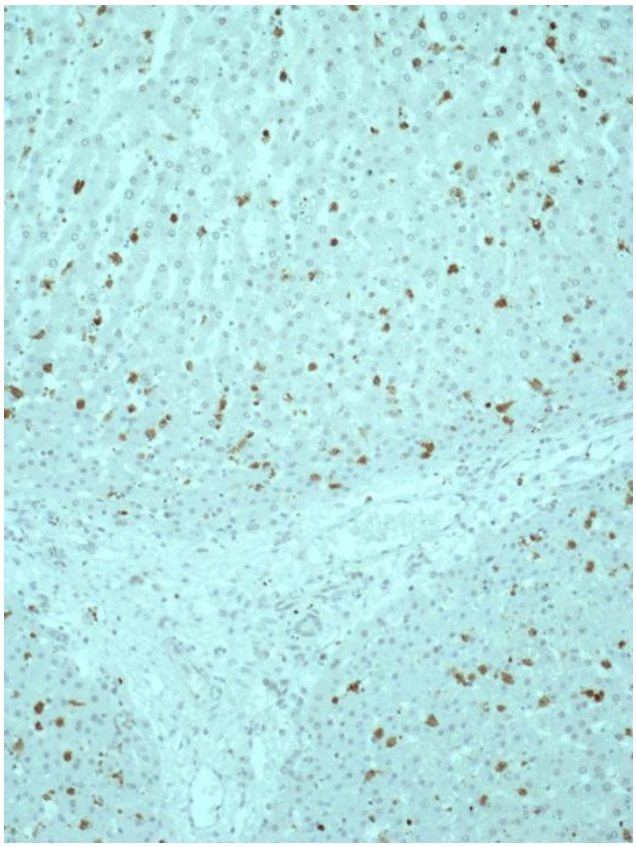

Figure 65[76]

Radiofrequency ablation

Morphologic analysis

Macroscopically are evident two zones in the parenchyma, the first one is a central white area close to the electrode and the second one a brown-red intermediate area interposed between the first and the normal liver parenchyma (Figure 66). Diameters and radii of the lesions produced are reported in Table 23. Microscopically the central white area corresponds to the coagulative necrosis of hepatocytes while the intermediate area to sinusoidal congestions and hemorrhages (Figure 67-68).

[76] Figures 62-63: Comparison between normal morphology (*Fig.62*) and apoptotic cells (*Fig.63*) at the end of the perfusion (*both figures: 100x*).

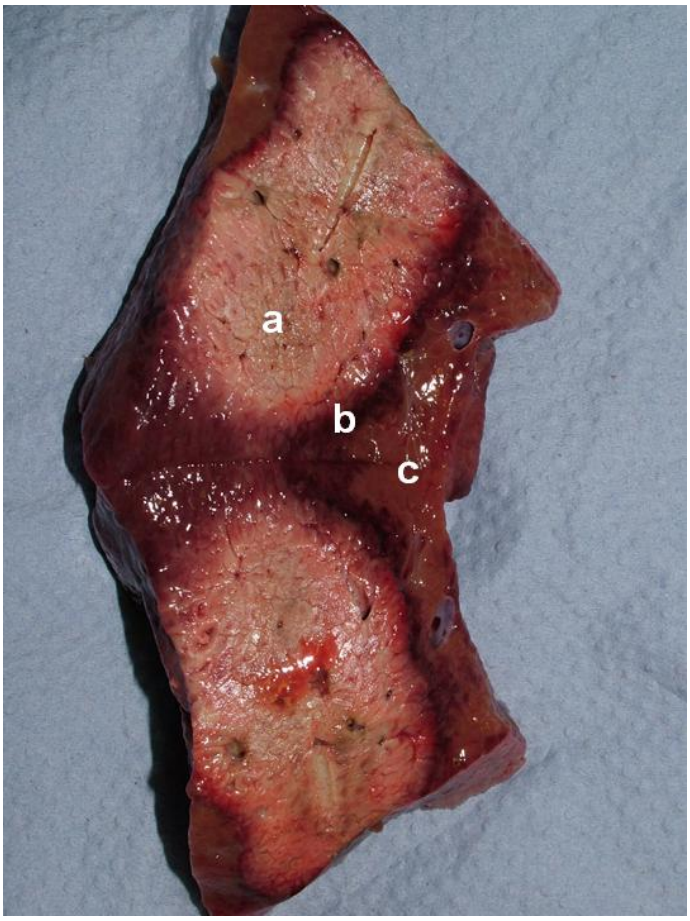

Figure 66[77]

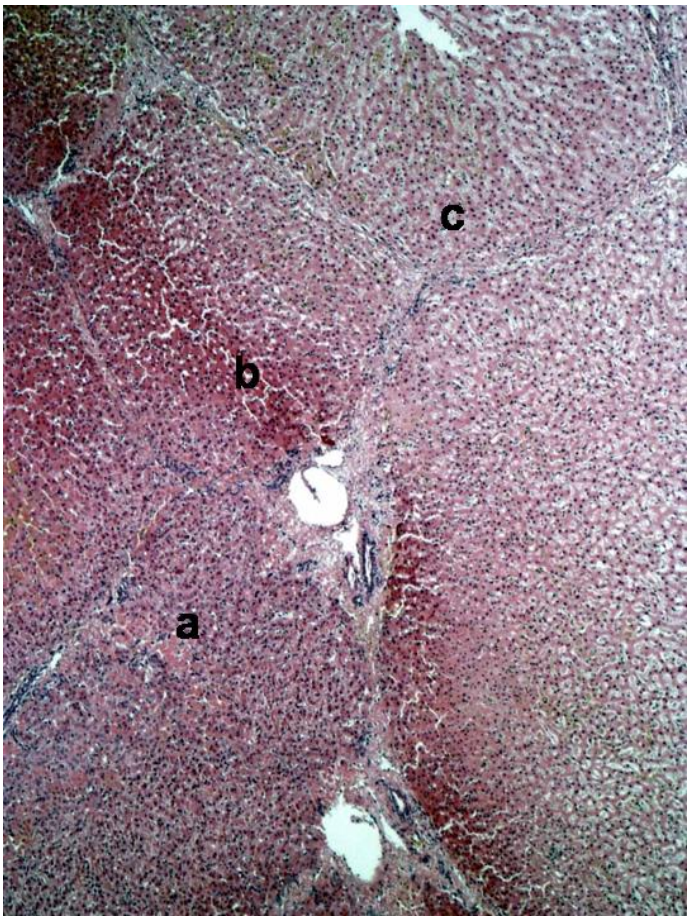

Figure 67[78]

Immunohistochemistry

No significant changes of the amount of apoptotic and regenerative cells were observed over the controls and no peculiar morphologic patterns were present according to the ablation zones (Figure 68-69). With regards to the hypothesis of the study, no significant differences were found between EA and RFA for the radii of ablations created and the amount of apoptotic and regenerative cells (ANOVA one-way test and ANOVA for repeated measures, p=NS). Therefore the null hypothesis has been true and the alternative hypothesis has been rejected. However,

[77] Macroscopic appearance of the radiofrequency ablated lesion. Two distinct zones of ablation, the central white area and the brown-red intermediate area before the normal liver parenchyma.
[78] Microscopic appearance of the ablated zones. a = normal liver parenchyma, b = intermediate transitional zone, c = coagulative necrosis (*40x*).

significant differences between the EA and RFA were observed for the morphology of ablations achieved; in this case the null hypothesis has been rejected and the alternative hypothesis is true.

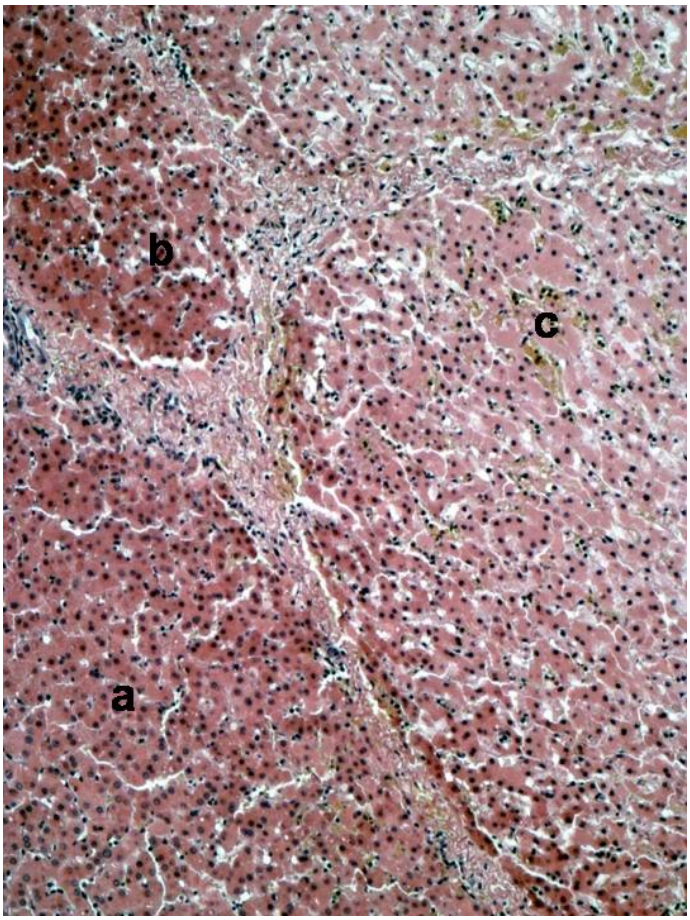

Figure 68

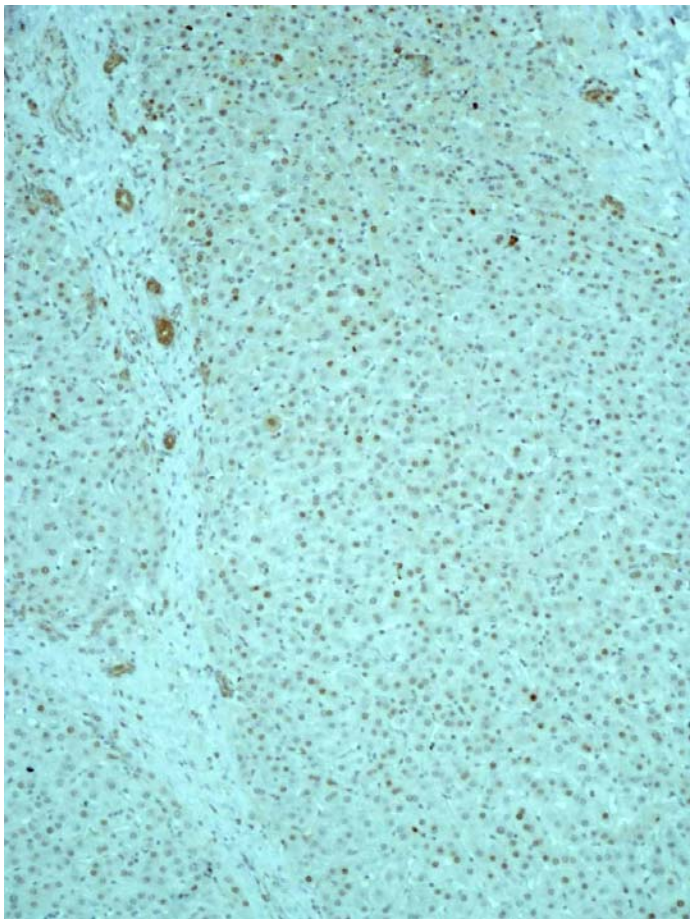

Figure 69[79]

[79] Figures 66-67: Comparison between normal morphology (*Fig.66*) and apoptotic cells (*Fig.67*) at the end of the perfusion (*both figures: 100x*).a = normal liver parenchyma, b = intermediate transitional zone, c = coagulative necrosis (*100x*).

Discussion

Hemodynamic parameters

The greatest variability in the physiological parameters (HA pressure and flow, PV pressure) was observed during the first hour of reperfusion, after which it subsequently stabilized with more predictable values. These data demonstrates that the hepatic vascular hemodynamic response to the reperfusion and the hypoxia is initially very variable while the vessels stabilize their response. This process always occurs during the first hour of perfusion and therefore this period of time cannot be used for experimental work. Subsequently the model is stable enough to study responses to artificially induced changes. The only parameter where there is any variability beyond this period of time is the PV flow. In this case such variability could persist until the 5^{th} hour of perfusion.

The choice of the PV pressures, based on the hematocrit values adopted in our study and on previous results on acellular buffer solutions (225-227), may have influenced all subsequent results. It is well-known that high perfusion pressures can produce tissue damage, cause hepatic barotrauma and enlarge sinusoidal fenestrations (237). It is possible that such pressures could have accounted for any or all the results achieved.

Acid-base changes

Controls

The use of our isolated *ex-vivo* perfused liver provides a peculiar experimental model in which the separation of the liver from organs that normally compensate for acid-base modifications (kidneys and lungs) allows the observation in the blood of any alteration produced during the perfusion without any external influence. At the same time, the interpretation of the acid-base changes may be biased by the characteristics peculiar to our model that needs to be considered.

In our experiments, initial values of the acid-base balance (time 0) were those of a normal standard arterial blood gas. However, after one hour of reperfusion an acute respiratory acidosis manifested due to the lack of gas-exchanging organs (the oxygenator allows only oxygen to be added to the circuit).The measured pH exactly reflected the value estimated from the CO_2 levels ($\Delta PH = 0.008 \times (CO_2 - 40)$) and confirmed the interpretation of a respiratory modification. Still, in our circuit other explanations are responsible for the increased CO_2 observed, such as the initial massive release of H^+ immediately after the reperfusion (ischemia-reperfusion injury) and the normal cellular metabolism which continuously contributes H^+ to the circulation. H^+ subtracts HCO_3^- and converts it into CO_2. For this reason, in the first hour HCO_3^- levels remains within normal limits and BE becomes mildly negative despite the initial HCO_3^- boost and the continuous infusion added throughout the experiment. Furthermore, the accumulation of H^+ is also evidenced from the AG that, although normal at hour 1 (AG = 12), was definitely increased from the hour 0 (AG = 4). All these issues point towards the presence of an additional second acid-base modification, a metabolic acidosis, present at hour 1 and explained by the absence of the kidneys.

From the third to the sixth hour three combined acid-base modifications were present. On one side, the metabolic and respiratory acidoses were even more evident due to the increased values

of the AG and the CO_2. From the third hour, lactic acid is significant elevated compared to baseline levels. The lack of organs that normally consumes lactic acid implies that all the acid produced is delivered into the circulation and accumulates over the hours. The increased total lactic acid in the circuit contributes to augment the H^+ and the metabolic acidosis observed. On the other side, a metabolic alkalosis appeared that was produced from the continuous infusion and accumulation of HCO_3^- necessary to compensate for the H^+ and the lactic acid released in the mainstream. The alkalosis was confirmed by the high values of pH and HCO_3^-.

Electrolytic and radiofrequency ablation

Changes observed in the EA group were similar to those of the controls. After the first hour the respiratory acidosis (increased CO_2) and metabolic acidosis (increased AG) were exactly balanced by the metabolic alkalosis (increased HCO_3^- and positive BE) and the resulting pH was normal. From the second hour, as in the control group, the effect of the metabolic alkalosis was predominant dominant resulting in an alkalosis despite the increased lactate and AG. More importantly, no significant differences were observed between groups for any acid-base balance parameters of the. As the experimental conditions were identical in each group apart from the EA treatment this implies that the EA did not contribute any increased acidotic or alkalotic stress to the overall acid-base balance.

Our findings confirm previous reports concerning the lack of pH modifications during EA (89, 238), but provide additional information. It is likely that, during EA, the additional production of H^+ is exactly balanced by the bases released into the circulation and explains why the procedure does not produce any overall pH changes. The lack of pH changes even persists when several ablations are performed in each liver (previous studies have only performed single ablations) (89, 238). Our studies are closer to the likely clinical scenario where multiple lesions will be treated (it is unusual for single lesions to be unsuitable for surgical treatment) for palliation. Despite the greater

number of ablations, longer duration of the procedure and increased overall ablated volume in our model the acid-base balance of the EA group did not differ from controls. The lack of any additional changes in the EA group, compared to controls, suggests that the procedure could be safely performed in patients with significant renal or pulmonary disease where normal compensatory mechanisms are significantly impaired. Similar results were also found for RFA.

Assessment of liver viability

Although the bile production was constantly greater than 10ml/hour and the arteriovenous oxygen and carbon dioxide extraction ratios were also constant during the perfusion in all experiments, it is still possible that livers were ischaemic or non-viable due to the high PV pressures adopted and the long warm ischemia times registered. These factors could have significantly influenced the results achieved in the current thesis.

Biochemical changes

Despite the myriad different causes of clinical changes that occur following prolonged hypoxia, end-results are remarkably similar due to the same final common pathway, and have profound effects on the organism. Such changes may be observed for example during cardiopulmonary bypass (CPB) surgery where the hemodilution values adopted range from moderate (hematocrit ≥ 27%) to profound (hematocrit 15-18%). These values produce isovolemic anaemia and a resulting decreased oxygen binding capacity of the blood culminating in a prolonged tissue hypoxia (239). In the present experiments organ perfusion was maintained for six hours in order to allow sufficient time for changes in liver function to manifest with hematocrit values comparable to those obtained with profound haemodilutions. The "*a posteriori"* evaluation of hematocrit obtained surprisingly showed that the dilution obtained was even greater than that initially planned (60% of the initial hematocrit values as opposed to a planned 50%), probably because some of the perfusion fluid present in the liver remained trapped in the circuit after that hepatic vessels were connected to circuit. Even with such low hematocrit values, the hepatic arteriovenous oxygen difference corresponded to approximately 260-290 mmHg and no significant differences were observed throughout the perfusion.

Prolonged hypoxic states produce a number of profound effects on the body's metabolism. In the study of Stratford et al., glycogenolysis was activated after four hours of reduced blood flow, thereby increasing blood glucose levels, and reduced after 24 hours due to enzyme inhibition. Circulating epinephrine and norepinephrine concentrations were still high at 24 hours, indicating that some inhibitory mechanism (as opposed to a reduction in levels of hormones) must be present and responsible for the reduction in glycogenolitic activity (240), and this apparent discrepancy has also been observed in humans exposed to altitude hypoxia (241). With hypoxia resulting from high altitude the increase of glucose blood levels does not correspond to a concomitant increase in the

hyperglycaemic hormones (glucagon, adrenaline and growth hormone) (241). Both these studies suggest that regulating factors other than changes in the concentration of circulating hormones are responsible for the rise of glucose and for its modulation during prolonged periods of hypoxemia.

Normothermic *ex-vivo* perfusion allows the "disconnection" of the liver from other variables that may exert an influence (autonomic nervous control, circulating hormones). For levels of blood glucose, a progressive and significant increase was present throughout the experimental period, with the greatest changes being observed immediately after the beginning of the perfusion and during the first two hours. Results suggest an intrinsic hepatocyte response to hypoxia but it is possible that an ischemia-reperfusion injury could elicit the same response (when oxygenated blood begins to flow through the liver). Previous studies have described increases in levels of glucose, lactate, and glycerol levels following reperfusion, and also that the rate of these increases continues to rise (242). However a direct link between liver cell hypoxia and increasing glucose mobilization is supported by reports of elevated blood sugar levels in the clinical setting following inflow occlusion (during a surgical 'Pringle' manoeuvre) before the liver is reperfused (243). Furthermore, in ischemia-reperfusion experiments the glucose rise is transient and lasts for only 60 minutes, returning to normal within that period (242). In the present experiments, values peaked between the first and second hour and remained significantly higher throughout the experiment. The data thus supports the hypothesis that while the ischemia-reperfusion injury is likely to contribute to the hyperglycaemia in the initial phase of the perfusion the responses to the subsequent prolonged hypoxia noted in the second phase must be due to an intrinsic mechanism. This intrinsic hyperglycaemic response observed following exposure of the hepatocytes to hypoxia would also explain the inconsistency found in some earlier experimental and clinical studies where just hyperglycaemic hormones and blood sugar levels were examined (240, 241, 244, 245).

Other important parameters examined were the transaminases as markers of hepatocyte necrosis, albumin and total bilirubin as markers of the hepatic function, and the alkaline phosphatase to look for biliary stasis. In the study of Fukusaki et al., 30 patients were divided into

three groups and received controlled hypotension, hemodilution or both during their hip surgery. Patients undergoing hemodilution alone were diluted to final hematocrit values of 21-22%, but did not manifest any change in hepatic parameters (transaminases, lactate dehydrogenase and total bilirubin) (246). In the present experiments transaminases were similar to those obtained in other studies involving *ex-vivo* perfused liver models (228) but still significantly higher than baseline values obtained immediately after the reperfusion was started. It is probable that unlike the study of Fukusaki (246), our model suffered from an ischemia-reperfusion injury due to the harvesting process and the period of cold preservation. This is similar to the findings in other *ex-vivo* perfused models (228) and in the clinical setting following liver transplantation. However, although plasma transaminases levels rose significantly during the first hour there were no changes thereafter possibly suggesting that hemodilution per se did not contribute further to the hepatocyte necrosis following the initial injury sustained after reperfusion. This is further supported by the finding of normal values for total bilirubin and by the high rate of bile production and HMRO throughout the experiment. These findings suggest a stable and essentially normal liver function in the remaining period of the study.

Cytokines

The mammalian immune system consists of innate and adaptive components that cooperate to protect the host against microbial infections. The innate immune system senses pathogens through pattern-recognition receptors, which trigger the activation of antimicrobial defences and stimulate the adaptive immune response. The adaptive immune system, in turn, activates innate effector mechanisms in an antigen-specific manner (247). The innate immune system is composed of various defense mechanisms. Among those, the complement system and Toll-like receptors (TLRs) are key innate defense systems that are rapidly triggered upon infection (248). They both are important to recognise non-self molecules and to provide critical danger signals instructing adaptive immune responses (249). Different TLRs recognize distinct types of microbial structures, giving the innate response a degree of specificity (250). After recognition of specific microbial proteins, TLRs induce intracellular signaling cascades that result in the production of both pro- and anti-inflammatory cytokines (251). The complement system includes serum and membrane-bound proteins that act as a cascade via three distinct pathways (classical, lectin or alternative) and converge on a final crossroad molecule C3 (252). C3 activation leads to the recruitment and activation of inflammatory cells, opsonization and phagocytosis of microbes, and direct lysis of microbial cell membranes (252). Complement activation stimulates the production of cytokines via direct stimulation of inflammatory and immune cells, and through the enhancement of TLR-induced production of proinflammatory cytokines (253, 254).

Controls

The use of an *ex-vivo* perfused porcine liver model provided a different biologic insight to the modifications of cytokines that occur following various stimuli to the hepatic parenchyma. Our isolated model excludes the liver from the influence of factors such as hormones, autonomic

nervous system or regulatory substances produced elsewhere in the organism, allowing a clearer interpretation of resulting changes. Apart from the warm and cold ischemic time during the organ harvesting and preservation, the only potential explanation for changes in circulating cytokines occurring in this model is ischemia/reperfusion injury.

Only two of the nine cytokines analysed demonstrated statistically significant increases (IL-6 and IL-8), consistent with results obtained from preclinical and clinical studies on ischemia/reperfusion injury of the liver (255-260). In fact, similar changes have also been demonstrated before surgery (in patients with advanced diseases), during the anhepatic phase of liver transplantation, and postoperatively in patients with poor early graft function (261). Our observations suggest that the ischemia/reperfusion injury to the liver also contribute to the increased cytokines concentrations and it is conceivable that elevated IL-6 and IL-8 are an epiphenomenon of different contributing factors in the setting of liver transplantation.

IL-6 is a potent regenerative and pro-inflammatory molecule produced mainly by perivenous hypoxic hepatocytes that belongs to the category of acute phase proteins (259, 262). Different studies have demonstrated a protective effect of this cytokine against ischemia/reperfusion mediated oxidative damage through a number of mechanisms including reduction of cell damage, enhancement of the compensatory hepatocyte proliferation, maintenance of the acute phase response, increase of the heat shock stress response and substitution of dysfunctional proteins (263, 264). The cytokine levels inversely correlates with the post-transplant liver function (265-268) and its protective effects are exaggerated following ischemic preconditioning in animal models (264, 269). It is interesting to note that a retrospective clinical study revealed a statistically significant correlation between low IL-6 mRNA expression and the occurrence of acute rejection episodes within the first 30 postoperative days, while high IL-6 mRNA levels coincided with the absence of signs of rejection (270).

Changes in IL-8 produce inconsistent results with regard to their ability to predict postoperative liver graft function or complications (271-273). IL-8 levels are not influenced by cold

ischemia times (272), unless it is longer than 12 hours (260) and the cold ischemia times in our experiments were consistently less than three and a half hours and unlikely to be responsible for changes in the IL-8 levels. In addition, the TNF-α and IL-10 levels did not demonstrate significant increases following reperfusion, contradicting the findings from other studies (257, 258, 274, 275). During the anhepatic phase of liver transplantation, mesenteric venous congestion and associated accumulation of endotoxin in the splancnic circulation stimulate Kupffer cells to produce TNF-α (276). The lack of TNF-α surge in our study could be explained by the absence of the anhepatic phase and the lack of a mesenteric splancnic accumulation of endotoxin.

IL-10 is a macrophage and T-cell-derived cytokine with potent immunosuppressive properties and it has been suggested that it is one of the reasons for the peculiar immune tolerance present in liver transplantation (275). Portal endotoxemia is not involved in IL-10 production, as endotoxin levels remain low before and after liver allograft reperfusion in patients with increased IL-10 (275). IL-10 levels did not change significantly throughout our experiments and while the lack of endotoxin may explain this, it is also possible that the ischemia/reperfusion alone is not sufficient to trigger release of this cytokine and that a more complex series of interactions is required. Nevertheless, this negative observation is important because our model has removed these additional factors and studied early changes in isolation. We believe that the model could also facilitate their incremental reintroduction in future studies that will allow the mechanisms to be further elucidated.

Electrolytic and radiofrequency ablation

Four *in-vivo* experimental studies have examined the inflammatory response elicited after EA (121, 168, 183, 277). Two studies were conducted on the pancreas (183, 277) and two on the liver (121, 168). The two reported studies on the liver analysed three cytokines including TNF-α, IL-1 and IL-8. Although hepatic EA seemed to elicit lower inflammatory responses compared to the

more common techniques of thermal ablation, the results presented were somewhat conflicting. The *ex-vivo* experiment presented here was designed to undertake these aforementioned studies with the analysis of all of the possible cytokines from an *ex-vivo* porcine liver model.

TNF-α is a strong pro-inflammatory cytokine that is frequently altered after RFA (119). The two hepatic EA studies reported contrasting results, as no significant modifications (168) and increased TNF-α values (121) were found. The results of this study showed significantly higher TNF-α values after the 4^{th} hour of perfusion when compared to the non-ablated controls. This is in agreement with a previous study conducted on non-ablated *ex-vivo* perfused livers, in which no significant changes in TNF-α levels were elicited *ex-vivo* by the ischemia-reperfusion injury (278). However, it remains a possibility that the ischemia-reperfusion injury primed the liver to respond in this way, as a result of the application of noxious ablative stimuli. The results presented here concur with those of Berry *et al.* and Teague *et al.* that found no significant changes in IL-1β and IL-8 levels when the EA group was compared to controls (121, 168).

The other cytokines investigated have rarely been measured after hepatic EA or other ablative techniques, such that it has not been possible to meaningfully interpret the findings. The results presented here describe significant difference for IL-2, IL-4 and IL-10 when comparing the EA group to the control group. It seems that EA decreases the expression of a Th1-type cytokine (IL-2), a Th2-type cytokine (IL-4), and increase the expression of IL-10. These results would suggest that EA is able to elicit an anti-inflammatory response that may counteract the effects of the increased pro-inflammatory TNF-α. It is now necessary to confirm these findings in experimental *in-vivo* studies and human studies, in order to evaluate whether these changes are influenced by systemic factors and to correlate them with clinical outcomes respectively. Similar considerations are valid fo the significant increase of IL-8 and IL-10 after RFA.

Histology

Controls

Different methods have been used for the evaluation of the viability of isolated perfused livers: the oxygen extraction rate (calculated as the arteriovenous oxygen difference) and the bile production are two parameters easily measured with the advantage that may give a rough estimation of the organ status during the experiment (228). Others include liver transaminases, alkaline phosphatase, lactate dehydrogenase, protrombin time, coagulations factors V and VIII, blood urea, clearance of ammonia and lactate, blood and bile bilirubin levels (228, 279). The assessment of the viability of isolated perfused livers with the histological analysis of serially collected specimen produced so far contrasting results. Some authors claimed that the histology of the liver parenchyma was normal throughout the experiments (280) especially in the periportal and the centrolobular zones (228) and a good architectural preservation of the lobule was found even after 72 hours of perfusion. Different authors found specific histological abnormalities during the perfusions. Areas of pericentral necrosis, mild septal hemorrhage, edema and sinusoidal dilatation were described in some experiments (215) and their presence appeared to relate with the duration of perfusion: scattered necrosis of single hepatocytes, apoptotic cells (especially in underperfused septa) (281) and increasing Kupffer cell hypertrophy with lysosomal overload were constant features since the beginning of perfusion and indicated an exacerbated renewal of hepatocytes (228, 230). Microvesicular steatotic vacuolization of liver cells (228, 230, 282) and the granulocytic infiltration of the portal space and septa were present from the 3rd hour (282), the sinusoidal mediolobular dilatation from the 4th hour (228, 230, 283), the trabecular fragmentation from the 5th hour (282), sinusoidal endothelial damage with red cells extravasation and mediolobular necrosis from the 6th hour (228).

Results of our study confirm that necrosis is the main mode of hepatic cell destruction in *ex-vivo* perfused porcine livers. In our studies cellular necrosis follows the ischemia/reperfusion injury that derives from the organ harvesting and cold preservation (284). The histological changes described are similar to those already presented (215, 228, 230, 282, 283), but their intensity varied and followed specific patterns throughout the perfusion. The first peak corresponds to end of the cold ischemia time, while the second peak derives from the hemodynamic disturbances that result from the artificial perfusion. These produced a state called low-flow hypoxia where isolated ischemic lobules manifest centrilobular and confluent necrosis (284). The analysis of factors influencing the liver damage demonstrated the importance of the anion gap acidosis on the ISHAK score and on the ALT values. The relationship of pH on the occurrence of hepatic necrosis following the ischemia/reperfusion injury has been well described (284). In our model the anion gap acidosis was mainly associated with the production of lactate and urea, suggesting that it probably derived from lack of lactate consumption and from the acute renal failure in the experiments. Hyperglycemia, although present during *ex-vivo* liver perfusions (285), does not influence the anion gap acidosis. The characteristics of the model used do explain these changes because of the lack of organs able to detoxify the blood (kidneys) or to consume the lactate (muscles and heart).

Changes in the ISHAK score were paralleled inversely by changes in the regenerative index. Immediately before reperfusion and at four hours the regeneration index was at its lowest level, while at six hours it produced the highest values when the ISHAK score decreased to normal values. The regenerative index was found to correlate with the liver weight, and this influence was also confirmed by the logistic regression analysis. The inverse correlation between liver weight and regeneration has already been described in experimental studies of liver transplantation in which a small graft-to-host size stimulated a higher liver regeneration following transplantation (286, 287). One possible explanation is that small organs regenerate more to meet the host's metabolic demands compared to larger organs. Our experiments seem to confirm this hypothesis although regenerative rates observed were inferior to those present after liver transplantation. Finally, liver apoptosis is an

infrequent cause of hepatic cell destruction following ischemia/reperfusion injury (288). Caspase activation is minimal or absent and apoptosis is only found in about 2% of cells (284). The apoptotic index observed in our experiments corresponded to these values and no significant modifications were present over the period of the study. This confirms that in isolated hemoperfused livers no specific pro-apoptotic stimuli act during the perfusion.

Electrolytic and radiofrequency ablation

Thermal techniques of liver ablation are a well-established palliative treatment that destroys liver tumors by delivering physical energy (RFA or MTA) and developing high tissue temperatures through the Joule effect. The histologic lesion created, in both normal liver and cancerous tissue, roughly resemble a set of concentric spheres or ovoids with the centre on the tip of the cannula delivering the energy and different histologic layers according to the gradient of temperature (10, 59). These mainly consist of a central zone of coagulative necrosis surrounded by a peripheral transitional zone of hemorrhage, stasis, sinusoidal dilatation and apoptosis (10, 59). Compared to thermal techniques, EA destroys tissues through extreme changes in the microenviromental acid-base balance. The anodes and catodes accumulate highly acidotic or extracellular fluids resulting in a toxic pH gradient (289, 290). The characteristics of non-thermal destruction of the liver parenchyma (73, 291) combined to the lack of any systemic effects despite the extreme local tissue changes in pH (81, 89) create for this technique a niche of application represented by the destruction of cancerous lesions "awkwardly" positioned as those close to major vessels that cannot be otherwise safely ablated (70, 289).

Histopathologic changes obtained after EA have been already presented in previous experimental studies. Macroscopically, ellipsoidal zones of hepatic necroses are created around the electrode tips (89). Increased volumes of ablation may be obtained with separated (70, 74) or multiple electrodes and by the use of a Pringle manoeuvre (88). Microscopically the central cavity corresponding to the electrode is surrounded by necrosis. The transitional zone is thin and with numerous microvascular thrombi (81). Anodic lesions characteristically desiccate and become well demarcated, and hepatocytes in this area have a pycnotic nucleus with little or absent cytoplasm (69, 75, 80, 81). Conversely cathodic lesions attract water and show generalized oedema (69, 75, 80, 81), hepatocyte nuclear and cytoplasmic swelling and occasional disruption of the plasma membranes (69, 81). What is peculiar to EA compared to the more common thermal ablative

techniques is the morphologic distribution of the damage within the hepatic lobules. With thermal ablation the histologic lesion created, in both normal liver and cancerous tissue, roughly resemble a set of concentric spheres or ovoids with the centre on the tip of the cannula delivering the energy and different histologic layers according to the gradient of temperature (10, 59). These mainly consist of a central zone of coagulative necrosis surrounded by a peripheral transitional zone of hemorrhage, stasis, sinusoidal dilatation and apoptosis (10, 59). In EA the distribution of the damage is mainly localed in the periphery of the hepatic lobule (necrosis) or around the centrolobular vein (sinusoidal congestion) to different degrees of severity. Furthermore EA produces a thinner transitional zone compared to the RFA (171). This could be derived from the increased time spent in producing the ablation that could allow tissues to undergo a more complete and definitive necrosis compared to RFA.

Conclusions

The *ex-vivo* normothermic perfused liver model theoretically allows the liver to be completely dissociated from systemic influences (whether neurological, hormonal or chemical) that confound the interpretation of intrinsic responses of the organ to external stimuli. While this model could be useful for experimental studies of liver physiology, it was not the correct choice for the purpose of this thesis that aimed to compare an experimental technique of liver ablation (EA) vs. the current gold standard (RFA). In fact, ablation techniques are conducted on live patients where systemic responses elicited by ablation therapies are important (i.e. metabolic and immune modifications). In this case, an in-vivo animal model would have been probably the best choice. Furthermore, the technical complexity of the *ex-vivo* model increased the number of parameters to monitor, especially concerning the liver viability and the administration of external substances to maintain a physiologic environment. Finally, the choice of high PV pressures and the long warm ischemia times registered could have further altered the results achieved.

Summary

Tables

Figures

References

1. van den Broek, M. A., Olde Damink, S. W., Dejong, C. H., Lang, H., Malago, M., Jalan, R., and Saner, F. H. Liver failure after partial hepatic resection: definition, pathophysiology, risk factors and treatment. *Liver Int* **28**: 767-780, 2008.

2. Wemyss-Holden, S. A., Dennison, A. R., Berry, D. P., and Maddern, G. J. Local ablation for unresectable liver tumors: is thermal best? *Journal of hepato-biliary-pancreatic surgery* **11**: 97-106, 2004.

3. Goldberg, S. N., Grassi, C. J., Cardella, J. F., Charboneau, J. W., Dodd, G. D. r., Dupuy, D. E., Gervais, D., Gillams, A. R., Kane, R. A., Lee, F. T. J., Livraghi, T., McGahan, J., Phillips, D. A., Rhim, H., and Silverman, S. G. Image-guided tumor ablation: standardization of terminology and reporting criteria. *Radiology* **235**: 728-739, 2005.

4. Mulier, S., Ni, Y., Frich, L., Burdio, F., Denys, A. L., De Wispelaere, J. F., Dupas, B., Habib, N., Hoey, M., Jansen, M. C., Lacrosse, M., Leveillee, R., Miao, Y., Mulier, P., Mutter, D., Ng, K. K., Santambrogio, R., Stippel, D., Tamaki, K., van Gulik, T. M., Marchal, G., and Michel, L. Experimental and clinical radiofrequency ablation: proposal for standardized description of coagulation size and geometry. *Annals of surgical oncology* **14**: 1381-1396, 2007.

5. Mulier, S., Miao, Y., Mulier, P., Dupas, B., Pereira, P., De Baere, T., Lencioni, R., Leveillee, R., Marchal, G., Michel, L., and Ni, Y. Electrodes and multiple electrode systems for radio frequency ablation: a proposal for updated terminology. *Adv Exp Med Biol* **574**: 57-73, 2006.

6. Sarantou, T., Bilchik, A., and Ramming, K. P. Complications of hepatic cryosurgery. *Semin Surg Oncol* **14**: 156-162, 1998.

7. Ong, S. L., Gravante, G., Metcalfe, M. S., Strickland, A. D., Dennison, A. R., and Lloyd, D. M. Efficacy and safety of microwave ablation for primary and secondary liver malignancies: a systematic review. *Eur J Gastroenterol Hepatol* **21**: 599-605, 2009.

8. Mulier, S., Mulier, P., Ni, Y., Miao, Y., Dupas, B., Marchal, G., De Wever, I., and Michel, L. Complications of radiofrequency coagulation of liver tumours. *The British journal of surgery* **89**: 1206-1222, 2002.

9. Gravante, G., Sconocchia, G., Ong, S. L., Dennison, A. R., and Lloyd, D. M. Immunoregulatory effects of liver ablation therapies for the treatment of primary and metastatic liver malignancies. *Liver Int* **29**: 18-24, 2009.

10. Gravante, G., Ong, S. L., Metcalfe, M. S., Strickland, A., Dennison, A. R., and Lloyd, D. M. Hepatic microwave ablation: a review of the histological changes following thermal damage. *Liver Int* **28**: 911-921, 2008.

11. Bhardwaj, N., Strickland, A. D., Ahmad, F., Atanesyan, L., West, K., and Lloyd, D. M. A comparative histological evaluation of the ablations produced by microwave, cryotherapy and radiofrequency in the liver. *Pathology* **41**: 168-172, 2009.

12. D'Arsonval, A. Action physiologique des courants alternatifs. *Soc. Biol* **43**: 283-286, 1891.

13. D'Arsonval, A. Action physiologique des courants alternatifs a grande frequence. *Arch Physiol Norm Pathol* **5**: 401-408, 1893.

14. Hertz, H. Recherches sur les Ondulations Électriques. *Archives des Sciences Physiques et Naturelles* **21**: 281-308, 1889.

15. Riviere, A. Action des courants de haute frequence et des effleuves du resonateur Oudin sur certaines tumeur malignes. *J Med Intern* **4**: 6-7, 1900.

16. De Forest, L. *Father of Radio*. Chicago: 1950.

17. Bovie, W. T. A preliminary note on a new surgical-current generator. 1928. *Clinical orthopaedics and related research*: 3-5, 1995.

18. Paliwal, B. R., Gibbs, F. A., Jr., and Wiley, A. L., Jr. Heating patterns induced by a 13.56 MHz radiofrequency generator in large phantoms and pig abdomen and thorax. *International journal of radiation oncology, biology, physics* **8**: 857-864, 1982.

19. Smialowicz, R. J., Weil, C. M., Kinn, J. B., and Elder, J. A. Exposure of rats to 425-MHz (cW) radiofrequency radiation: effects on lymphocytes. *The Journal of microwave power* **17**: 211-221, 1982.

20. Lotz, W. G., and Saxton, J. L. Metabolic and vasomotor responses of rhesus monkeys exposed to 225-MHz radiofrequency energy. *Bioelectromagnetics* **8**: 73-89, 1987.

21. Scheiblich, J., and Petrowicz, O. Radiofrequency-induced hyperthermia in the prostate. *The Journal of microwave power* **17**: 203-209, 1982.

22. Weigert, N., Eckel, F., Born, P., Erhardt, W., Henke, J., Werner, M., Classen, M., and Rosch, T. Endohyperthermia--experimental evaluation of a new therapeutic approach for treatment of biliary carcinoma. *Endoscopy* **32**: 306-310, 2000.

23. Morrison, P. R., vanSonnenberg, E., Shankar, S., Godleski, J., Silverman, S. G., Tuncali, K., Jaklitsch, M. T., and Jolesz, F. A. Radiofrequency ablation of thoracic lesions: part 1, experiments in the normal porcine thorax. *Ajr* **184**: 375-380, 2005.

24. Huang, S. K., Graham, A. R., and Wharton, K. Radiofrequency catheter ablation of the left and right ventricles: anatomic and electrophysiologic observations. *Pacing Clin Electrophysiol* **11**: 449-459, 1988.

25. Hindricks, G., Haverkamp, W., Dute, U., and Gulker, H. [The incidence of ventricular arrhythmia following direct current ablation, high-frequency current ablation and laser photo-ablation]. *Zeitschrift fur Kardiologie* **77**: 696-703, 1988.

26. Barry, K. J., Kaplan, J., Connolly, R. J., Nardella, P., Lee, B. I., Becker, G. J., Waller, B. F., and Callow, A. D. The effect of radiofrequency-generated thermal energy on the mechanical and histologic characteristics of the arterial wall in vivo: implications for radiofrequency angioplasty. *American heart journal* **117**: 332-341, 1989.

27. Haverkamp, W., Hindricks, G., Gulker, H., Rissel, U., Pfennings, W., Borggrefe, M., and Breithardt, G. Coagulation of ventricular myocardium using radiofrequency alternating current: bio-physical aspects and experimental findings. *Pacing Clin Electrophysiol* **12**: 187-195, 1989.

28. Verdaasdonk, R. M., Holstege, F. C., Jansen, E. D., and Borst, C. In vitro comparison of radiofrequency-heated and laser-heated metal probes for angioplasty. *Investigative radiology* **25**: 686-691, 1990.

29. Idikio, H. A., and Humen, D. P. Fine structural alterations in radiofrequency energy-induced lesions in dog hearts: possible basis for reduced arrhythmic complications. *The Canadian journal of cardiology* **7**: 270-274, 1991.

30. Mackey, S., Thornton, L., He, D. S., Marcus, F. I., and Lampe, L. F. Simultaneous multipolar radiofrequency ablation in the monopolar mode increases lesion size. *Pacing Clin Electrophysiol* **19**: 1042-1048, 1996.

31. Mantiply, E. D., Pohl, K. R., Poppell, S. W., and Murphy, J. A. Summary of measured radiofrequency electric and magnetic fields (10 kHz to 30 GHz) in the general and work environment. *Bioelectromagnetics* **18**: 563-577, 1997.

32. Repacholi, M. H. Low-level exposure to radiofrequency electromagnetic fields: health effects and research needs. *Bioelectromagnetics* **19**: 1-19, 1998.

33. Schwan, H. P. Biological effects of non-ionizing radiations: cellular properties and interactions. *Annals of biomedical engineering* **16**: 245-263, 1988.

34. Meltz, M. L. Radiofrequency exposure and mammalian cell toxicity, genotoxicity, and transformation. *Bioelectromagnetics* **Suppl 6**: S196-213, 2003.

35. Brusick, D., Albertini, R., McRee, D., Peterson, D., Williams, G., Hanawalt, P., and Preston, J. Genotoxicity of radiofrequency radiation. DNA/Genetox Expert Panel. *Environmental and molecular mutagenesis* **32**: 1-16, 1998.

36. Verschaeve, L., and Maes, A. Genetic, carcinogenic and teratogenic effects of radiofrequency fields. *Mutation research* **410**: 141-165, 1998.

37. Cosman, E. R., Nashold, B. S., and Ovelman-Levitt, J. Theoretical aspects of radiofrequency lesions in the dorsal root entry zone. *Neurosurgery* **15**: 945-950, 1984.

38. Hansen, P. D., Rogers, S., Corless, C. L., Swanstrom, L. L., and Siperstien, A. E. Radiofrequency ablation lesions in a pig liver model. *The Journal of surgical research* **87**: 114-121, 1999.

39. Goldberg, S. N., Solbiati, L., Hahn, P. F., Cosman, E., Conrad, J. E., Fogle, R., and Gazelle, G. S. Large-volume tissue ablation with radio frequency by using a clustered, internally cooled electrode technique: laboratory and clinical experience in liver metastases. *Radiology* **209**: 371-379, 1998.

40. Lorentzen, T., Christensen, N. E., Nolsle, C. P., and Torp-Pedersen, S. T. Radiofrequency tissue ablation with a cooled needle in vitro: ultrasonography, dose response, and lesion temperature. *Academic radiology* **4**: 292-297, 1997.

41. Sugimori, K., Morimoto, M., Shirato, K., Kokawa, A., Tomita, N., Saito, T., Nozawa, A., Hara, M., Sekihara, H., and Tanaka, K. Radiofrequency ablation in a pig liver model: effect of transcatheter arterial embolization on coagulation diameter and histologic characteristics. *Hepatol Res* **24**: 164, 2002.

42. McGahan, J. P., Brock, J. M., Tesluk, H., Gu, W. Z., Schneider, P., and Browning, P. D. Hepatic ablation with use of radio-frequency electrocautery in the animal model. *J Vasc Interv Radiol* **3**: 291-297, 1992.

43. Kettenbach, J., Kostler, W., Rucklinger, E., Gustorff, B., Hupfl, M., Wolf, F., Peer, K., Weigner, M., Lammer, J., Muller, W., and Goldberg, S. N. Percutaneous saline-enhanced radiofrequency ablation of unresectable hepatic tumors: initial experience in 26 patients. *Ajr* **180**: 1537-1545, 2003.

44. Pereira, P. L., Trubenbach, J., Schenk, M., Subke, J., Kroeber, S., Schaefer, I., Remy, C. T., Schmidt, D., Brieger, J., and Claussen, C. D. Radiofrequency ablation: in vivo comparison of four commercially available devices in pig livers. *Radiology* **232**: 482-490, 2004.

45. Curley, S. A., Davidson, B. S., Fleming, R. Y., Izzo, F., Stephens, L. C., Tinkey, P., and Cromeens, D. Laparoscopically guided bipolar radiofrequency ablation of areas of porcine liver. *Surgical endoscopy* **11**: 729-733, 1997.

46. Nikfarjam, M., Muralidharan, V., and Christophi, C. Mechanisms of focal heat destruction of liver tumors. *The Journal of surgical research* **127**: 208-223, 2005.

47. Curley, S. A., Izzo, F., Delrio, P., Ellis, L. M., Granchi, J., Vallone, P., Fiore, F., Pignata, S., Daniele, B., and Cremona, F. Radiofrequency ablation of unresectable primary and metastatic hepatic malignancies: results in 123 patients. *Annals of surgery* **230**: 1-8, 1999.

48. Rossi, S., Fornari, F., Pathies, C., and Buscarini, L. Thermal lesions induced by 480 KHz localized current field in guinea pig and pig liver. *Tumori* **76**: 54-57, 1990.

49. Goldberg, S. N., Gazelle, G. S., Compton, C. C., Mueller, P. R., and Tanabe, K. K. Treatment of intrahepatic malignancy with radiofrequency ablation: radiologic-pathologic correlation. *Cancer* **88**: 2452-2463, 2000.

50. Mulier, S., Miao, Y., Mulier, P., Dupas, B., Pereira, P., de Baere, T., Lencioni, R., Leveillee, R., Marchal, G., Michel, L., and Ni, Y. Electrodes and multiple electrode systems for radiofrequency ablation: a proposal for updated terminology. *Eur Radiol* **15**: 798-808, 2005.

51. Goldberg, S. N., Grassi, C. J., Cardella, J. F., Charboneau, J. W., Dodd, G. D., 3rd, Dupuy, D. E., Gervais, D. A., Gillams, A. R., Kane, R. A., Lee, F. T., Jr., Livraghi, T., McGahan, J., Phillips, D. A., Rhim, H., Silverman, S. G., Solbiati, L., Vogl, T. J., Wood, B. J., Vedantham, S., and Sacks, D. Image-guided tumor ablation: standardization of terminology and reporting criteria. *J Vasc Interv Radiol* **20**: S377-390, 2009.

52. Sutherland, L. M., Williams, J. A., Padbury, R. T., Gotley, D. C., Stokes, B., and Maddern, G. J. Radiofrequency ablation of liver tumors: a systematic review. *Arch Surg* **141**: 181-190, 2006.

53. Mulier, S., Ni, Y., Jamart, J., Ruers, T., Marchal, G., and Michel, L. Local recurrence after hepatic radiofrequency coagulation: multivariate meta-analysis and review of contributing factors. *Annals of surgery* **242**: 158-171, 2005.

54. Mulier, S., Ni, Y., Jamart, J., Michel, L., Marchal, G., and Ruers, T. Radiofrequency ablation versus resection for resectable colorectal liver metastases: time for a randomized trial? *Annals of surgical oncology* **15**: 144-157, 2008.

55. Liang, P., Dong, B., Yu, X., Yu, D., Wang, Y., Feng, L., and Xiao, Q. Prognostic factors for survival in patients with hepatocellular carcinoma after percutaneous microwave ablation. *Radiology* **235**: 299-307, 2005.

56. Gravante, G. Thermal ablation for unresectable liver tumours, time to move forward? *World J Gastrointest Surg* **2**: 1-5, 2010.

57. Seifert, J. K., and Morris, D. L. Prognostic factors after cryotherapy for hepatic metastases from colorectal cancer. *Annals of surgery* **228**: 201-208, 1998.

58. Seifert, J. K., and Morris, D. L. Indicators of recurrence following cryotherapy for hepatic metastases from colorectal cancer. *Br J Surg* **86**: 234-240, 1999.

59. Gravante, G., Ong, S. L., Metcalfe, M. S., Bhardwaj, N., Lloyd, D. M., and Dennison, A. R. The effects of radiofrequency ablation on the hepatic parenchyma: Histological bases for tumor recurrences. *Surgical oncology*.

60. Griffin, D. T., Dodd, N. J., Zhao, S., Pullan, B. R., and Moore, J. V. Low-level direct electrical current therapy for hepatic metastases. I. Preclinical studies on normal liver. *Br J Cancer* **72**: 31-34, 1995.

61. Samuelsson, L., Jonsson, L., Lamm, I. L., Linden, C. J., and Ewers, S. B. Electrolysis with different electrode materials and combined with irradiation for treatment of experimental rat tumors. *Acta Radiol* **32**: 178-181, 1991.

62. Samuelsson, L., Olin, T., and Berg, N. O. Electrolytic destruction of lung tissue in the rabbit. *Acta radiologica: diagnosis* **21**: 447-454, 1980.

63. Cockburn, J. F., Maddern, G. J., and Wemyss-Holden, S. A. Bimodal electric tissue ablation (BETA) - in-vivo evaluation of the effect of applying direct current before and during radiofrequency ablation of porcine liver. *Clinical radiology* **62**: 213-220, 2007.

64. Dobbins, C., Wemyss-Holden, S. A., Cockburn, J., and Maddern, G. J. Bimodal electric tissue ablation-modified radiofrequency ablation with a le veen electrode in a pig model. *J Surg Res* **144**: 111-116, 2008.

65. Dobbins, C., Brennan, C., Wemyss-Holden, S., Cockburn, J., and Maddern, G. Bimodal electric tissue ablation-long term studies of morbidity and pathological change. *J Surg Res* **148**: 251-259, 2008.

66. Dobbins, C., Brennan, C., Wemyss-Holden, S. A., Cockburn, J., and Maddern, G. J. Bimodal electric tissue ablation: positive electrode studies. *ANZ journal of surgery* **78**: 568-572, 2008.

67. Nordenstrom, B. E. Survey of mechanisms in electrochemical treatment (ECT) of cancer. *Eur J Surg Suppl*: 93-109, 1994.

68. Finch, J. G., Fosh, B., Anthony, A., Slimani, E., Texler, M., Berry, D. P., Dennison, A. R., and Maddern, G. J. Liver electrolysis: pH can reliably monitor the extent of hepatic ablation in pigs. *Clin Sci (Lond)* **102**: 389-395, 2002.

69. von Euler, H., Nilsson, E., Olsson, J. M., and Lagerstedt, A. S. Electrochemical treatment (EChT) effects in rat mammary and liver tissue. In vivo optimizing of a dose-planning model for EChT of tumours. *Bioelectrochemistry (Amsterdam, Netherlands)* **54**: 117-124, 2001.

70. Wemyss-Holden, S. A., Dennison, A. R., Finch, G. J., Hall Pd Pde, L., and Maddern, G. J. Electrolytic ablation as an adjunct to liver resection: experimental studies of predictability and safety. *Br J Surg* **89**: 579-585, 2002.

71. Hagedorn, R., and Fuhr, G. Steady state electrolysis and isoelectric focusing. *Electrophoresis* **11**: 281-289, 1990.

72. Baumgartl, H., Zimelka, W., and Lubbers, D. W. pH changes in front of the hydrogen generating electrode during measurements with an electrolytic hydrogen clearance sensor. *Adv Exp Med Biol* **277**: 107-113, 1990.

73. Baxter, P. S., Wemyss-Holden, S. A., Dennison, A. R., and Maddern, G. J. Electrochemically induced hepatic necrosis: the next step forward in patients with unresectable liver tumours? *Aust N Z J Surg* **68**: 637-640, 1998.

74. Robertson, G. S., Wemyss-Holden, S. A., Dennison, A. R., Hall, P. M., Baxter, P., and Maddern, G. J. Experimental study of electrolysis-induced hepatic necrosis. *Br J Surg* **85**: 1212-1216, 1998.

75. Li, K., Xin, Y., Gu, Y., Xu, B., Fan, D., and Ni, B. Effects of direct current on dog liver: possible mechanisms for tumor electrochemical treatment. *Bioelectromagnetics* **18**: 2-7, 1997.

76. Turler, A., Schaefer, H., Schaefer, N., Maintz, D., Wagner, M., Qiao, J. C., and Hoelscher, A. H. Local treatment of hepatic metastases with low-level direct electric current: experimental results. *Scand J Gastroenterol* **35**: 322-328, 2000.

77. Marino, A. A., Morris, D., and Arnold, T. Electrical treatment of Lewis lung carcinoma in mice. *J Surg Res* **41**: 198-201, 1986.

78. Grossi, E. A., Parish, M. A., Kralik, M. R., Glassman, L. R., Esposito, R. A., Ribakove, G. H., Galloway, A. C., and Colvin, S. B. Direct-current injury from external pacemaker results in tissue electrolysis. *The Annals of thoracic surgery* **56**: 156-157, 1993.

79. David, S. L., Absolom, D. R., Smith, C. R., Gams, J., and Herbert, M. A. Effect of low level direct current on in vivo tumor growth in hamsters. *Cancer research* **45**: 5625-5631, 1985.

80. Berendson, J., and Simonsson, D. Electrochemical aspects of treatment of tissue with direct current. *Eur J Surg Suppl* **574)**: 111-115, 1994.

81. von Euler, H., Olsson, J. M., Hultenby, K., Thorne, A., and Lagerstedt, A. S. Animal models for treatment of unresectable liver tumours: a histopathologic and ultra-structural study of cellular toxic changes after electrochemical treatment in rat and dog liver. *Bioelectrochemistry (Amsterdam, Netherlands)* **59**: 89-98, 2003.

82. Jarm, T., Cemazar, M., Steinberg, F., Streffer, C., Sersa, G., and Miklavcic, D. Perturbation of blood flow as a mechanism of anti-tumour action of direct current electrotherapy. *Physiol Meas* **24**: 75-90, 2003.

83. Jarm, T., Wickramasinghe, Y. A., Deakin, M., Cemazar, M., Elder, J., Rolfe, P., Sersa, G., and Miklavcic, D. Blood perfusion of subcutaneous tumours in mice following the application of low-level direct electric current. *Adv Exp Med Biol* **471**: 497-506, 1999.

84. Lin, X. Z., Jen, C. M., Chou, C. K., Chou, C. S., Sung, M. J., and Chou, T. C. Saturated saline enhances the effect of electrochemical therapy. *Digestive diseases and sciences* **45**: 509-514, 2000.

85. Finch, J. G., Fosh, B. G., Anthony, A. A., Texler, M., Pearson, S., Dennison, A. R., and Maddern, G. J. The use of a "liquid" electrode in hepatic electrolysis. *J Surg Res* **120**: 272-277, 2004.

86. Samuelsson, L., and Jonsson, L. Electrolytic destruction of tissue in the normal lung of the pig. *Acta radiologica: diagnosis* **22**: 9-14, 1981.

87. Turler, A., Schaefer, H., Schaefer, N., Wagner, M., Maintz, D., Qiao, J. C., and Hoelscher, A. H. Experimental low-level direct current therapy in liver metastases: influence of polarity and current dose. *Bioelectromagnetics* **21**: 395-401, 2000.

88. Berry, D. P., Garcea, G., Vanderzon, P., Slimani, E., Chong, C., Dennison, A. R., and Maddern, G. J. Augmenting the ablative effect of liver electrolysis: using two electrodes and the pringle maneuver. *J Invest Surg* **17**: 105-112, 2004.

89. Wemyss-Holden, S. A., de la M Hall, P., Robertson, G. S., Dennison, A. R., Vanderzon, P. S., and Maddern, G. J. The safety of electrolytically induced hepatic necrosis in a pig model. *Aust N Z J Surg* **70**: 607-612, 2000.

90. Fosh, B. G., Finch, J. G., Lea, M., Black, C., Wong, S., Wemyss-Holden, S., and Maddern, G. J. Use of electrolysis as an adjunct to liver resection. *Br J Surg* **89**: 999-1002, 2002.

91. Berry, D. P., Dennison, A. R., Ward, R., and Maddern, G. J. Electrolytic ablation of colorectal liver metastases: 1-year histological patient follow-up. *Digestive surgery* **17**: 518-519, 2000.

92. Mannelli, L., Padia, S. A., Yeung, R. S., and Green, D. E. Irreversible electroporation of a liver metastasis. *Liver Int* **33**: 104.

93. Lee, E. W., Thai, S., and Kee, S. T. Irreversible electroporation: a novel image-guided cancer therapy. *Gut and liver* **4 Suppl 1**: S99-S104, 2010.

94. Charpentier, K. P. Irreversible electroporation for the ablation of liver tumors: are we there yet? *Arch Surg* **147**: 1053-1061, 2012.

95. Appelbaum, L., Ben-David, E., Faroja, M., Nissenbaum, Y., Sosna, J., and Goldberg, S. N. Irreversible Electroporation Ablation: Creation of Large-Volume Ablation Zones in in Vivo Porcine Liver with Four-Electrode Arrays. *Radiology*.

96. Lee, Y. J., Lu, D. S., Osuagwu, F., and Lassman, C. Irreversible electroporation in porcine liver: acute computed tomography appearance of ablation zone with histopathologic correlation. *Journal of computer assisted tomography* **37**: 154-158, 2013.

97. Lee, Y. J., Lu, D. S., Osuagwu, F., and Lassman, C. Irreversible electroporation in porcine liver: short- and long-term effect on the hepatic veins and adjacent tissue by CT with pathological correlation. *Investigative radiology* **47**: 671-675, 2012.

98. Ben-David, E., Appelbaum, L., Sosna, J., Nissenbaum, I., and Goldberg, S. N. Characterization of irreversible electroporation ablation in in vivo porcine liver. *AJR Am J Roentgenol* **198**: W62-68, 2012.

99. Fuchs, E. J., and Matzinger, P. Is cancer dangerous to the immune system? *Seminars in immunology* **8**: 271-280, 1996.

100. Gallucci, S., Lolkema, M., and Matzinger, P. Natural adjuvants: endogenous activators of dendritic cells. *Nature medicine* **5**: 1249-1255, 1999.

101. Schueller, G., Kettenbach, J., Sedivy, R., Stift, A., Friedl, J., Gnant, M., and Lammer, J. Heat shock protein expression induced by percutaneous radiofrequency ablation of hepatocellular carcinoma in vivo. *International journal of oncology* **24**: 609-613, 2004.

102. Schueller, G., Kettenbach, J., Sedivy, R., Bergmeister, H., Stift, A., Fried, J., Gnant, M., and Lammer, J. Expression of heat shock proteins in human hepatocellular carcinoma after radiofrequency ablation in an animal model. *Oncology reports* **12**: 495-499, 2004.

103. Harding, C. V. Class I MHC presentation of exogenous antigens. *Journal of clinical immunology* **16**: 90-96, 1996.

104. Hansler, J., Wissniowski, T. T., Schuppan, D., Witte, A., Bernatik, T., Hahn, E. G., and Strobel, D. Activation and dramatically increased cytolytic activity of tumor specific T lymphocytes after radio-frequency ablation in patients with hepatocellular carcinoma and colorectal liver metastases. *World J Gastroenterol* **12**: 3716-3721, 2006.

105. Hansler, J., Neureiter, D., Strobel, D., Muller, W., Mutter, D., Bernatik, T., Hahn, E. G., and Becker, D. Cellular and vascular reactions in the liver to radio-frequency thermo-ablation with wet needle applicators. Study on juvenile domestic pigs. *European surgical research. Europaische chirurgische Forschung* **34**: 357-363, 2002.

106. Wissniowski, T. T., Hansler, J., Neureiter, D., Frieser, M., Schaber, S., Esslinger, B., Voll, R., Strobel, D., Hahn, E. G., and Schuppan, D. Activation of tumor-specific T lymphocytes by radio-frequency ablation of the VX2 hepatoma in rabbits. *Cancer research* **63**: 6496-6500, 2003.

107. den Brok, M. H., Sutmuller, R. P., van der Voort, R., Bennink, E. J., Figdor, C. G., Ruers, T. J., and Adema, G. J. In situ tumor ablation creates an antigen source for the generation of antitumor immunity. *Cancer research* **64**: 4024-4029, 2004.

108. Ali, M. Y., Grimm, C. F., Ritter, M., Mohr, L., Allgaier, H. P., Weth, R., Bocher, W. O., Endrulat, K., Blum, H. E., and Geissler, M. Activation of dendritic cells by local ablation of hepatocellular carcinoma. *Journal of hepatology* **43**: 817-822, 2005.

109. den Brok, M. H., Sutmuller, R. P., Nierkens, S., Bennink, E. J., Frielink, C., Toonen, L. W., Boerman, O. C., Figdor, C. G., Ruers, T. J., and Adema, G. J. Efficient loading of dendritic cells following cryo and radiofrequency ablation in combination with immune modulation induces anti-tumour immunity. *British journal of cancer* **95**: 896-905, 2006.

110. Zerbini, A., Pilli, M., Fagnoni, F., Pelosi, G., Pizzi, M. G., Schivazappa, S., Laccabue, D., Cavallo, C., Schianchi, C., Ferrari, C., and Missale, G. Increased immunostimulatory activity conferred to antigen-presenting cells by exposure to antigen extract from hepatocellular carcinoma after radiofrequency thermal ablation. *J Immunother* **31**: 271-282, 2008.

111. Zerbini, A., Pilli, M., Penna, A., Pelosi, G., Schianchi, C., Molinari, A., Schivazappa, S., Zibera, C., Fagnoni, F. F., Ferrari, C., and Missale, G. Radiofrequency thermal ablation of hepatocellular carcinoma liver nodules can activate and enhance tumor-specific T-cell responses. *Cancer research* **66**: 1139-1146, 2006.

112. Napoletano, C., Taurino, F., Biffoni, M., De Majo, A., Coscarella, G., Bellati, F., Rahimi, H., Pauselli, S., Pellicciotta, I., Burchell, J. M., Gaspari, L. A., Ercoli, L., Rossi, P., and Rughetti, A. RFA strongly modulates the immune system and anti-tumor immune responses in metastatic liver patients. *International journal of oncology* **32**: 481-490, 2008.

113. Evrard, S., Menetrier-Caux, C., Biota, C., Neaud, V., Mathoulin-Pelissier, S., Blay, J. Y., and Rosenbaum, J. Cytokines pattern after surgical radiofrequency ablation of liver colorectal metastases. *Gastroenterologie clinique et biologique* **31**: 141-145, 2007.

114. Schell, S. R., Wessels, F. J., Abouhamze, A., Moldawer, L. L., and Copeland, E. M., 3rd Pro- and antiinflammatory cytokine production after radiofrequency ablation of unresectable hepatic tumors. *Journal of the American College of Surgeons* **195**: 774-781, 2002.

115. Meredith, K., Haemmerich, D., Qi, C., and Mahvi, D. Hepatic resection but not radiofrequency ablation results in tumor growth and increased growth factor expression. *Annals of surgery* **245**: 771-776, 2007.

116. Schueller, G., Stift, A., Friedl, J., Dubsky, P., Bachleitner-Hofmann, T., Benkoe, T., Jakesz, R., and Gnant, M. Hyperthermia improves cellular immune response to human hepatocellular carcinoma subsequent to co-culture with tumor lysate pulsed dendritic cells. *International journal of oncology* **22**: 1397-1402, 2003.

117. Rughetti, A., Rahimi, H., Rossi, P., Frati, L., Nuti, M., Gaspari, A., Danza, F. M., and Ercoli, L. Modulation of blood circulating immune cells by radiofrequency tumor ablation. *J Exp Clin Cancer Res* **22**: 247-250, 2003.

118. Chapman, W. C., Debelak, J. P., Wright Pinson, C., Washington, M. K., Atkinson, J. B., Venkatakrishnan, A., Blackwell, T. S., and Christman, J. W. Hepatic cryoablation, but not radiofrequency ablation, results in lung inflammation. *Annals of surgery* **231**: 752-761, 2000.

119. Ng, K. K., Lam, C. M., Poon, R. T., Shek, T. W., To, J. Y., Wo, Y. H., Ho, D. W., and Fan, S. T. Comparison of systemic responses of radiofrequency ablation, cryotherapy, and surgical resection in a porcine liver model. *Annals of surgical oncology* **11**: 650-657, 2004.

120. Ng, K. K., Lam, C. M., Poon, R. T., Shek, T. W., Ho, D. W., and Fan, S. T. Safety limit of large-volume hepatic radiofrequency ablation in a rat model. *Arch Surg* **141**: 252-258, 2006.

121. Teague, B. D., Court, F. G., Morrison, C. P., Kho, M., Wemyss-Holden, S. A., and Maddern, G. J. Electrolytic liver ablation is not associated with evidence of a systemic inflammatory response syndrome. *Br J Surg* **91**: 178-183, 2004.

122. Gillams, A. R. The use of radiofrequency in cancer. *British journal of cancer* **92**: 1825-1829, 2005.

123. Lau, W. Y., and Lai, E. C. The current role of radiofrequency ablation in the management of hepatocellular carcinoma: a systematic review. *Annals of surgery* **249**: 20-25, 2009.

124. Cho, Y. K., Kim, J. K., Kim, M. Y., Rhim, H., and Han, J. K. Systematic review of randomized trials for hepatocellular carcinoma treated with percutaneous ablation therapies. *Hepatology (Baltimore, Md* **49**: 453-459, 2009.

125. Patterson, E. J., Scudamore, C. H., Owen, D. A., Nagy, A. G., and Buczkowski, A. K. Radiofrequency ablation of porcine liver in vivo: effects of blood flow and treatment time on lesion size. *Annals of surgery* **227**: 559-565, 1998.

126. Tamaki, K., Shimizu, I., Oshio, A., Fukuno, H., Inoue, H., Tsutsui, A., Shibata, H., Sano, N., and Ito, S. Influence of large intrahepatic blood vessels on the gross and histological characteristics of lesions produced by radiofrequency ablation in a pig liver model. *Liver Int* **24**: 696-701, 2004.

127. Rossi, S., Garbagnati, F., De Francesco, I., Accocella, F., Leonardi, L., Quaretti, P., Zangrandi, A., Paties, C., and Lencioni, R. Relationship between the shape and size of radiofrequency induced thermal lesions and hepatic vascularization. *Tumori* **85**: 128-132, 1999.

128. Chinn, S. B., Lee, F. T., Jr., Kennedy, G. D., Chinn, C., Johnson, C. D., Winter, T. C., 3rd, Warner, T. F., and Mahvi, D. M. Effect of vascular occlusion on radiofrequency ablation of the liver: results in a porcine model. *Ajr* **176**: 789-795, 2001.

129. de Baere, T., Deschamps, F., Briggs, P., Dromain, C., Boige, V., Hechelhammer, L., Abdel-Rehim, M., Auperin, A., Goere, D., and Elias, D. Hepatic malignancies: percutaneous radiofrequency ablation during percutaneous portal or hepatic vein occlusion. *Radiology* **248**: 1056-1066, 2008.

130. Gravante, G., Delogu, D., Palmieri, M. B., Santeusanio, G., Montone, A., and Esposito, G. Inverse relationship between the apoptotic rate and the time elapsed from thermal injuries in deep partial thickness burns. *Burns* **34**: 228-233, 2008.

131. Hoffman, A. L., Wu, S. S., Obaid, A. K., French, S. W., Lois, J., McMonigle, M., Ramos, H. C., Sher, L. S., and Lopez, R. R. Histologic evaluation and treatment outcome after sequential radiofrequency ablation and hepatic resection for primary and metastatic tumors. *The American surgeon* **68**: 1038-1043, 2002.

132. Goldberg, S. N., Hahn, P. F., Tanabe, K. K., Mueller, P. R., Schima, W., Athanasoulis, C. A., Compton, C. C., Solbiati, L., and Gazelle, G. S. Percutaneous radiofrequency tissue ablation:

does perfusion-mediated tissue cooling limit coagulation necrosis? *J Vasc Interv Radiol* **9**: 101-111, 1998.

133. Oshio, A., Tamaki, K., Shimizu, I., Fukuno, H., Urata, M., Ito, S., and Sano, N. Double radiofrequency ablation is more extensive with a spherical zone shape compared to single ablation in a pig liver model. *J Med Invest* **54**: 28-34, 2007.

134. Ng, K. K., Lam, C. M., Poon, R. T., Shek, T. W., Fan, S. T., and Wong, J. Delayed portal vein thrombosis after experimental radiofrequency ablation near the main portal vein. *The British journal of surgery* **91**: 632-639, 2004.

135. Denys, A. L., De Baere, T., Mahe, C., Sabourin, J. C., Sa Cunha, A., Germain, S., and Roche, A. Radio-frequency tissue ablation of the liver: effects of vascular occlusion on lesion diameter and biliary and portal damages in a pig model. *European radiology* **11**: 2102-2108, 2001.

136. Raman, S. S., Lu, D. S., Vodopich, D. J., Sayre, J., and Lassman, C. Creation of radiofrequency lesions in a porcine model: correlation with sonography, CT, and histopathology. *Ajr* **175**: 1253-1258, 2000.

137. Morimoto, M., Nozawa, A., Numata, K., Shirato, K., Sugimori, K., Kokawa, A., Tomita, N., Saitou, T., Nakatani, Y., Imada, T., and Tanaka, K. Evaluation using contrast-enhanced harmonic gray scale sonography after radio frequency ablation of small hepatocellular carcinoma: sonographic-histopathologic correlation. *J Ultrasound Med* **24**: 273-283, 2005.

138. Ni, Y., Chen, F., Mulier, S., Sun, X., Yu, J., Landuyt, W., Marchal, G., and Verbruggen, A. Magnetic resonance imaging after radiofrequency ablation in a rodent model of liver tumor: tissue characterization using a novel necrosis-avid contrast agent. *European radiology* **16**: 1031-1040, 2006.

139. Scudamore, C. H., Lee, S. I., Patterson, E. J., Buczkowski, A. K., July, L. V., Chung, S. W., Buckley, A. R., Ho, S. G., and Owen, D. A. Radiofrequency ablation followed by resection of malignant liver tumors. *American journal of surgery* **177**: 411-417, 1999.

140. Kuromatsu, R., Tanaka, M., Shimauchi, Y., Harada, R., Ando, E., Itano, S., Kumashiro, R., Fukuda, S., Okuda, K., and Sata, M. Light and electron microscopic analyses of immediate and late tissue damage caused by radiofrequency ablation in porcine liver. *International journal of molecular medicine* **11**: 199-204, 2003.

141. Lee, J. D., Lee, J. M., Kim, S. W., Kim, C. S., and Mun, W. S. MR imaging-histopathologic correlation of radiofrequency thermal ablation lesion in a rabbit liver model: observation during acute and chronic stages. *Korean J Radiol* **2**: 151-158, 2001.

142. Rai, R., Richardson, C., Flecknell, P., Robertson, H., Burt, A., and Manas, D. M. Study of apoptosis and heat shock protein (HSP) expression in hepatocytes following radiofrequency ablation (RFA). *The Journal of surgical research* **129**: 147-151, 2005.

143. Anderson, C. D., Lin, W. C., Beckham, J., Mahadevan-Jansen, A., Buttemere, C. R., Pierce, J., Nicoud, I. B., Wright Pinson, C., and Chari, R. S. Fluorescence spectroscopy accurately detects irreversible cell damage during hepatic radiofrequency ablation. *Surgery* **136**: 524-531, 2004.

144. Ng, K. K., Lam, C. M., Poon, R. T., Shek, T. W., Yu, W. C., To, J. Y., Wo, Y. H., Lau, C. P., Tang, T. C., Ho, D. W., and Fan, S. T. Porcine liver: morphologic characteristics and cell viability at experimental radiofrequency ablation with internally cooled electrodes. *Radiology* **235**: 478-486, 2005.

145. Anderson, C. D., Lin, W. C., Buttemere, C. R., Washington, M. K., Mahadevan-Jansen, A., Pierce, J., Nicoud, I. B., Pinson, C. W., and Chari, R. S. Real-time spectroscopic assessment of thermal damage: implications for radiofrequency ablation. *J Gastrointest Surg* **8**: 660-669, 2004.

146. Hsu, C. P., Razavi, M. K., So, S. K., Parachikov, I. H., and Benaron, D. A. Liver tumor gross margin identification and ablation monitoring during liver radiofrequency treatment. *J Vasc Interv Radiol* **16**: 1473-1478, 2005.

147. Ritz, J. P., Roggan, A., Isbert, C., Muller, G., Buhr, H. J., and Germer, C. T. Optical properties of native and coagulated porcine liver tissue between 400 and 2400 nm. *Lasers in surgery and medicine* **29**: 205-212, 2001.

148. Ritz, J. P., Roggan, A., Germer, C. T., Isbert, C., Muller, G., and Buhr, H. J. Continuous changes in the optical properties of liver tissue during laser-induced interstitial thermotherapy. *Lasers in surgery and medicine* **28**: 307-312, 2001.

149. Germer, C. T., Roggan, A., Ritz, J. P., Isbert, C., Albrecht, D., Muller, G., and Buhr, H. J. Optical properties of native and coagulated human liver tissue and liver metastases in the near infrared range. *Lasers in surgery and medicine* **23**: 194-203, 1998.

150. Kruskal, J. B., Oliver, B., Huertas, J. C., and Goldberg, S. N. Dynamic intrahepatic flow and cellular alterations during radiofrequency ablation of liver tissue in mice. *J Vasc Interv Radiol* **12**: 1193-1201, 2001.

151. Lin, S. M., Shen, C. H., Lin, D. Y., Kuo, S. H., Lin, C. J., Hsu, C. W., Chung, H. J., and Peng, C. Y. Cytologic changes in small hepatocellular carcinomas after radiofrequency ablation. *Acta cytologica* **46**: 490-494, 2002.

152. Cha, C. H., Lee, F. T., Jr., Gurney, J. M., Markhardt, B. K., Warner, T. F., Kelcz, F., and Mahvi, D. M. CT versus sonography for monitoring radiofrequency ablation in a porcine liver. *Ajr* **175**: 705-711, 2000.

153. Lu, D. S., Raman, S. S., Vodopich, D. J., Wang, M., Sayre, J., and Lassman, C. Effect of vessel size on creation of hepatic radiofrequency lesions in pigs: assessment of the "heat sink" effect. *Ajr* **178**: 47-51, 2002.

154. Sato, K., Nakamura, K., Hamuro, M., Sakai, Y., Nishida, N., Yamada, R., Ikura, Y., Ueda, M., and Inoue, Y. The influence of radiofrequency ablation on hepatic vessels in porcine liver. *Hepato-gastroenterology* **52**: 571-574, 2005.

155. Sofocleous, C. T., Klein, K. M., Hubbi, B., Brown, K. T., Weiss, S. H., Kannarkat, G., Hinrichs, C. R., Contractor, D., Bahramipour, P., Barone, A., and Baker, S. R. Histopathologic evaluation of tissue extracted on the radiofrequency probe after ablation of liver tumors: preliminary findings. *Ajr* **183**: 209-213, 2004.

156. Morimoto, M., Sugimori, K., Shirato, K., Kokawa, A., Tomita, N., Saito, T., Tanaka, N., Nozawa, A., Hara, M., Sekihara, H., Shimada, H., Imada, T., and Tanaka, K. Treatment of hepatocellular carcinoma with radiofrequency ablation: radiologic-histologic correlation during follow-up periods. *Hepatology (Baltimore, Md* **35**: 1467-1475, 2002.

157. Sofocleous, C. T., Nascimento, R. G., Petrovic, L. M., Klimstra, D. S., Gonen, M., Brown, K. T., Brody, L. A., Covey, A. M., Thornton, R. H., Fong, Y., Solomon, S. B., Schwartz, L. H., DeMatteo, R. P., and Getrajdman, G. I. Histopathologic and immunohistochemical features of tissue adherent to multitined electrodes after RF ablation of liver malignancies can help predict local tumor progression: initial results. *Radiology* **249**: 364-374, 2008.

158. Yoshimoto, T., Kotoh, K., Horikawa, Y., Kohjima, M., Morizono, S., Yamashita, S., Enjoji, M., and Nakamuta, M. Decreased portal flow volume increases the area of necrosis caused by radio frequency ablation in pigs. *Liver Int* **27**: 368-372, 2007.

159. Goldberg, S. N., Walovitch, R. C., Straub, J. A., Shore, M. T., and Gazelle, G. S. Radio-frequency-induced coagulation necrosis in rabbits: immediate detection at US with a synthetic microsphere contrast agent. *Radiology* **213**: 438-444, 1999.

160. Leyendecker, J. R., Dodd, G. D., 3rd, Halff, G. A., McCoy, V. A., Napier, D. H., Hubbard, L. G., Chintapalli, K. N., Chopra, S., Washburn, W. K., Esterl, R. M., Cigarroa, F. G., Kohlmeier, R. E., and Sharkey, F. E. Sonographically observed echogenic response during intraoperative radiofrequency ablation of cirrhotic livers: pathologic correlation. *Ajr* **178**: 1147-1151, 2002.

161. Chang, C. K., Hendy, M. P., Smith, J. M., Recht, M. H., and Welling, R. E. Radiofrequency ablation of the porcine liver with complete hepatic vascular occlusion. *Annals of surgical oncology* **9**: 594-598, 2002.

162. Shen, P., Fleming, S., Westcott, C., and Challa, V. Laparoscopic radiofrequency ablation of the liver in proximity to major vasculature: effect of the Pringle maneuver. *Journal of surgical oncology* **83**: 36-41, 2003.

163. Bangard, C., Gossmann, A., Kasper, H. U., Hellmich, M., Fischer, J. H., Holscher, A., Lackner, K., and Stippel, D. L. Experimental radiofrequency ablation near the portal and the hepatic veins in pigs: differences in efficacy of a monopolar ablation system. *The Journal of surgical research* **135**: 113-119, 2006.

164. Wemyss-Holden, S. A., Robertson, G. S., Dennison, A. R., de la M Hall, P., Fothergill, J. C., Jones, B., and Maddern, G. J. Electrochemical lesions in the rat liver support its potential for treatment of liver tumors. *J Surg Res* **93**: 55-62, 2000.

165. Wemyss-Holden, S. A., Robertson, G. S., Dennison, A. R., Vanderzon, P. S., Hall, P. M., and Maddern, G. J. A new treatment for unresectable liver tumours: long-term studies of electrolytic lesions in the pig liver. *Clin Sci (Lond)* **98**: 561-567, 2000.

166. Wemyss-Holden, S. A., Robertson, G. S., Hall, P. D., Dennison, A. R., and Maddern, G. J. Electrolytic treatment of colorectal liver tumour deposits in a rat model: a technique with potential for patients with unresectable liver tumours. *Dig Dis* **18**: 50-57, 2000.

167. Berry, D. P., Dennison, A. R., Vanderzon, P. S., Wemyss-Holden, S. A., and Maddern, G. J. Electrolytic ablation of the liver: the effect of multiple electrodes. *Gastroenterology* **116**: A377, 1999.

168. Berry, D., Garcea, G., Chong, C., Silman, E., Finch, G., Dennison, A., and Maddern, G. J. Systematic reaction to electrolytic treatment of pig livers in vivo. *ANZ journal of surgery* **74**: 586-590, 2004.

169. Metcalfe, M. S., Mullin, E. J., Texler, M., Berry, D. P., Dennison, A. R., and Maddern, G. J. The safety and efficacy of radiofrequency and electrolytic ablation created adjacent to large hepatic veins in a porcine model. *Eur J Surg Oncol* **33**: 662-667, 2007.

170. Wemyss-Holden, S. A., Berry, D. P., Robertson, G. S., Dennison, A. R., De La M Hall, P., and Maddern, G. J. Electrolytic ablation as an adjunct to liver resection: Safety and efficacy in patients. *ANZ journal of surgery* **72**: 589-593, 2002.

171. Hinz, S., Egberts, J. H., Pauser, U., Schafmayer, C., Fandrich, F., and Tepel, J. Electrolytic ablation is as effective as radiofrequency ablation in the treatment of artificial liver metastases in a pig model. *Journal of surgical oncology* **98**: 135-138, 2008.

172. Schaefer, N., Schafer, H., Maintz, D., Wagner, M., Overhaus, M., Hoelscher, A. H., and Turler, A. Efficacy of direct electrical current therapy and laser-induced interstitial thermotherapy in local treatment of hepatic colorectal metastases: an experimental model in the rat. *J Surg Res* **146**: 230-240, 2008.

173. Dobbins, C., Wemyss-Holden, S., Cockburn, J., and Maddern, G. Beta is better than radiofrequency ablation. *ANZ J. Surg* **77**: A41, 2007.

174. Xin, Y. L. Advances in the treatment of malignant tumours by electrochemical therapy (ECT). *Eur J Surg Suppl* **574**: 31-35, 1994.

175. Wang, H. L. Electrochemical therapy of 74 cases of liver cancer. *Eur J Surg Suppl* **574**: 55-57, 1994.

176. Lao, Y. H., Ge, T. G., Zheng, X. L., Zhang, J. Z., Hua, Y. W., Mao, S. M., and Feng, X. Electrochemical therapy for intermediate and advanced liver cancer: a report of 50 cases. *Eur J Surg Suppl* **574**: 51-53, 1994.

177. Fosh, B. G., Finch, J. G., Anthony, A. A., Lea, M. M., Wong, S. K., Black, C. L., and Maddern, G. J. Use of electrolysis for the treatment of non-resectable hepatocellular carcinoma. *ANZ journal of surgery* **73**: 1068-1070, 2003.

178. Fosh, B. G., Finch, J. G., Anthony, A. A., Texler, M., and Maddern, G. J. Electrolytic ablation of the rat pancreas: a feasibility trial. *BMC gastroenterology* **1**: 9, 2001.

179. Wemyss-Holden, S. A., Court, F. G., Morrison, C. P., Teague, B. D., Burrell, A., Morales, D. R., Rodgers, N., Anthony, A. A., Metcalfe, M. S., Dennison, A. R., and Maddern, G. J. Palliation of pancreatic cancer using electrolytic ablation. *Surgical endoscopy* **17**: 207-211, 2003.

180. Morrison, C. P., Court, F. G., Wemyss-Holden, S. A., Teague, B. D., Burrell, A., Texler, M., Metcalfe, M. S., Dennison, A. R., and Maddern, G. J. Perductal electrolytic ablation of the porcine

pancreas: a minimally invasive option-studies of morbidity and mortality. *Surgical endoscopy* **18**: 1435-1441, 2004.

181. Morrison, C. P., Court, F. G., Teague, B. D., Metcalfe, M. S., Wemyss-Holden, S. A., Texler, M., Dennison, A. R., and Maddern, G. J. Endoscopic perductal electrolytic ablation of the pancreas: experimental studies of morbidity and mortality. *Dig Dis* **23**: 83-91, 2005.

182. Teague, B. D., Morrison, C. P., Court, F. G., Nguyen, T., Wemyss-Holden, S. A., Dennison, A. R., and Maddern, G. J. The lack of a systemic inflammatory response syndrome supports the safety of pancreatic electrolysis: experimental studies. *J Surg Res* **116**: 121-123, 2004.

183. Morrison, C. P., Teague, B. D., Court, F. G., Wemyss-Holden, S. A., Metcalfe, M. S., Dennison, A. R., and Maddern, G. J. Experimental studies of serum cytokine concentration following pancreatic electrolytic ablation. *Med Sci Monit* **9**: BR43-46, 2003.

184. Finch, J. G., Berry, D. P., Wemyss-Holden, S. A., Fosh, B. G., Dennison, A. R., and Maddern, G. J. Electrolytic induced hepatic necrosis: the lack of a systemic response to treatment is confirmed in a large animal model. *HPB* **2**: 237, 2000.

185. Limmer, S., Huppert, P. E., Juette, V., Lenhart, A., Welte, M., and Wietholtz, H. Radiofrequency ablation of solitary pancreatic insulinoma in a patient with episodes of severe hypoglycemia. *Eur J Gastroenterol Hepatol* **21**: 1097-1101, 2009.

186. Finch, J. G., Berry, D. P., Wemyss-Holden, S. A., Vanderzon, P. S., Fosh, B. G., Dennison, A. R., and Maddern, G. J. Electrolytic destruction of liver tumours. Multiple electrodes reduce treatment times. *HPB* **2**: 237, 2000.

187. Finch, J. G., Fosh, B. G., Anthony, A., Wemyss-Holden, S. A., Dennison, A. R., and Maddern, G. J. Electrolysis. A new method for treating unresectable liver metastases: real-time monitoring of treatment. *HPB* **2**: 237, 2000.

188. Metcalfe, M. S., Mullin, E. J., Texler, M., Berry, D. P., Dennison, A. R., and Maddern, G. J. The safety and efficacy of radiofrequency and electrolytic ablation created adjacent to large hepatic veins in a porcine model. *European Journal of Surgical Oncology* **33**: 662-667, 2007.

189. Teratani, T., Yoshida, H., Shiina, S., Obi, S., Sato, S., Tateishi, R., Mine, N., Kondo, Y., Kawabe, T., and Omata, M. Radiofrequency ablation for hepatocellular carcinoma in so-called high-risk locations. *Hepatology* **43**: 1101-1108, 2006.

190. Welp, C., Siebers, S., Ermert, H., and Werner, J. Investigation of the influence of blood flow rate on large vessel cooling in hepatic radiofrequency ablation. *Biomedizinische Technik (Biomedical Engineering)* **51**: 337-346, 2006.

191. Thanos, L., Mylona, S., Galani, P., Pomoni, M., Pomoni, A., and Koskinas, I. Overcoming the heat-sink phenomenon: successful radiofrequency thermal ablation of liver tumors in contact with blood vessels. *Diagnostic and Interventional Radiology* **14**: 51-56, 2008.

192. Brace, C. L., Laeseke, P. F., van der Weide, D. W., and Lee, F. T. Microwave ablation with a triaxial antenna: results in ex vivo bovine liver. *IEEE Trans Microw Theory Tech* **53**: 215-220, 2005.

193. Lee, J. M., Han, J. K., Kim, H. C., Choi, Y. H., Kim, S. H., Choi, J. Y., and Choi, B. I. Switching monopolar radiofequency ablation technique using multiple, internally cooled electrodes and a multichannel generator: ex vivo and in vivo pilot study. *Investigative Radiology* **42**: 163-171, 2007.

194. Navarro, A. C., Burdio, F., Berjano, E. J., Guemes, A., Burdio, J. M., Sousa, R., Lozano, R., Tejero, E., and de Gregorio, M. A. Small ablation zones created previous to saline infusion result in enlargement of the coagulated area during perfusion RF ablation: an ex vivo experimental study. *Physiological Measurement* **28**: N29-37, 2007.

195. O'Rourke, A. P., Lazebnik, M., Bertram, J. M., Converse, M. C., Hagness, S. C., Webster, J. G., and Mahvi, D. M. Dielectric properties of human normal, malignant, and cirrhotic liver tissue: in vivo and ex vivo measurements from 0.5 to 20 GHz using a precision open-ended coaxial probe. *Physics in medicine and biology* **52**: 4707-4719, 2007.

196. Crocetti, L., Lencioni, R., Debeni, S., See, T. C., Pina, C. D., and Bartolozzi, C. Targeting liver lesions for radiofrequency ablation: an experimental feasibility study using a CT-US fusion imaging system. *Investigative Radiology* **43**: 33-39, 2008.

197. Imber, C. J., St Peter, S. D., De Cenarruzabeitia, I. L., Lemonde, H., Rees, M., Butler, A., Clayton, P. T., and Friend, P. J. Optimisation of bile production during normothermic preservation of porcine livers. *American Journal of Transplantation* **2**: 593-599, 2002.

198. Imber, C. J., St Peter, S. D., De Cenarruzabeitia, I. L., Pigott, D., James, T., Taylor, R., McGuire, J., Hughes, D., Butler, A., Rees, M., and Friend, P. Advantages of normothermic perfusion over cold storage in liver preservation. *Transplantation* **73**: 701-709, 2002.

199. Butler, A. J., Rees, M. A., Wight, D. G., Casey, N. D., Alexander, G., White, D. J., and Friend, P. J. Successful extracorporeal porcine liver perfusion for 72 hr. *Transplantation* **73**: 1212-1218, 2002.

200. Carrel, A., and Lindbergh, C. A. The Culture of Whole Organs. *Science (New York, N.Y* **81**: 621-623, 1935.

201. Marchioro, T. L., Huntley, R. T., Waddell, W. R., and Starzl, T. E. Extracorporeal Perfusion for Obtaining Postmortem Homografts. *Surgery* **54**: 900-911, 1963.

202. Kestens, P. J., Mikaeloff, P., Haxhe, J. J., Dureau, G., Alexandre, G., Rassat, J. P., Cuilleret, J., Hassoun, A., Dubernard, M., Descotes, J., and Morelle, J. Homotransplantation of the canine liver after hypothermic perfusion of long duration. *Bulletin de la Societe internationale de chirurgie* **25**: 647-659, 1966.

203. Belzer, F. O., Ashby, B. S., Huang, J. S., and Dunphy, J. E. Etiology of rising perfusion pressure in isolated organ perfusion. *Annals of surgery* **168**: 382-391, 1968.

204. Slapak, M., Wigmore, R. A., and MacLean, L. D. Twenty-four hour liver preservation by the use of continuous pulsatile perfusion and hyperbaric oxygen. *Transplantation* **5**: Suppl:1154-1158, 1967.

205. Brettschneider, L., Daloze, P. M., Huguet, C., Porter, K. A., Groth, C. G., Kashiwagi, N., Hutchison, D. E., and Starzl, T. E. The Use of Combined Preservation Techniques for Extended Storage of Orthotopic Liver Homografts. *Surgery, gynecology & obstetrics* **126**: 263-274, 1968.

206. Belzer, F. O., May, R., Berry, M. N., and Lee, J. C. Short term preservation of porcine livers. *The Journal of surgical research* **10**: 55-61, 1970.

207. Petrie, C. R., and Woods, J. E. Successful 24-hour preservation of the canine liver. *Arch Surg* **107**: 461-464, 1973.

208. Pienaar, B. H., Lindell, S. L., Van Gulik, T., Southard, J. H., and Belzer, F. O. Seventy-two-hour preservation of the canine liver by machine perfusion. *Transplantation* **49**: 258-260, 1990.

209. Abouna, G. M., Ashcroft, T., Hull, C., Hodson, A., Kirkley, J., and Walder, D. N. The assessment of function of the isolated perfused porcine liver. *British Journal of Surgery* **56**: 289-295, 1969.

210. Abouna, G. M., Fisher, L. M., Still, W. J., and Hume, D. M. Acute hepatic coma successfully treated by extracorporeal baboon liver perfusions. *British Medical Journal* **1**: 23-25, 1972.

211. Powell, G. M., Hugher, H. M., and Curtis, C. G. Isolated perfused liver technology for studying metabolic and toxicological problems. *Drug Metabolism and Drug Interactions* **7**: 53-86, 1989.

212. Hobbs, K. E., Hunt, A. C., Palmer, D. B., Badric, F. E., Morris, A. M., Mitra, S. K., Peacock, J. H., Immelman, E. J., and Riddell, A. G. Hypothermic perfusion as a method of short-term porcine liver storage. *British Journal of Surgery* **55**: 862, 1968.

213. Hobbs, K. E., Hunt, A. C., Palmer, D. B., Badric, F. E., Morris, A. M., Mitra, S. K., Peacock, J. H., Immelman, E. J., and Riddell, A. G. Hypothermic low flow liver perfusion as a means of porcine hepatic storage for six hours. *British Journal of Surgery* **55**: 696-703, 1968.

214. Drapanas, T., Zemel, R., and Vang, J. O. Haemodynamics of the isolated perfused pig liver: metabolism according to routes of perfusion and rates of flow. *Annals of Surgery* **164**: 522-537, 1966.

215. Butler, A. J., Rees, M. A., Wight, D. G., Casey, N. D., Alexander, G., White, D. J., and Friend, P. J. Successful extracorporeal porcine liver perfusion for 72 hr. *Transplantation* **73**: 1212-1218, 2002.

216. Schon, M. R., Kollmar, O., Wolf, S., Schrem, H., Matthes, M., Akkoc, N., Schnoy, N. C., and Neuhaus, P. Liver transplantation after organ preservation with normothermic extracorporeal perfusion. *Annals of surgery* **233**: 114-123, 2001.

217. Neuhaus, P., and Blumhardt, G. Extracorporeal liver perfusion: applications of an improved model for experimental studies of the liver. *The International journal of artificial organs* **16**: 729-739, 1993.

218. Schon, M. R., Puhl, G., Frank, J., and Neuhaus, P. Hemodialysis improves results of pig liver perfusion after warm ischemic injury. *Transplantation proceedings* **25**: 3239-3243, 1993.

219. Naruse, K., Sakai, Y., Guo, L., Natori, T., Shindoh, J., Karasawa, Y., Iida, Y., Kojima, K., Michishita, K., and Makuuchi, M. Development of a new extracorporeal whole-liver perfusion system. *J Artif Organs* **6**: 211-217, 2003.

220. St Peter, S. D., Imber, C. J., Kay, J., James, T., and Friend, P. J. Hepatic control of perfusate homeostasis during normothermic extrocorporeal preservation. *Transplantation proceedings* **35**: 1587-1590, 2003.

221. Vogel, T., Brockmann, J. G., Coussios, C., and Friend, P. J. The role of normothermic extracorporeal perfusion in minimizing ischemia reperfusion injury. *Transplantation reviews (Orlando, Fla* **26**: 156-162, 2012.

222. Schmucker, D. L., and Curtis, J. C. A correlated study of the fine structure and physiology of the perfused rat liver. *Laboratory investigation; a journal of technical methods and pathology* **30**: 201-212, 1974.

223. Vogel, T., Brockmann, J. G., Coussios, C. C., and Friend, P. J. Normothermic machine perfusion of the liver. *Organ preservation and reengineering.* Boston: Artech House, 2011. Pp. 1-20.

224. Pegg, D. E., Foreman, J., and Rolles, K. Metabolism during preservation and viability of ischemically injured canine kidneys. *Transplantation* **38**: 78-81, 1984.

225. Motoyama, S., Minamiya, Y., Saito, S., Saito, R., Matsuzaki, I., Abo, S., Inaba, H., Enomoto, K., and Kitamura, M. Hydrogen peroxide derived from hepatocytes induces sinusoidal endothelial cell apoptosis in perfused hypoxic rat liver. *Gastroenterology* **114**: 153-163, 1998.

226. Felker, T. E., Gantz, D., Tercyak, A. M., Oliva, C., Clark, S. B., and Small, D. M. A comparison of lipoprotein secretion, bile production and hepatic morphology in isolated rat livers perfused with a perfluorocarbon emulsion or rat erythrocytes. *Hepatology (Baltimore, Md* **14**: 340-351, 1991.

227. Riedel, G. L., Scholle, J. L., Shepherd, A. P., and Ward, W. F. Effects of hematocrit on oxygenation of the isolated perfused rat liver. *The American journal of physiology* **245**: G769-774, 1983.

228. Adham, M., Peyrol, S., Chevallier, M., Ducerf, C., Vernet, M., Barakat, C., De La Roche, E., Taibi, A., Bizollon, T., Rigal, D., Pouyet, M., and Baulieux, J. The isolated perfused porcine liver: assessment of viability during and after six hours of perfusion. *Transpl Int* **10**: 299-311, 1997.

229. Aggarwal, S., Obrist, W., Yonas, H., Kramer, D., Kang, Y., Scott, V., and Planinsic, R. Cerebral hemodynamic and metabolic profiles in fulminant hepatic failure: relationship to outcome. *Liver Transpl* **11**: 1353-1360, 2005.

230. Ikeda, T., Yanaga, K., Lebeau, G., Higashi, H., Kakizoe, S., and Starzl, T. E. Hemodynamic and biochemical changes during normothermic and hypothermic sanguinous perfusion of the porcine hepatic graft. *Transplantation* **50**: 564-567, 1990.

231. St Peter, S. D., Imber, C. J., and Friend, P. J. Liver and kidney preservation by perfusion. *Lancet* **359**: 604-613, 2002.

232. Okafor, O., and Ojo, S. A comparative analysis of six current histological classification schemes and scoring systems used in chronic hepatitis reporting. *Rev Esp Patol* **37**: 269-277, 2004.

233. Knodell, R. G., Ishak, K. G., Black, W. C., Chen, T. S., Craig, R., Kaplowitz, N., Kiernan, T. W., and Wollman, J. Formulation and application of a numerical scoring system for assessing histological activity in asymptomatic chronic active hepatitis. *Hepatology (Baltimore, Md* **1**: 431-435, 1981.

234. Ishak, K., Baptista, A., Bianchi, L., Callea, F., De Groote, J., Gudat, F., Denk, H., Desmet, V., Korb, G., MacSween, R. N., and et al. Histological grading and staging of chronic hepatitis. *Journal of hepatology* **22**: 696-699, 1995.

235. Bedossa, P., and Poynard, T. An algorithm for the grading of activity in chronic hepatitis C. The METAVIR Cooperative Study Group. *Hepatology (Baltimore, Md* **24**: 289-293, 1996.

236. Nicholson, D. W., Ali, A., Thornberry, N. A., Vaillancourt, J. P., Ding, C. K., Gallant, M., Gareau, Y., Griffin, P. R., Labelle, M., Lazebnik, Y. A., and et al. Identification and inhibition of the ICE/CED-3 protease necessary for mammalian apoptosis. *Nature* **376**: 37-43, 1995.

237. Fraser, R., Bowler, L. M., Day, W. A., Dobbs, B., Johnson, H. D., and Lee, D. High perfusion pressure damages the sieving ability of sinusoidal endothelium in rat livers. *British journal of experimental pathology* **61**: 222-228, 1980.

238. Wemyss-Holden, S. A., Berry, D. P., Robertson, G. S., Dennison, A. R., De La, M. H. P., and Maddern, G. J. Electrolytic ablation as an adjunct to liver resection: Safety and efficacy in patients. *ANZ journal of surgery* **72**: 589-593, 2002.

239. Mathew, J. P., Mackensen, G. B., Phillips-Bute, B., Stafford-Smith, M., Podgoreanu, M. V., Grocott, H. P., Hill, S. E., Smith, P. K., Blumenthal, J. A., Reves, J. G., and Newman, M. F. Effects of extreme hemodilution during cardiac surgery on cognitive function in the elderly. *Anesthesiology* **107**: 577-584, 2007.

240. Stratford, L. L., and Hooper, S. B. Effect of hypoxemia on tissue glycogen content and glycolytic enzyme activities in fetal sheep. *The American journal of physiology* **272**: R103-110, 1997.

241. Larsen, J. J., Hansen, J. M., Olsen, N. V., Galbo, H., and Dela, F. The effect of altitude hypoxia on glucose homeostasis in men. *The Journal of physiology* **504 (Pt 1)**: 241-249, 1997.

242. Nowak, G., Ungerstedt, J., Wernerman, J., Ungerstedt, U., and Ericzon, B. G. Metabolic changes in the liver graft monitored continuously with microdialysis during liver transplantation in a pig model. *Liver Transpl* **8**: 424-432, 2002.

243. Kannerup, A. S., Funch-Jensen, P., Gronbaek, H., Jorgensen, R. L., and Mortensen, F. V. Metabolic changes in the pig liver during warm ischemia and reperfusion measured by microdialysis. *J Gastrointest Surg* **12**: 319-326, 2008.

244. Chen, X. Q., Dong, J., Niu, C. Y., Fan, J. M., and Du, J. Z. Effects of hypoxia on glucose, insulin, glucagon, and modulation by corticotropin-releasing factor receptor type 1 in the rat. *Endocrinology* **148**: 3271-3278, 2007.

245. Klaus, S., Heringlake, M., Gliemroth, J., Pagel, H., Staubach, K., and Bahlmann, L. Biochemical tissue monitoring during hypoxia and reoxygenation. *Resuscitation* **56**: 299-305, 2003.

246. Fukusaki, M., Maekawa, T., Yamaguchi, K., Matsumoto, M., Shibata, O., and Sumikawa, K. Combined effects of prolonged prostaglandin E1-induced hypotension and haemodilution on human hepatic function. *European journal of anaesthesiology* **14**: 157-163, 1997.

247. Medzhitov, R. Recognition of microorganisms and activation of the immune response. *Nature* **449**: 819-826, 2007.

248. Hajishengallis, G., and Lambris, J. D. Crosstalk pathways between Toll-like receptors and the complement system. *Trends in immunology* **31**: 154-163, 2010.

249. Hawlisch, H., and Kohl, J. Complement and Toll-like receptors: key regulators of adaptive immune responses. *Molecular immunology* **43**: 13-21, 2006.

250. Ishii, K. J., Koyama, S., Nakagawa, A., Coban, C., and Akira, S. Host innate immune receptors and beyond: making sense of microbial infections. *Cell host & microbe* **3**: 352-363, 2008.

251. Zeytun, A., Chaudhary, A., Pardington, P., Cary, R., and Gupta, G. Induction of cytokines and chemokines by Toll-like receptor signaling: strategies for control of inflammation. *Critical reviews in immunology* **30**: 53-67, 2010.

252. Markiewski, M. M., and Lambris, J. D. The role of complement in inflammatory diseases from behind the scenes into the spotlight. *The American journal of pathology* **171**: 715-727, 2007.

253. Zhang, X., Kimura, Y., Fang, C., Zhou, L., Sfyroera, G., Lambris, J. D., Wetsel, R. A., Miwa, T., and Song, W. C. Regulation of Toll-like receptor-mediated inflammatory response by complement in vivo. *Blood* **110**: 228-236, 2007.

254. Ricklin, D., Hajishengallis, G., Yang, K., and Lambris, J. D. Complement: a key system for immune surveillance and homeostasis. *Nature immunology* **11**: 785-797, 2010.

255. Ulukaya, S., Basturk, B., Kilic, M., and Ulukaya, E. Cytokine gene polymorphism and postreperfusion syndrome during orthotopic liver transplantation. *Transplantation proceedings* **40**: 1290-1293, 2008.

256. Ohkohchi, N., Hirano, T., Satake, M., and Satomi, S. Immunological reactions in liver graft perireperfusion in living donor liver transplantation--change of expression of adhesion molecules, deposition of immunoglobulins and cytokine level. *Hepato-gastroenterology* **50**: 1090-1096, 2003.

257. Kubala, L., Ciz, M., Vondracek, J., Cizova, H., Cerny, J., Nemec, P., Studenik, P., Duskova, M., and Lojek, A. Peri- and post-operative course of cytokines and the metabolic activity of neutrophils in human liver transplantation. *Cytokine* **16**: 97-101, 2001.

258. Wen, X. H., Kong, H. Y., Zhu, S. M., Xu, J. H., Huang, S. Q., and Chen, Q. L. Plasma levels of tumor necrotic factor-alpha and interleukin-6, -8 during orthotopic liver transplantation and their relations to postoperative pulmonary complications. *Hepatobiliary Pancreat Dis Int* **3**: 38-41, 2004.

259. Zhao, X., Koshiba, T., Fujimoto, Y., Pirenne, J., Yoshizawa, A., Ito, T., Kamei, H., Jobara, K., Ogawa, K., Uryuhara, K., Takada, Y., and Tanaka, K. Proinflammatory and antiinflammatory cytokine production during ischemia-reperfusion injury in a case of identical twin living donor liver transplantation using no immunosuppression. *Transplantation proceedings* **37**: 392-394, 2005.

260. Schmidt, A., Tomasdottir, H., and Bengtsson, A. Influence of cold ischemia time on complement activation, neopterin, and cytokine release in liver transplantation. *Transplantation proceedings* **36**: 2796-2798, 2004.

261. Boros, P., Suehiro, T., Curtiss, S., Sheiner, P., Emre, S., Guy, S., Schwartz, M. E., and Miller, C. M. Differential contribution of graft and recipient to perioperative TNF-alpha, IL-1 beta, IL-6 and IL-8 levels and correlation with early graft function in clinical liver transplantation. *Clinical transplantation* **11**: 588-592, 1997.

262. Broughan, T. A., Naukam, R., Tan, C., Van De Wiele, C. J., Refai, H., and Teague, T. K. Effects of hepatic zonal oxygen levels on hepatocyte stress responses. *The Journal of surgical research* **145**: 150-160, 2008.

263. Tiberio, L., Tiberio, G. A., Bardella, L., Cervi, E., Cerea, K., Dreano, M., Garotta, G., Fra, A., Montani, N., Ferrari-Bravo, A., Callea, F., Grigolato, P., Giulini, S. M., and Schiaffonati, L. Mechanisms of interleukin-6 protection against ischemia-reperfusion injury in rat liver. *Cytokine* **34**: 131-142, 2006.

264. Tacchini, L., Cairo, G., De Ponti, C., Massip, M., Rosello-Catafau, J., and Peralta, C. Up regulation of IL-6 by ischemic preconditioning in normal and fatty rat livers: association with reduction of oxidative stress. *Free radical research* **40**: 1206-1217, 2006.

265. Langdale, L. A., Hoagland, V., Benz, W., Riehle, K. J., Campbell, J. S., Liggitt, D. H., and Fausto, N. Suppressor of cytokine signaling expression with increasing severity of murine hepatic ischemia-reperfusion injury. *Journal of hepatology* **49**: 198-206, 2008.

266. Pulitano, C., Aldrighetti, L., Arru, M., Finazzi, R., Soldini, L., Catena, M., and Ferla, G. Prospective randomized study of the benefits of preoperative corticosteroid administration on

hepatic ischemia-reperfusion injury and cytokine response in patients undergoing hepatic resection. *HPB (Oxford)* **9**: 183-189, 2007.

267. Saidi, R. F., Chang, J., Verb, S., Brooks, S., Nalbantoglu, I., Adsay, V., and Jacobs, M. J. The effect of methylprednisolone on warm ischemia-reperfusion injury in the liver. *American journal of surgery* **193**: 345-347; discussion 347-348, 2007.

268. Aldrighetti, L., Pulitano, C., Arru, M., Finazzi, R., Catena, M., Soldini, L., Comotti, L., and Ferla, G. Impact of preoperative steroids administration on ischemia-reperfusion injury and systemic responses in liver surgery: a prospective randomized study. *Liver Transpl* **12**: 941-949, 2006.

269. Teoh, N., Field, J., and Farrell, G. Interleukin-6 is a key mediator of the hepatoprotective and pro-proliferative effects of ischaemic preconditioning in mice. *Journal of hepatology* **45**: 20-27, 2006.

270. Flach, R., Speidel, N., Flohe, S., Borgermann, J., Dresen, I. G., Erhard, J., and Schade, F. U. Analysis of intragraft cytokine expression during early reperfusion after liver transplantation using semi-quantitative RT-PCR. *Cytokine* **10**: 445-451, 1998.

271. Noguchi, T., Kitano, T., Ware, F., Board, J., Goto, S., Lynch, S. V., and Strong, R. W. The effects of circulating interleukin-8 and adhesion molecules on pulmonary dysfunction in pediatric orthotopic liver transplantation. *Surgery today* **29**: 1011-1016, 1999.

272. Gerlach, J., Jorres, A., Schon, M., Nohr, R., Berger, A., Spatkowski, G., Smith, M. D., and Neuhaus, P. Systemic liberation of interleukin-8 in the perioperative phase of liver transplantation. *Transpl Int* **10**: 401-404, 1997.

273. Tilg, H., Ceska, M., Vogel, W., Herold, M., Margreiter, R., and Huber, C. Interleukin-8 serum concentrations after liver transplantation. *Transplantation* **53**: 800-803, 1992.

274. Steininger, R., Roth, E., Fugger, R., Winkler, S., Langle, F., Grunberger, T., Gotzinger, P., Sautner, T., and Muhlbacher, F. Transhepatic metabolism of TNF-alpha, IL-6, and endotoxin in the

early hepatic reperfusion period after human liver transplantation. *Transplantation* **58**: 179-183, 1994.

275. Le Moine, O., Marchant, A., Durand, F., Ickx, B., Pradier, O., Belghiti, J., Abramowicz, D., Gelin, M., Goldman, M., and Deviere, J. Systemic release of interleukin-10 during orthotopic liver transplantation. *Hepatology (Baltimore, Md* **20**: 889-892, 1994.

276. Urata, K., Brault, A., Rocheleau, B., and Huet, P. M. Role of Kupffer cells in the survival after rat liver transplantation with long portal vein clamping times. *Transpl Int* **13**: 420-427, 2000.

277. Teague, B. D., Morrison, C. P., Court, F. G., Nguyen, T., Wemyss-Holden, S. A., Dennison, A. R., and Maddern, G. J. The lack of a systemic inflammatory response syndrome supports the safety of pancreatic electrolysis: experimental studies. *J Surg Res* **116**: 121-123, 2004.

278. Gravante, G., Ong, S. L., Metcalfe, M. S., Sorge, R., Sconocchia, G., Orlando, G., Lloyd, D. M., and Dennison, A. R. Cytokine response to ischemia/reperfusion injury in an ex vivo perfused porcine liver model. *Transplant Proc* **41**: 1107-1112, 2009.

279. Mora, N., Kaptanoglu, L., Zhang, Z., Niekrasz, M., Black, S., Ver Steeg, K., Wade, R., Siddall, V., Pao, W., Walsh, W., Ivancic, D., Kaufman, D., Abecassis, M., Stuart, F., Blei, A., Leventhal, J., and Fryer, J. Single vs. dual vessel porcine extracorporeal liver perfusion. *J Surg Res* **103**: 228-235, 2002.

280. Gong, J., Wang, X. M., Long, G., Guo, Z. T., Jiang, T., and Chen, S. Establishment and evaluation of the system of extracorporeal liver perfusion in pigs. *Hepatobiliary Pancreat Dis Int* **4**: 94-97, 2005.

281. Kusmic, C., Boggi, U., Bellini, R., Vistoli, F., Castellari, M., Taddei, G., Minervini, A., Filipponi, F., Mosca, F., and Barsacchi, R. Oxidative stress in fulminant hepatic failure: comparison of two pig models with and without liver necrosis. *Hepato-gastroenterology* **48**: 762-769, 2001.

282. Carraro, A., Gringeri, E., Calabrese, F., Violi, P., Brolese, A., Zanus, G., Boccagni, P., Valente, M. L., Bassi, D., D'Amico, F., Jr., D'Amico, D. F., and Cillo, U. A new experimental

model of isolated perfused pig liver to support acute hepatic failure. *Transplantation proceedings* **39**: 2028-2030, 2007.

283. Monbaliu, D., Vekemans, K., De Vos, R., Brassil, J., Heedfeld, V., Qiang, L., D'Hollander, M., Roskams, T., and Pirenne, J. Hemodynamic, biochemical, and morphological characteristics during preservation of normal porcine livers by hypothermic machine perfusion. *Transplantation proceedings* **39**: 2652-2658, 2007.

284. Malhi, H., Gores, G. J., and Lemasters, J. J. Apoptosis and necrosis in the liver: a tale of two deaths? *Hepatology (Baltimore, Md* **43**: S31-44, 2006.

285. Gravante, G., Ong, S., Metcalfe, M., Sorge, R., Birchandani, J., Lloyd, D., and Dennison, A. Effects of hypoxia due to isovolaemic hemodilution on an ex-vivo normothermic perfused liver model. *J Surg Res* (in press).

286. Dirsch, O., Li, J., He, Q., Ji, Y., Gu, Y. L., and Dahmen, U. Induction of rejection after small-for-size liver transplantation: size matters. *J Invest Surg* **21**: 288-298, 2008.

287. Maetani, Y., Itoh, K., Egawa, H., Shibata, T., Ametani, F., Kubo, T., Kiuchi, T., Tanaka, K., and Konishi, J. Factors influencing liver regeneration following living-donor liver transplantation of the right hepatic lobe. *Transplantation* **75**: 97-102, 2003.

288. Feldmann, G. [Liver apoptosis]. *Gastroenterologie clinique et biologique* **30**: 533-545, 2006.

289. Gravante, G., Ong, S. L., Metcalfe, M. S., Bhardwaj, N., Maddern, G. J., Lloyd, D. M., and Dennison, A. R. Experimental application of electrolysis in the treatment of liver and pancreatic tumours: Principles, preclinical and clinical observations and future perspectives. *Surgical oncology*, 2009.

290. Gravante, G., Ong, S. L., Metcalfe, M. S., Sorge, R., Fox, A. J., Lloyd, D. M., Maddern, G. J., and Dennison, A. R. Changes in acid-base balance during electrolytic ablation in an ex vivo perfused liver model. *American journal of surgery*.

291. Turler, A., Schaefer, H., Schaefer, N., Wagner, M., Maintz, D., Qiao, J. C., and Hoelscher, A. H. Experimental low-level direct current therapy in liver metastases: influence of polarity and current dose. *Bioelectromagnetics* **21**: 395-401, 2000.